LAWRENCE
LIVERMORE
NATIONAL
LABORATORY

LLNL-PROC-446991

Target Science and Technology: Thin Film and Small Scale Mechanical Behavior

A. V. Hamza

August 3, 2010

Gordon Research Confernce
Waterville, ME, United States
July 29, 2010 through July 29, 2010

Disclaimer

This document was prepared as an account of work sponsored by an agency of the United States government. Neither the United States government nor Lawrence Livermore National Security, LLC, nor any of their employees makes any warranty, expressed or implied, or assumes any legal liability or responsibility for the accuracy, completeness, or usefulness of any information, apparatus, product, or process disclosed, or represents that its use would not infringe privately owned rights. Reference herein to any specific commercial product, process, or service by trade name, trademark, manufacturer, or otherwise does not necessarily constitute or imply its endorsement, recommendation, or favoring by the United States government or Lawrence Livermore National Security, LLC. The views and opinions of authors expressed herein do not necessarily state or reflect those of the United States government or Lawrence Livermore National Security, LLC, and shall not be used for advertising or product endorsement purposes.

Target Science and Technology

Presentation to

Thin Film & Small Scale Mechanical Behavior

July 29th, 2010

Alex Hamza

This work performed under the auspices of the U.S. Department of Energy by Lawrence Livermore National Laboratory under Contract DE-AC52-07NA27344

Fusion is an extremely dense energy source

Fusion energy:
3 gal of DT ice

=

Chemical energy:
Supertanker full
of carbon dioxide rich oil

Could we build a miniature sun on earth?

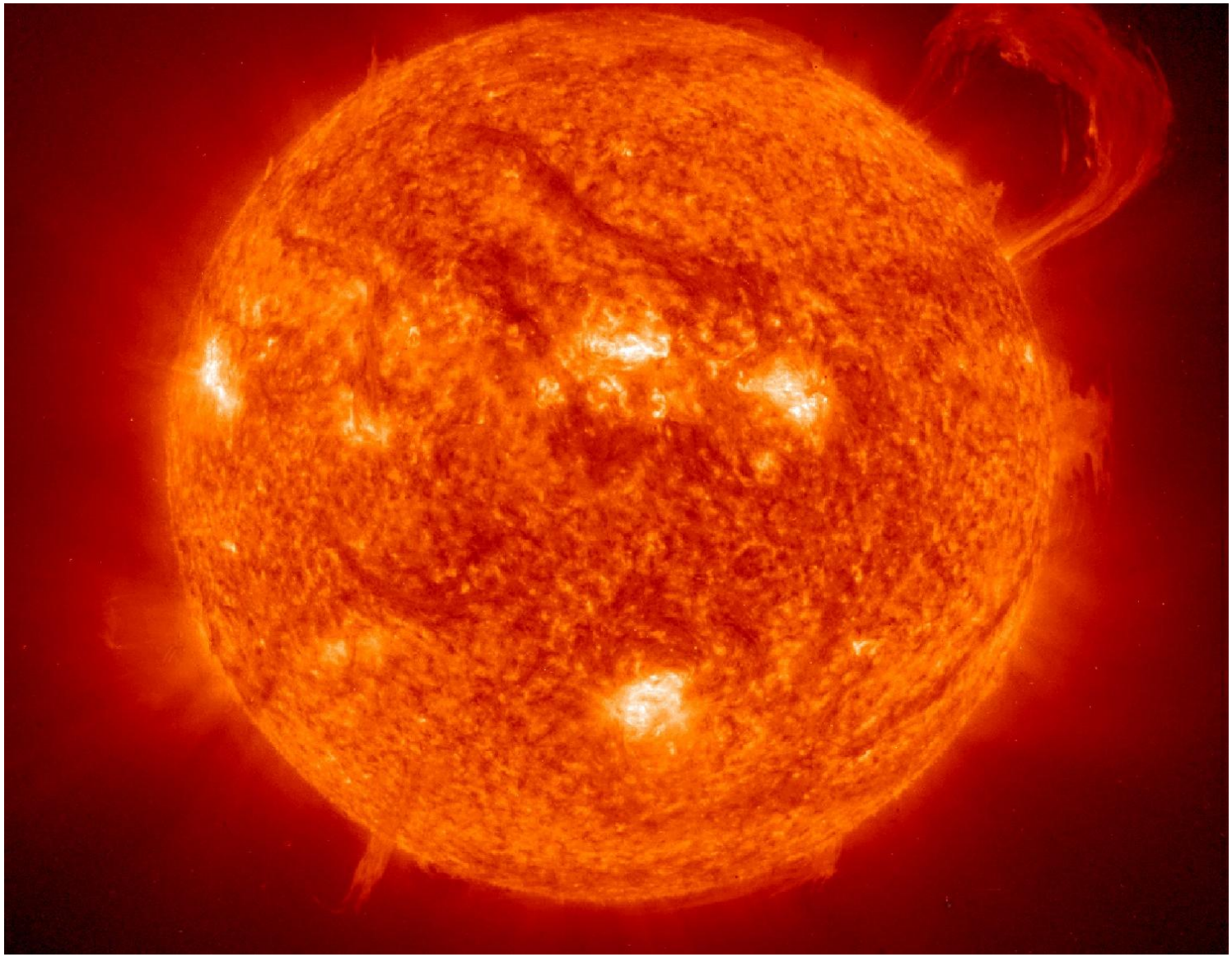

Laser-driven Inertial Confinement Fusion

Laser driven compression of a millimeter-sized capsule that contains a mixture of deuterium and tritium to extreme pressures and temperatures

- ~ 1MJ laser energy
- ~ 3 milllion degree X-ray bath
- ~ 100 million atmosphere ablative rocket drive
- Accelerates shell to ~ 350 km/s

Compresses & heats core, PdV

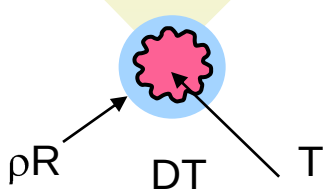

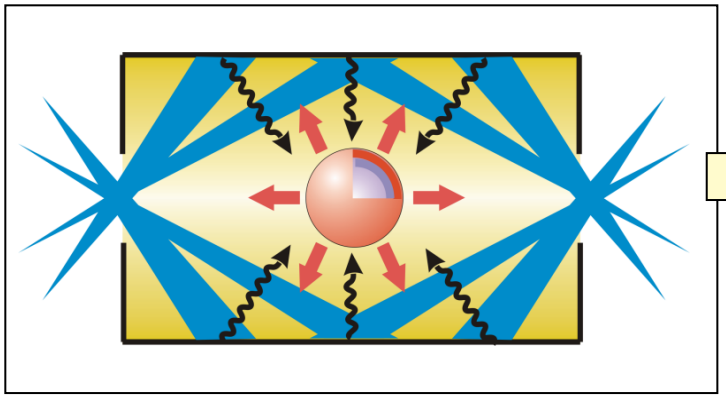

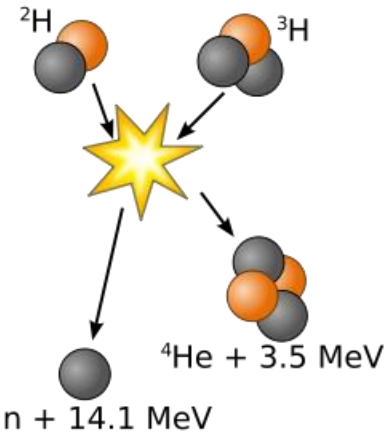

The experiment requires a thin-walled, millimeter-sized, perfectly spherical shell (ablator) made of a low atomic number element (Be, B, C)

National Ignition Facility

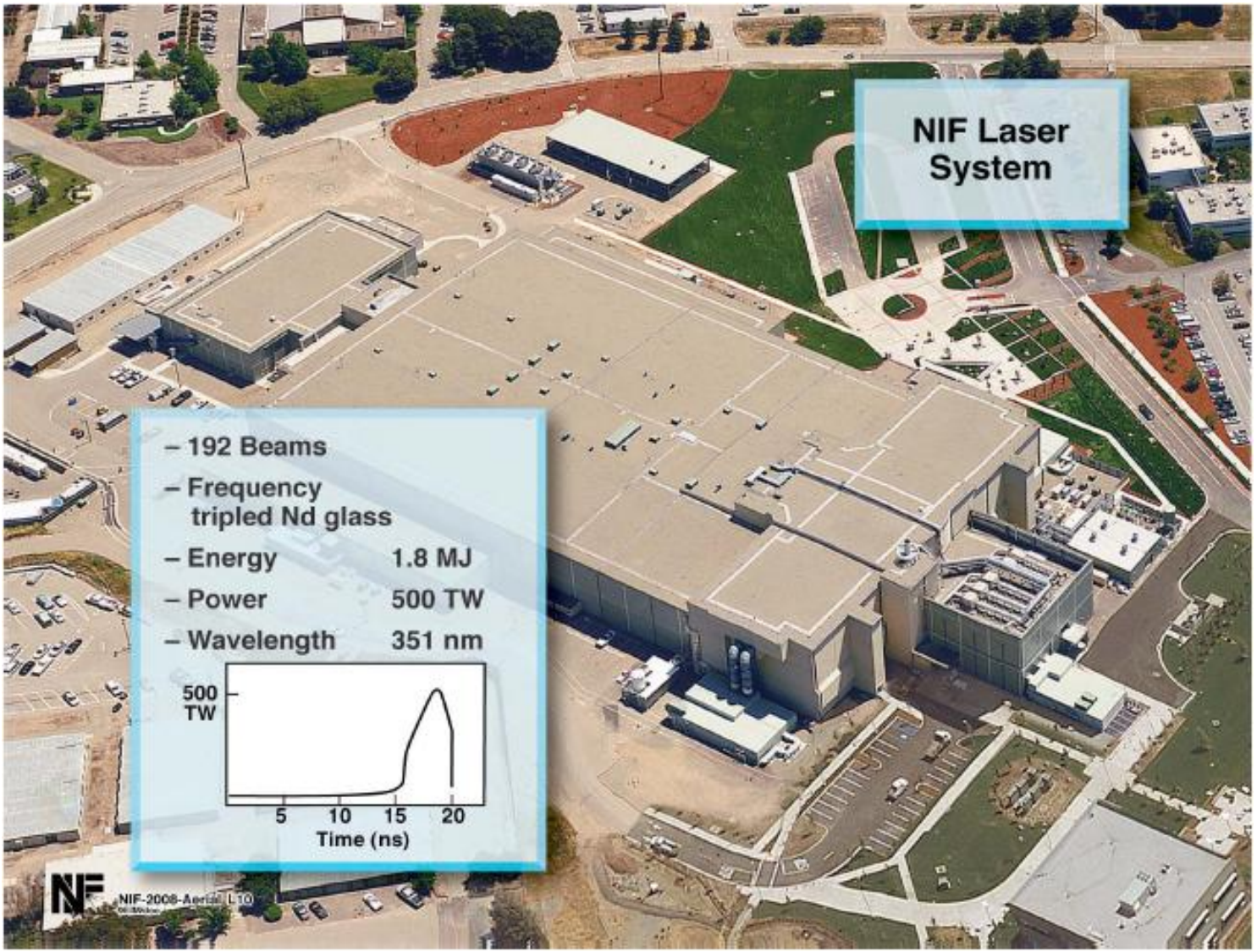

National Ignition Facility

National Ignition Facility

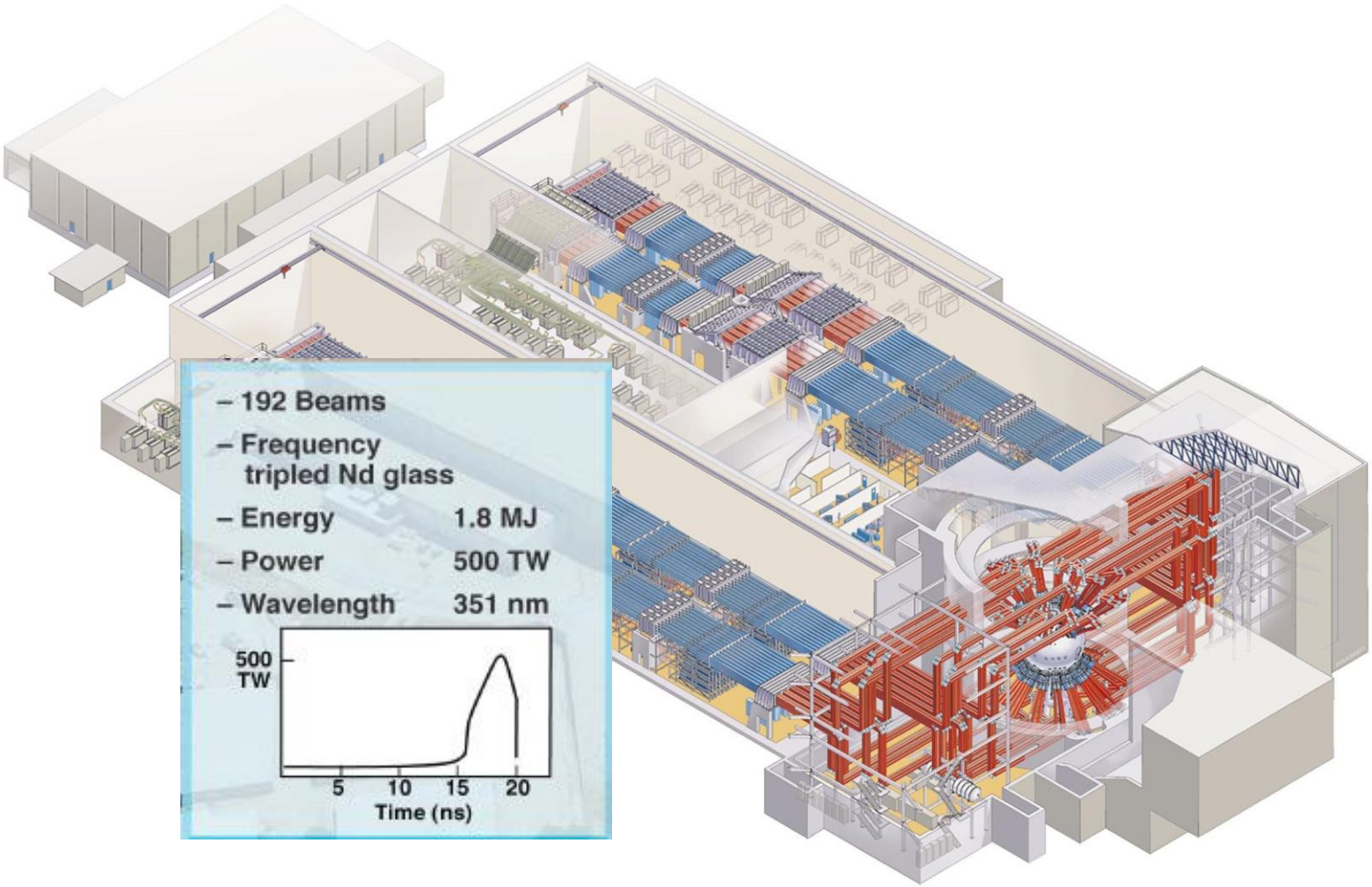

The NIF-laser beamline - One of 192 beams

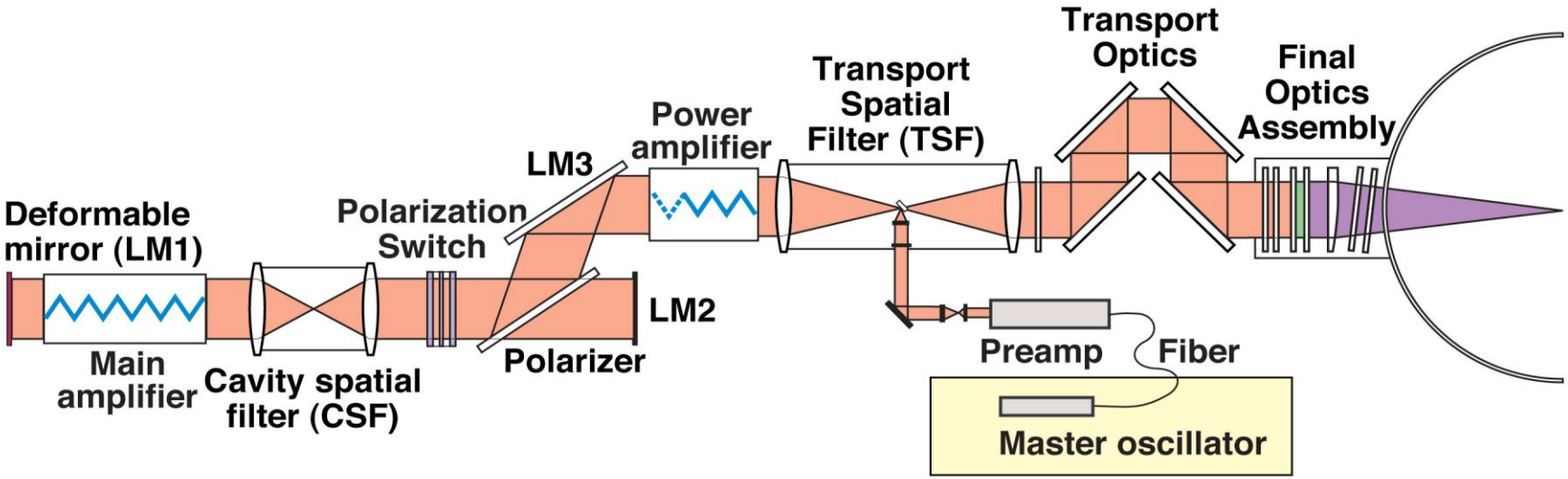

- The master oscillator is a flexible and accurate tool for pulse shaping

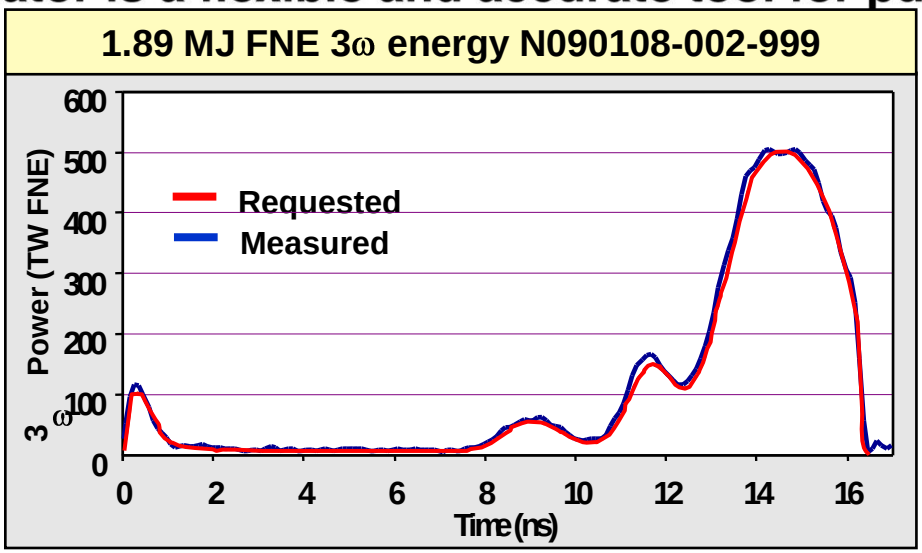

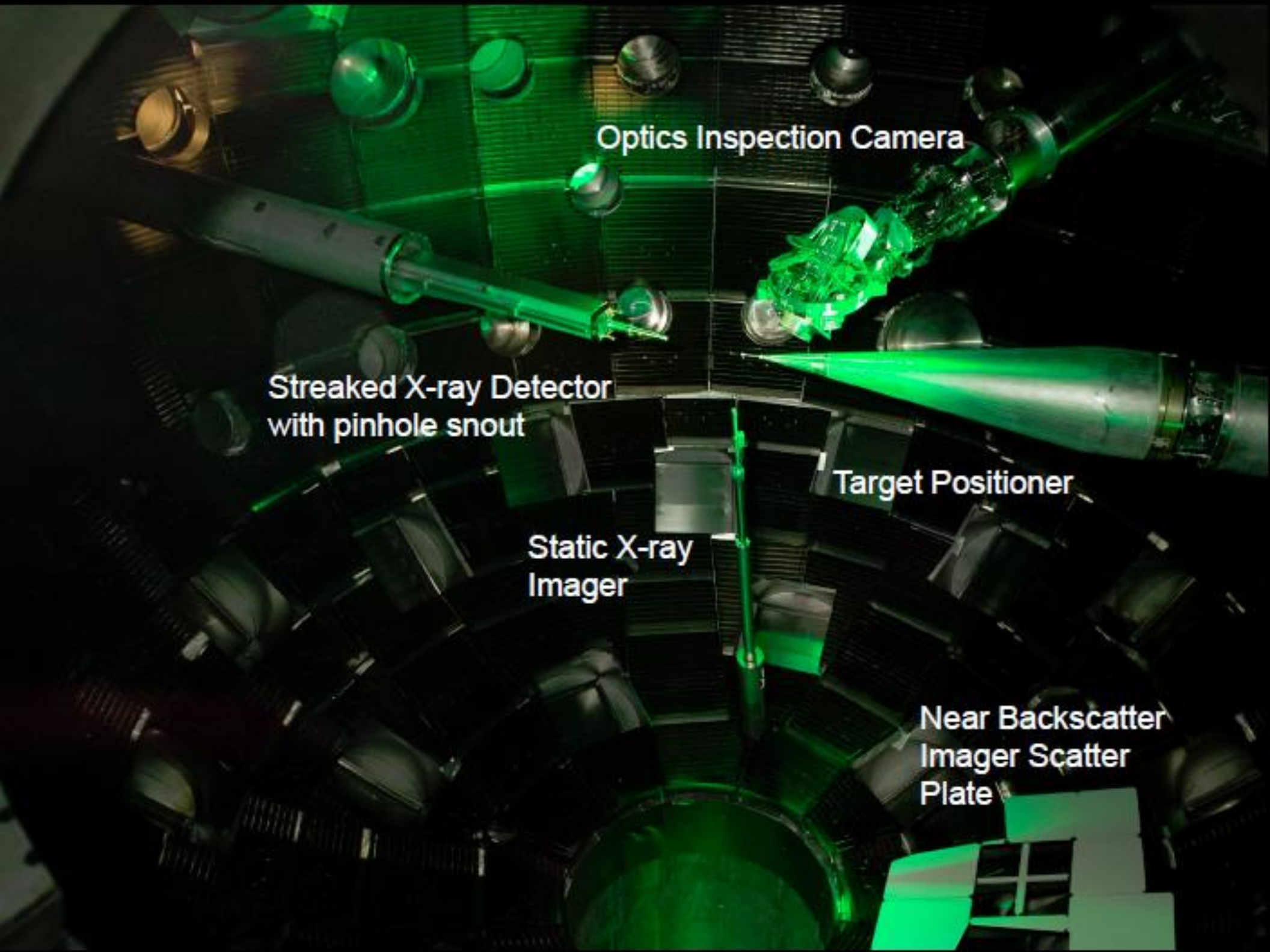
Optics Inspection Camera
Streaked X-ray Detector
with pinhole snout
Target Positioner
Static X-ray
Imager
Near Backscatter
Imager Scatter
Plate

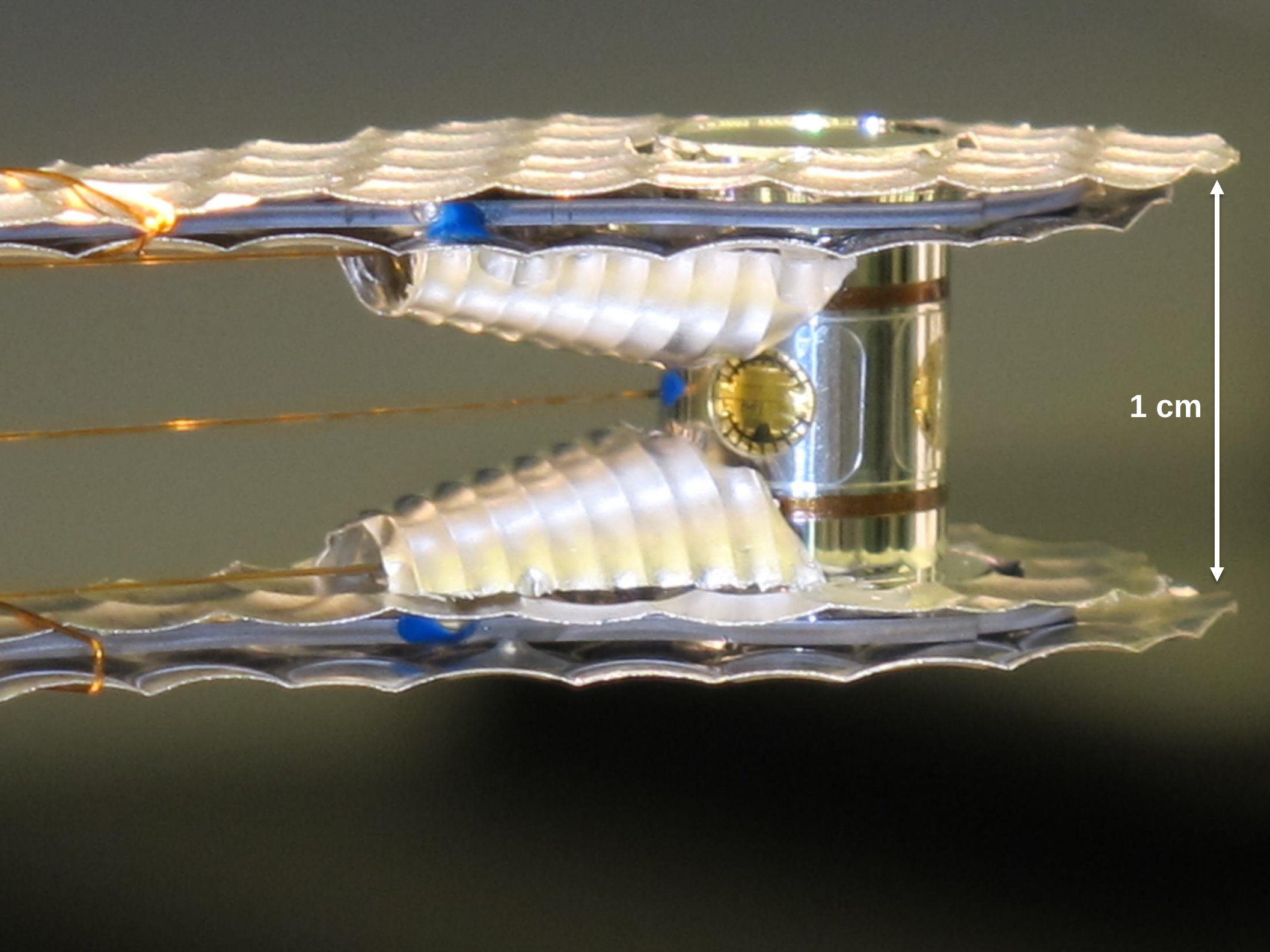
1 cm

There are various designs to achieve ignition

NIC Ignition Platform

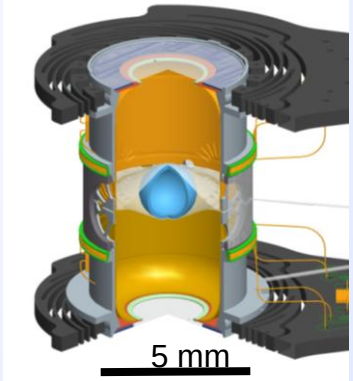

NIC Ignition Target

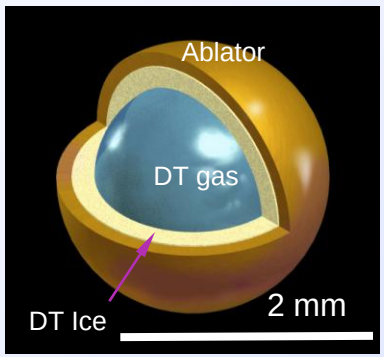

Fast Ignition Target

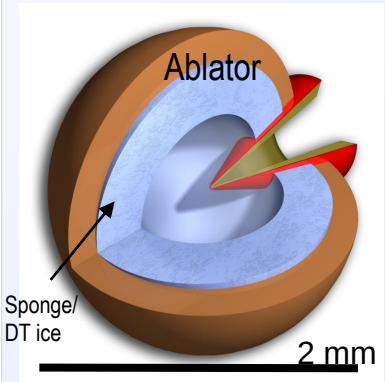

Ignition Double Shell

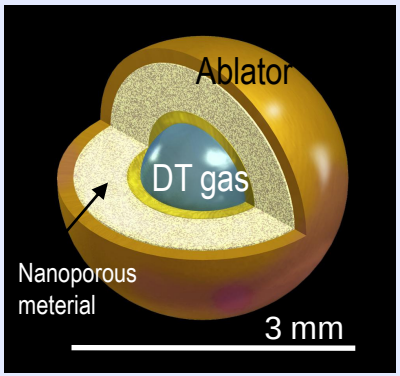

The NIF point design has a graded-doped, CH capsule in a U hohlraum driven at 285 eV by 1.22 MJ

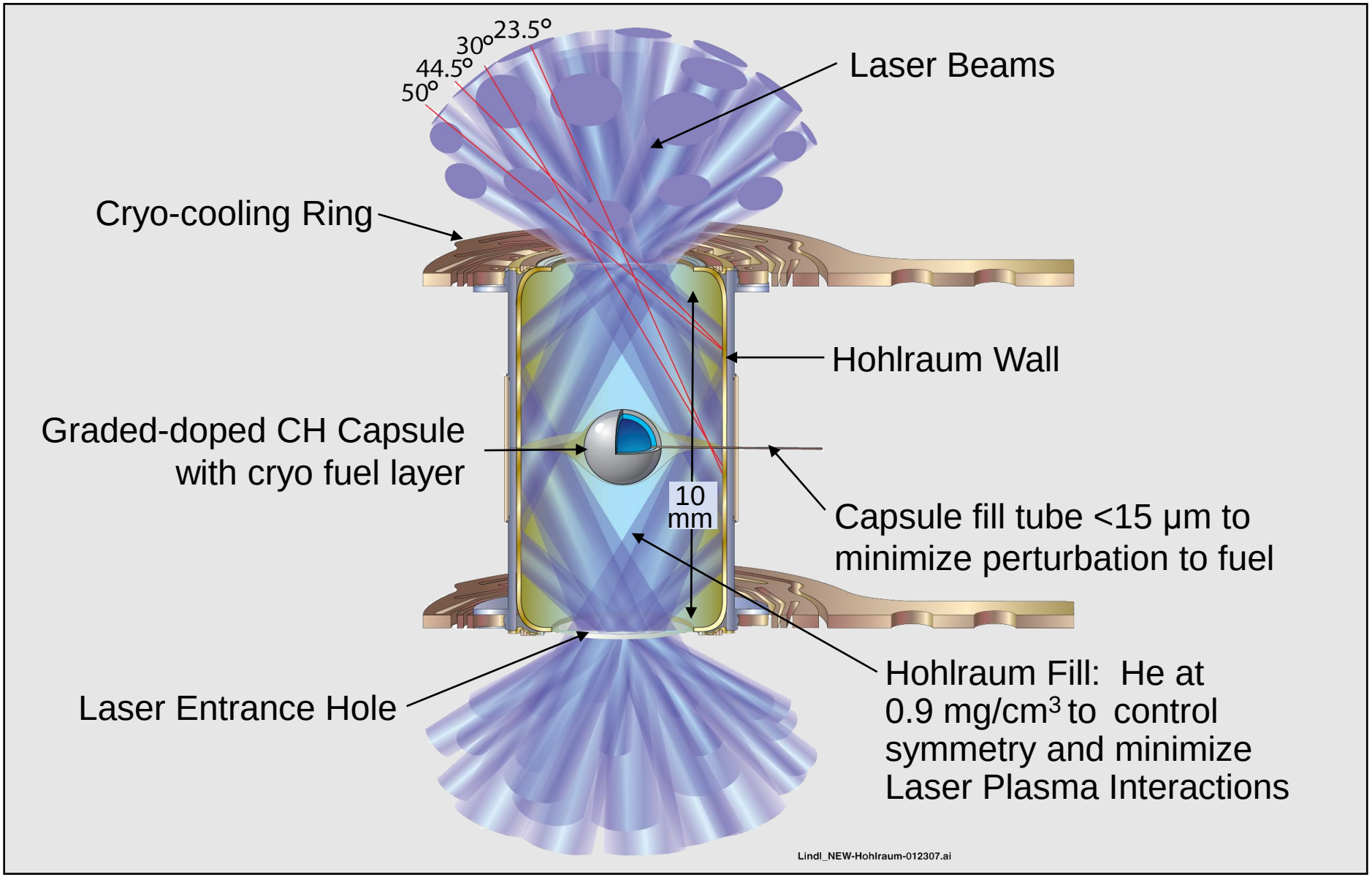

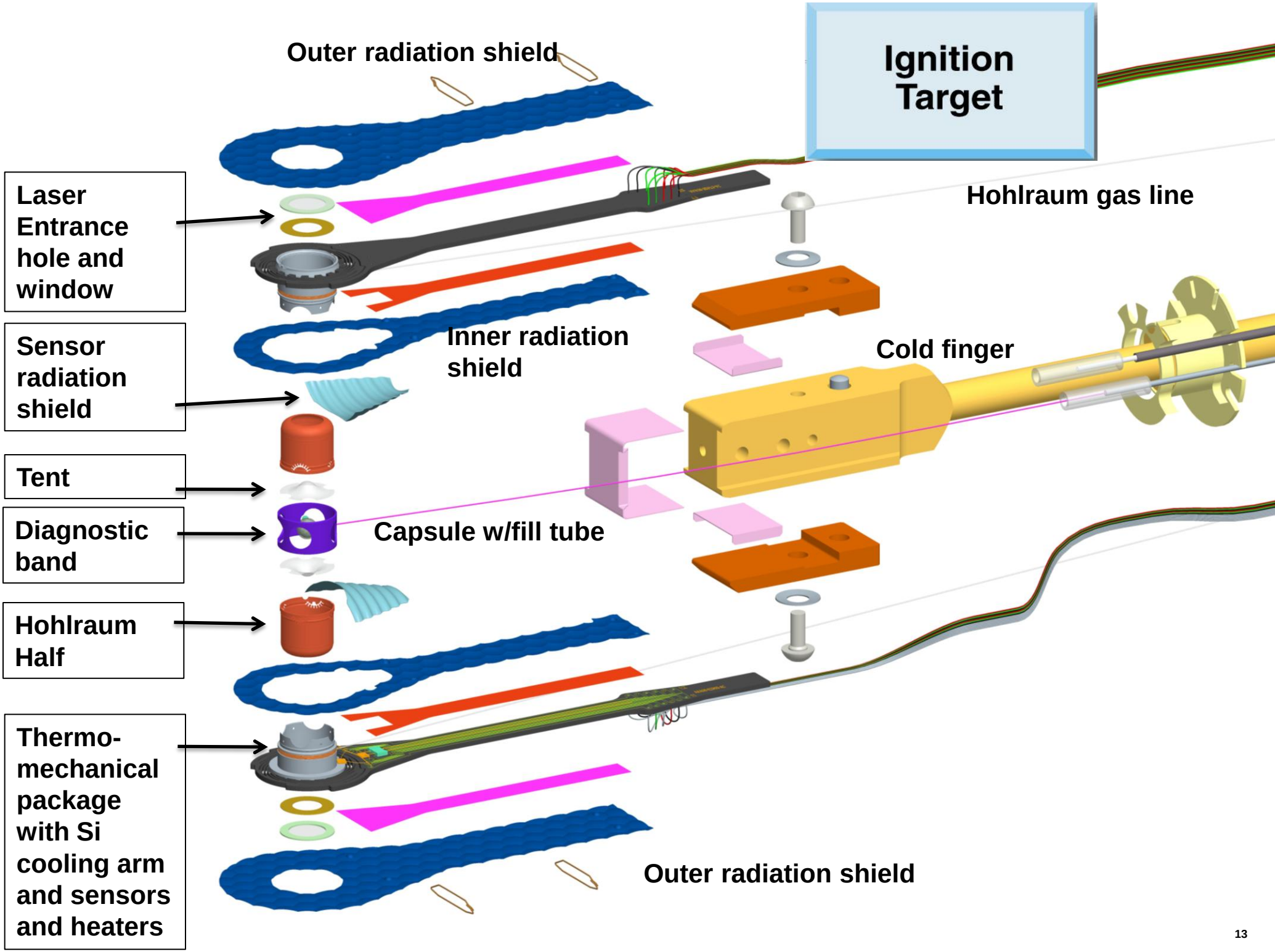
Ignition Target
Outer radiation shield
Laser Entrance hole and window
Sensor radiation shield
Tent
Diagnostic band
Hohlraum Half
Thermo-mechanical package with Si cooling arm and sensors and heaters
Inner radiation shield
Capsule w/fill tube
Hohlraum gas line
Cold finger
Outer radiation shield

CH Rev5

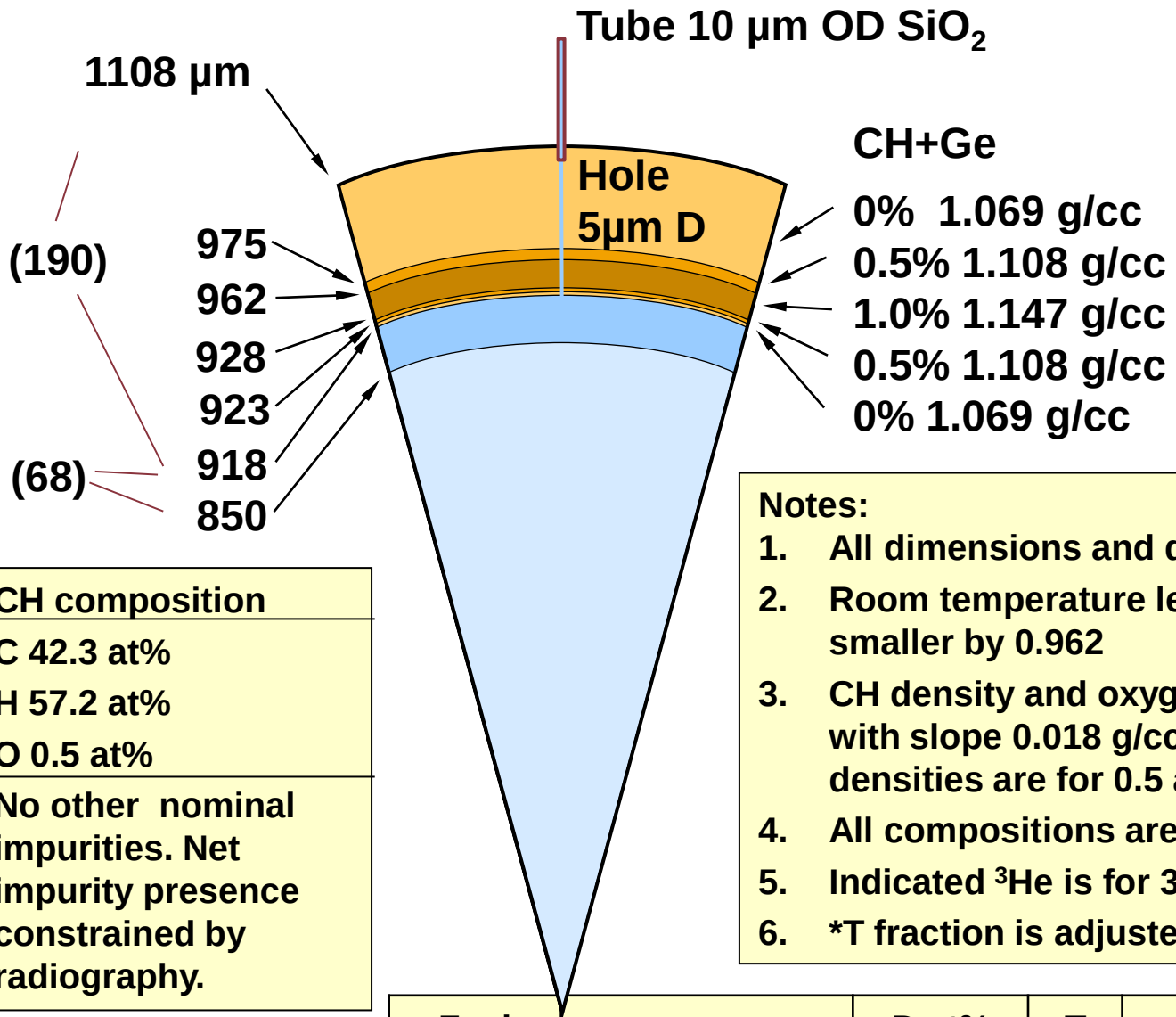

CH composition
C 42.3 at%
H 57.2 at%
O 0.5 at%
No other nominal impurities. Net impurity presence constrained by radiography.

Notes:

1. All dimensions and densities are at cryogenic temp
2. Room temperature lengths bigger by 1.013, densities smaller by 0.962
3. CH density and oxygen fraction are linearly related with slope 0.018 g/cc per at% oxygen. Indicated densities are for 0.5 at% oxygen.
4. All compositions are atom-%
5. Indicated ^{3}He is for 31 hours age
6. *T fraction is adjusted to achieve 100% total atom-%

Fuel	ρ	D at%	T	^{1}H	^{3}He
Solid	0.255 g/cc	50±3	*	0.75±0.25	0.01±0.01
Gas	0.3 mg/cc	60±3	*	1.0±0.25	$1.0^{+0.2}_{-1.0}$

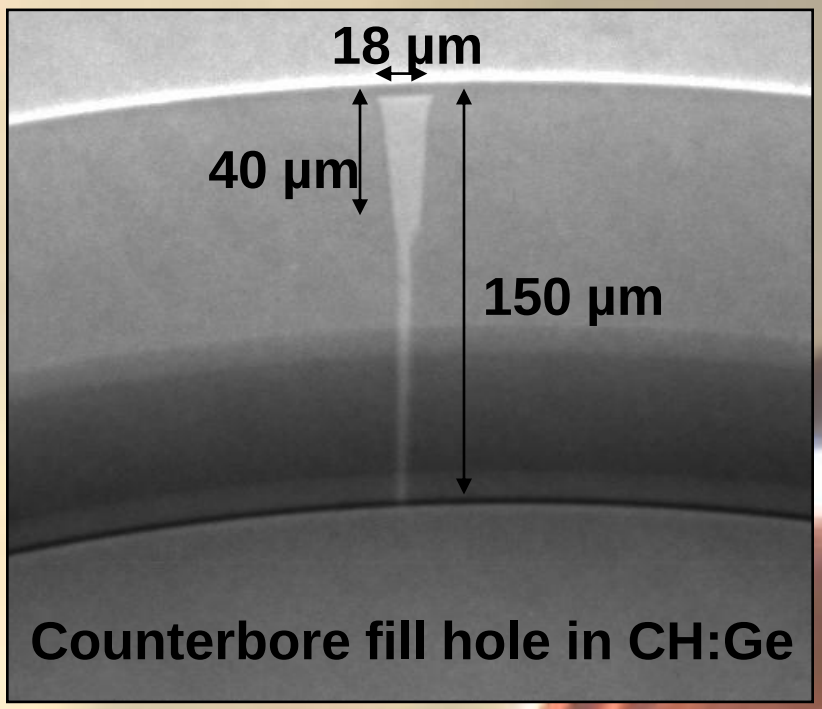

~ 2 mm diameter

Ignition design CH shells have been developed that meet NIF specifications

Target fabrication issue: defects on mandrels will grow into “domes” which affect mix mass

- GDP coating is omni-directional
- Can predict dome size from seed size

$$w = \left(h(2t - h)\right)^{1/2} + s_w / 2$$

- Height is unchanged
- Tested by using seeds of known size

Defect of initial height h & width 2w

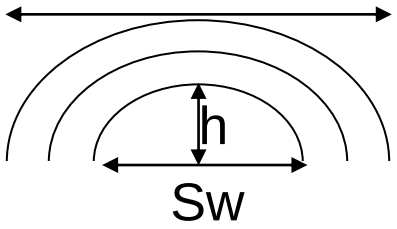

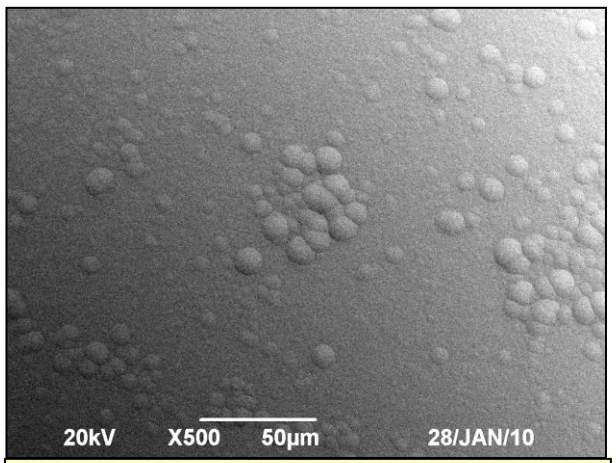

SEM of “isolated” defects

1 um spherical seed after 200 um coating:
~ 40 um wide, 1 um tall dome , 150 ng of mix mass

Surface quality of CH capsule has greatly improved with new finishing techniques

As-deposited CH Capsule

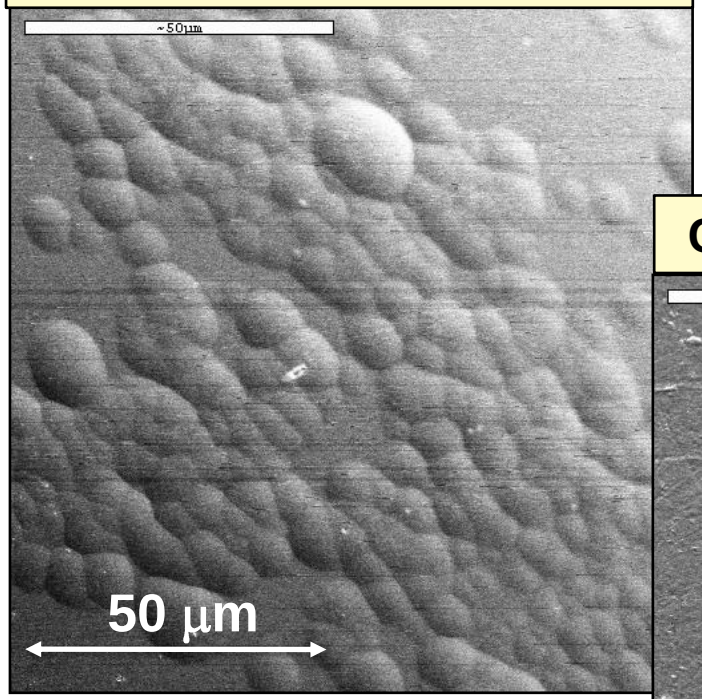

Conventional Polish (2009)

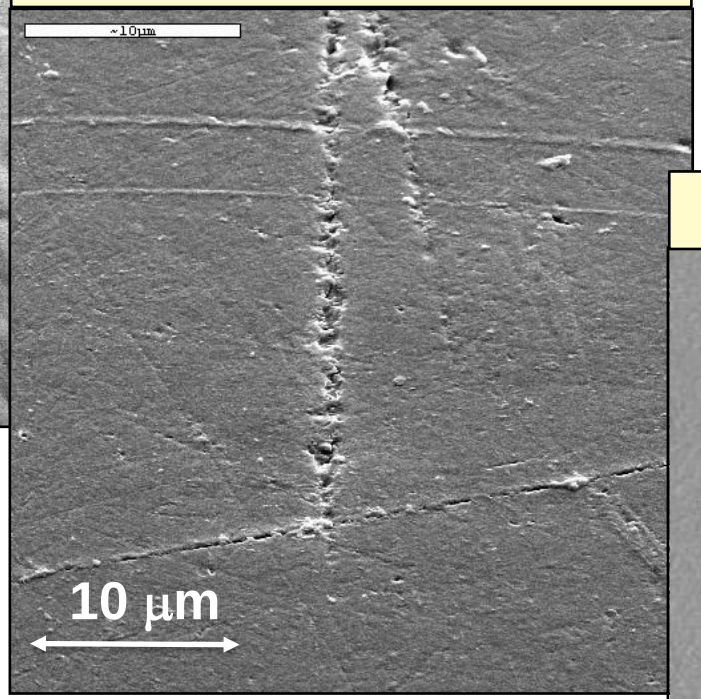

Advanced Finishing (2010)

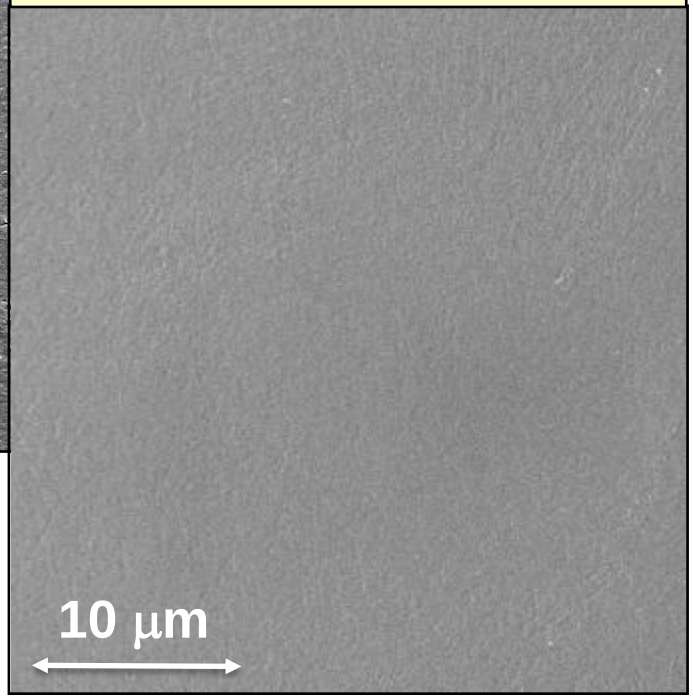

Mid-modes (10-100) still meet specification after polishing measured by atomic force microscopy

Unpolished Capsule 10CH89-02

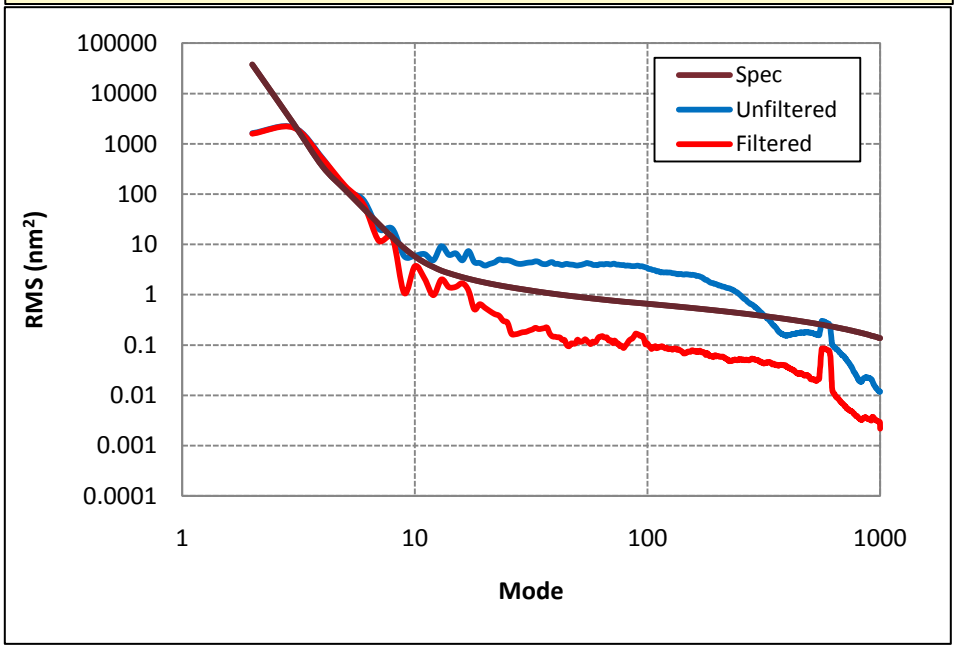

Polished Capsule 10CH89-02P

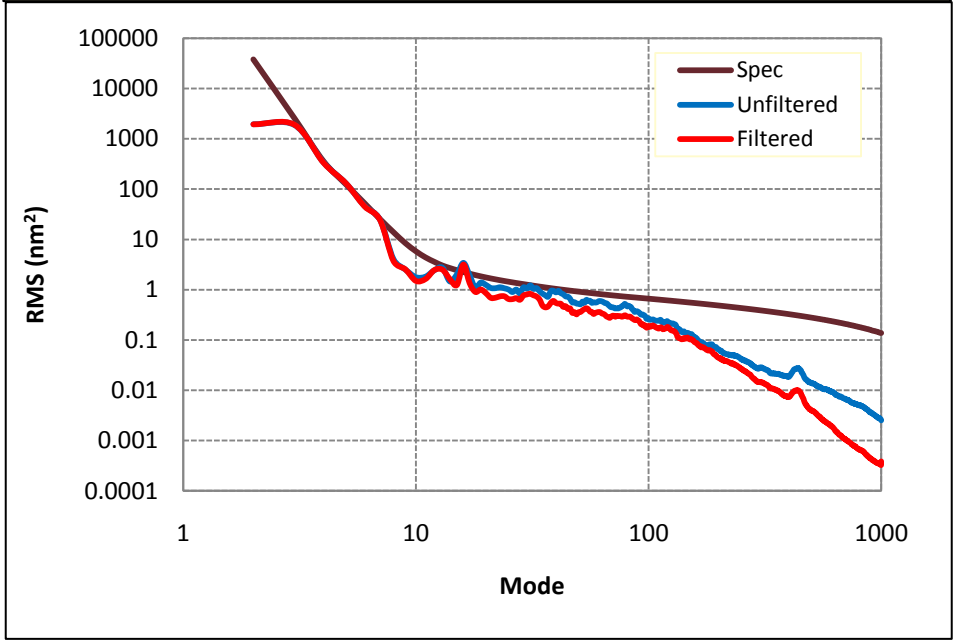

We are working on reducing polishing induced mid-mode roughness

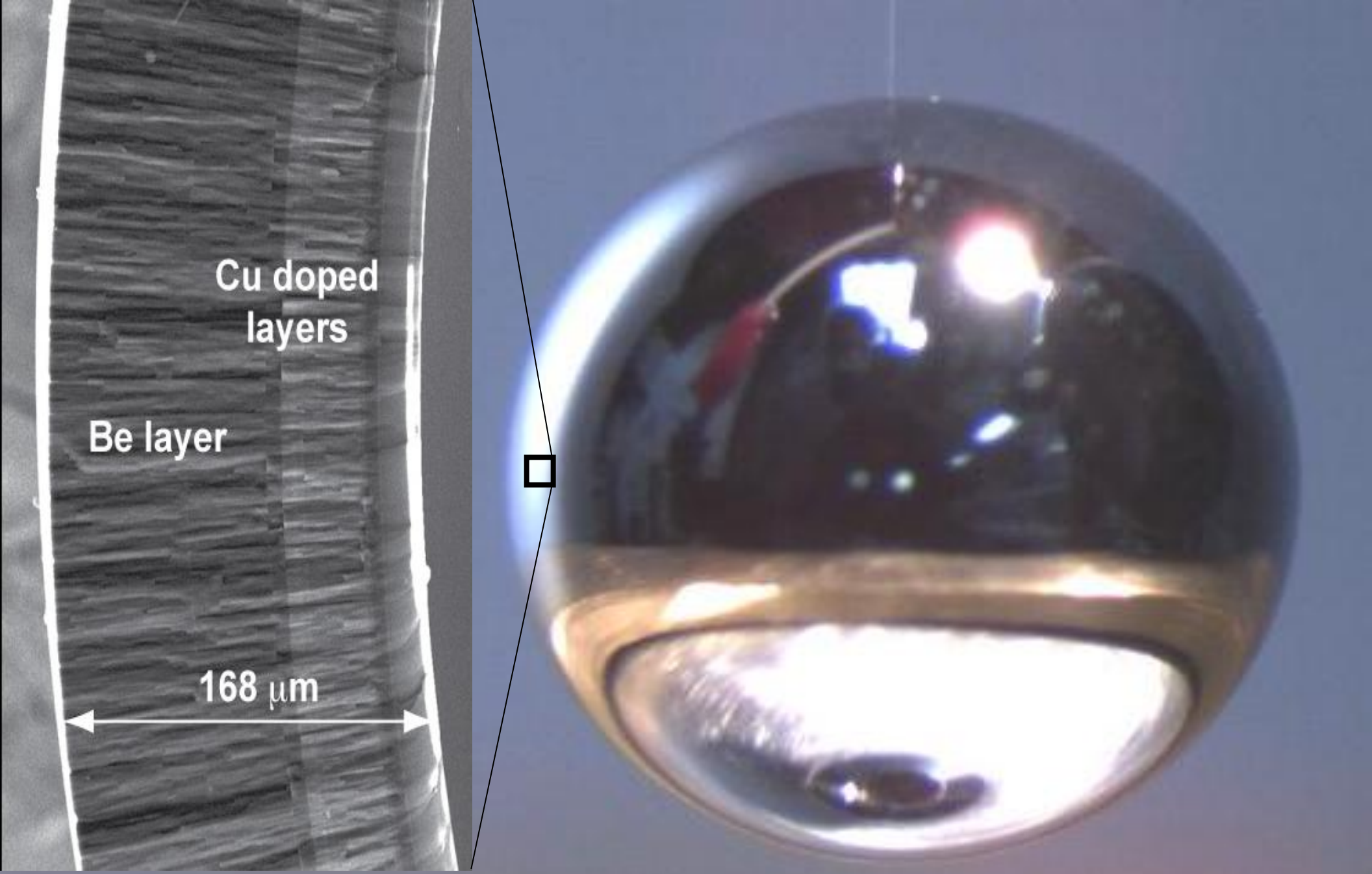
Cu doped
layers
Be layer
168 μm
2mm

Using ion assisted deposition we have improved the microstructure of the Be shells

Transmission electron micrograph of twisted structure/ leaky shells ca 2005

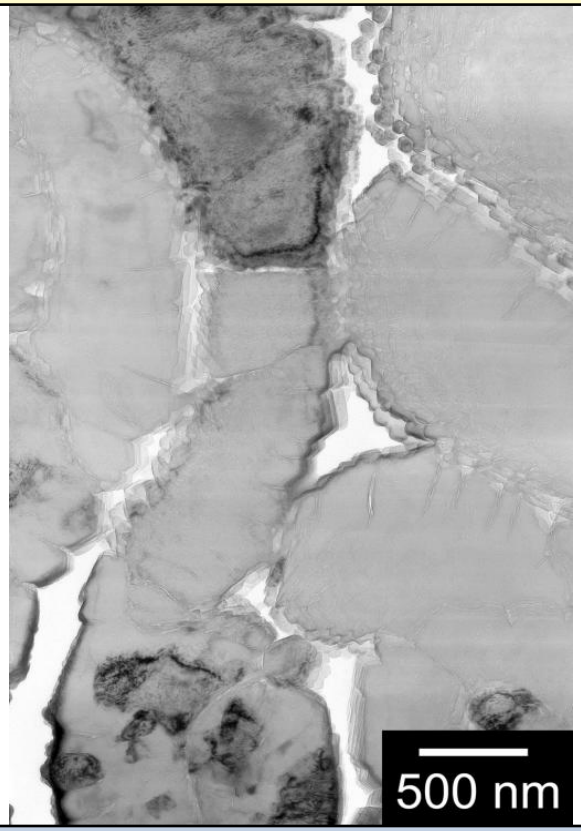

Maximum void size ~10 μm

— Volume > 1 μm^3

Transmission electron micrograph of high density/gas retentive shell

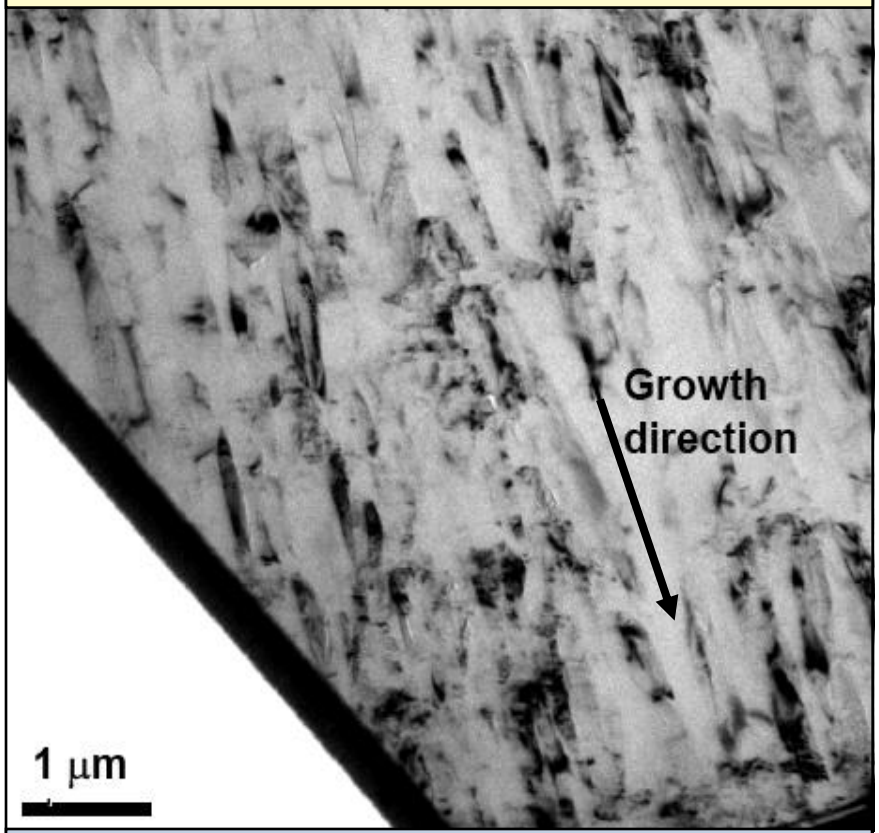

Maximum void size ~200nm

— Volume < 0.04 μm^3

Effect of ion-assist on morphology of sputter deposited Be

No bias

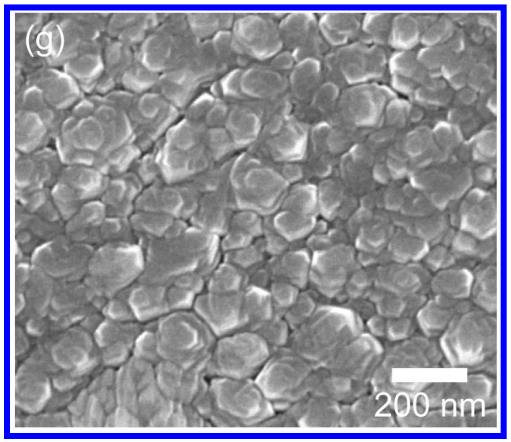

(002) basal texture

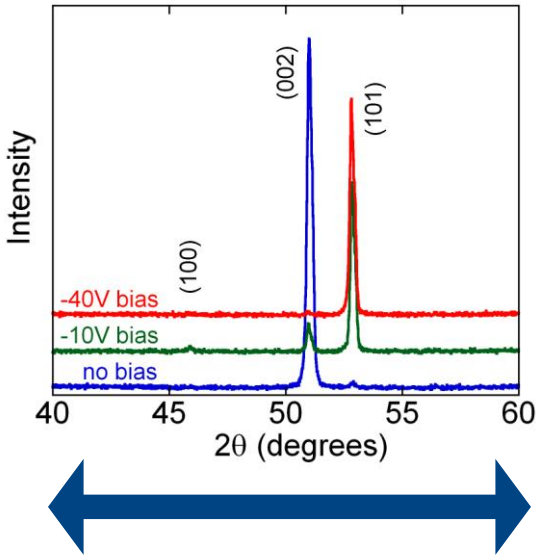

40V bias

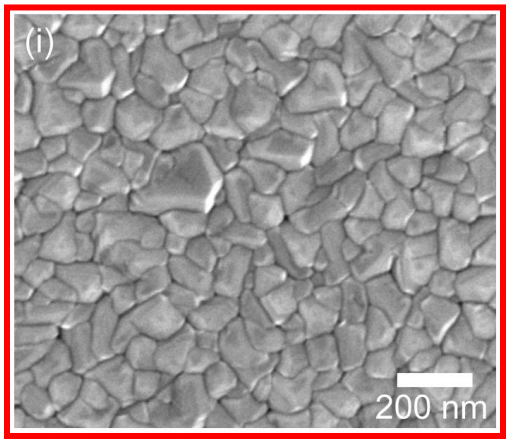

(101) texture

Ion-assist in sputtered beryllium leads to a texture transition

Simulations indicate the lower Ehrlich-Schwoebel barrier on the (101) texture leads to denser microstructure and smoother surface

Effect of the Ehrlich-Schwoebel barrier

Large ES barrier leads to 3D growth and porosity

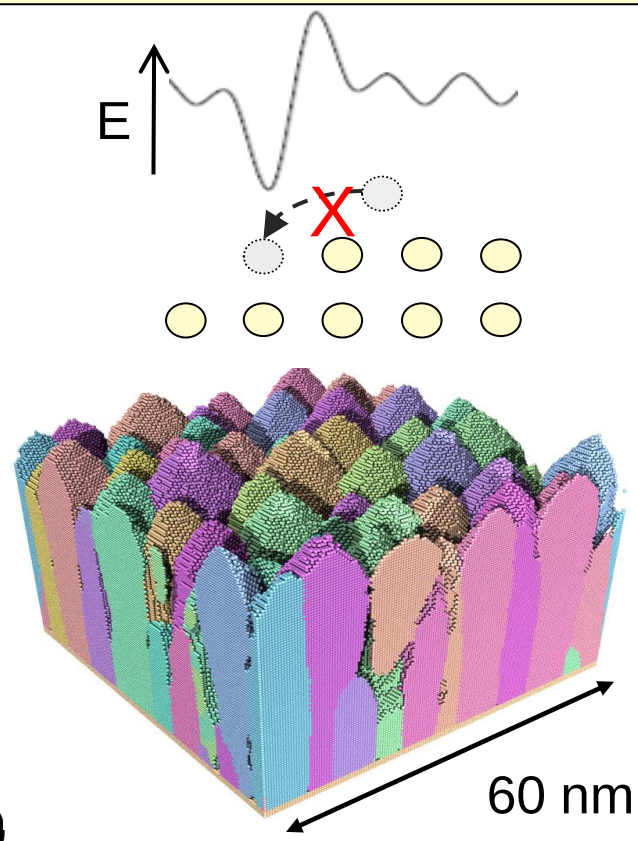

(0002) texture

ΔE_{ES} = 0.25 eV

Small ES barrier leads to 2D step flow and higher density

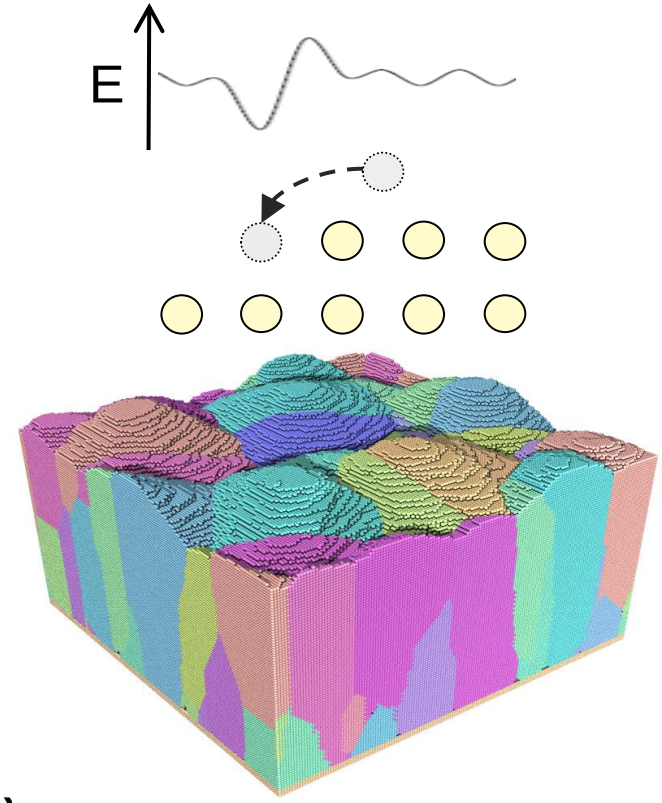

(1011) texture

ΔE_{ES} ~ 0.06 - 0.09 eV

The size of the Ehrlich-Schwoebel (ES) controls the growth mode (2D step flow versus 3D)

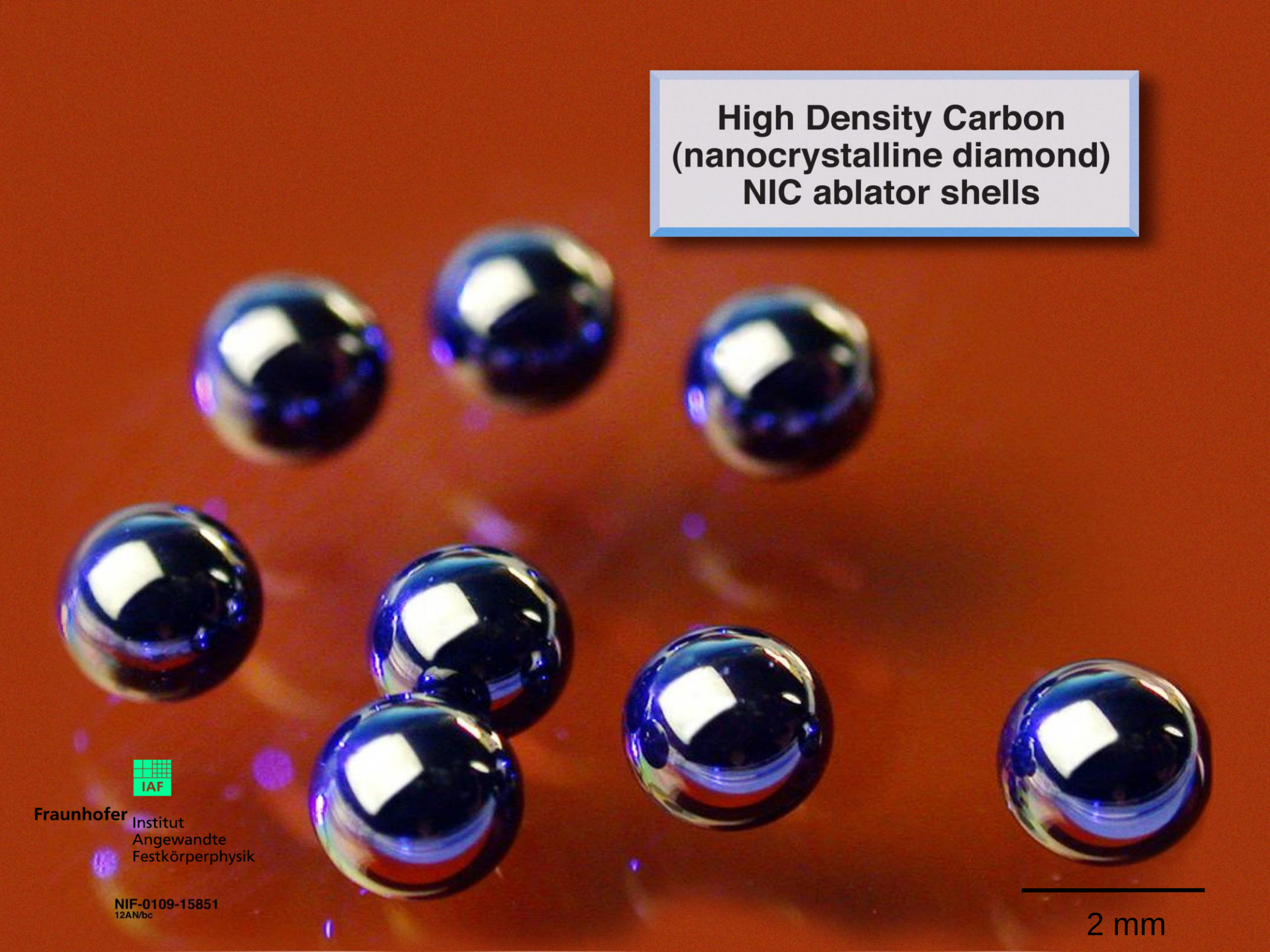
High Density Carbon
(nanocrystalline diamond)
NIC ablator shells
IAF
Fraunhofer
Institut
Angewandte
Festkörperphysik
NIF-0109-15851
12AN/bc
2 mm

HDC inner and outer surface finish

White light interferometry of HDC capsule inner surface

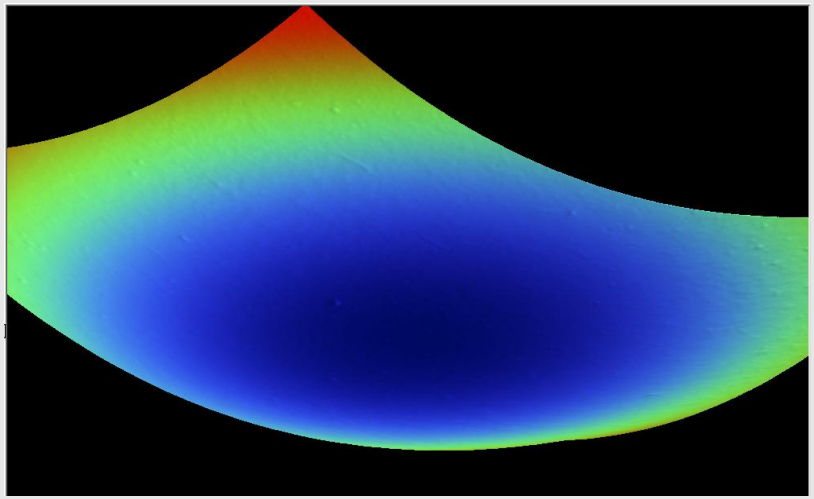

< 5 nm colloidial diamond seed particles lead to 3 nm rms inner surface roughness

Power spectrum for HDC capsule outer surface from atomic force sphere mapping

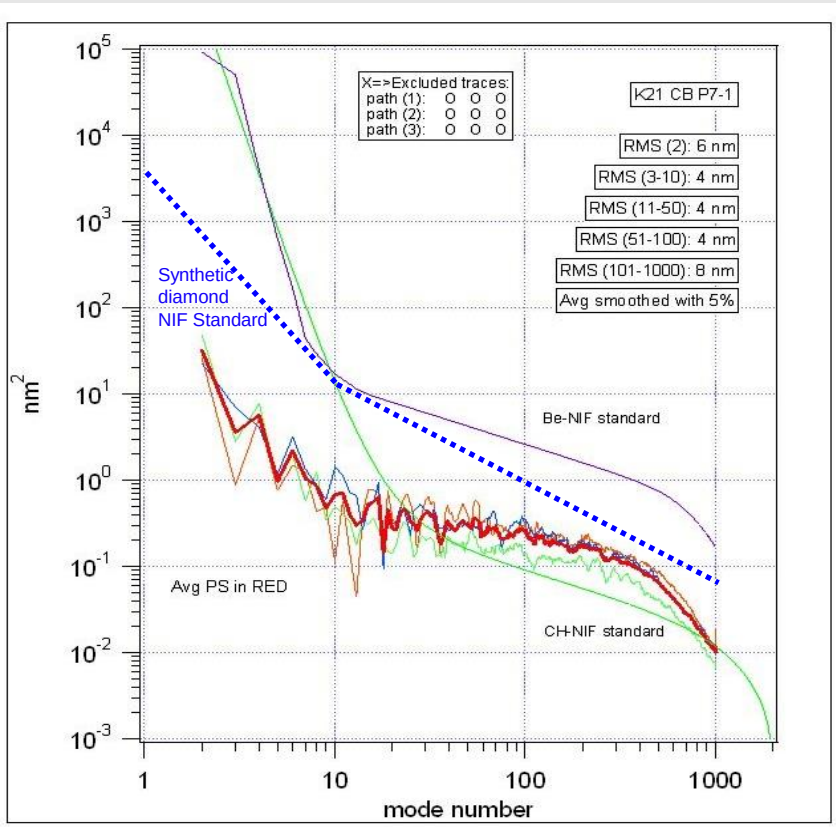

Forming layers of solid hydrogen

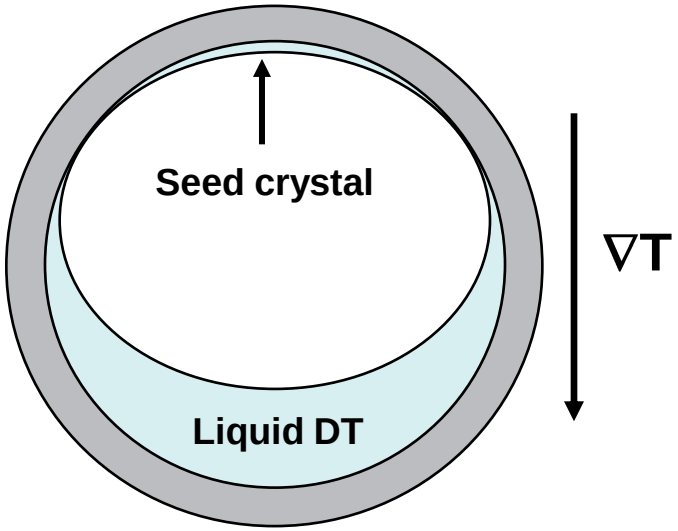

Liquid self heating provides thermal gradient during formation that helps limit rate of solid growth

The power generated by the DT divided by the heat of sublimation gives a natural time constant

T ~ 1500 J/mole/(0.977 watts/mole) = 25.6 min

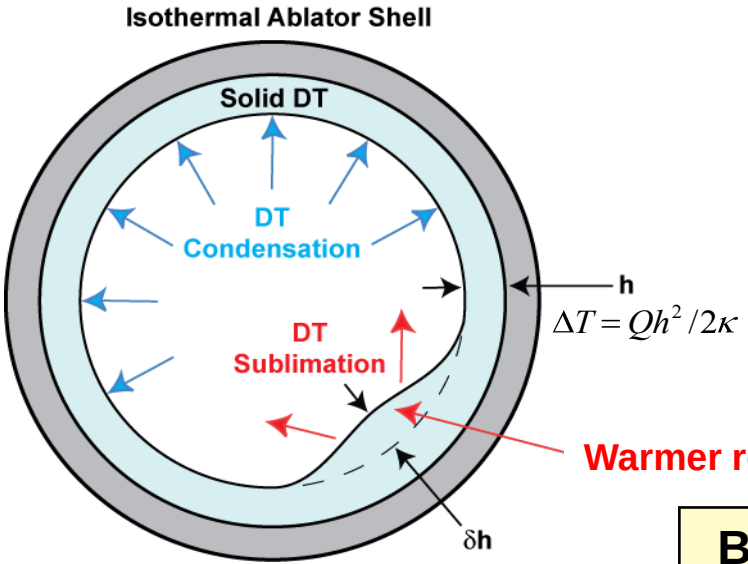

Beta-layering* reduces the bump height as DT sublimes from the warmer region (due to beta-decay of tritium) and condenses on colder surfaces

** J. K. Hoffer and L. R. Foreman, PRL 60, 1310 (1988)*

Beta-layering helps produce a spherical shape, but does not smooth small-scale roughness

Key DT fuel layer specifications

Low Modes

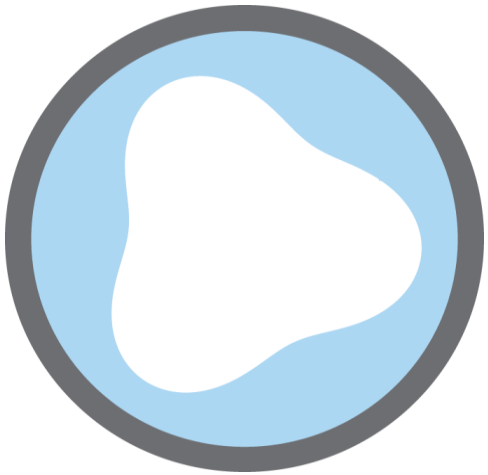

Hohlraum Thermal Eng

High Modes

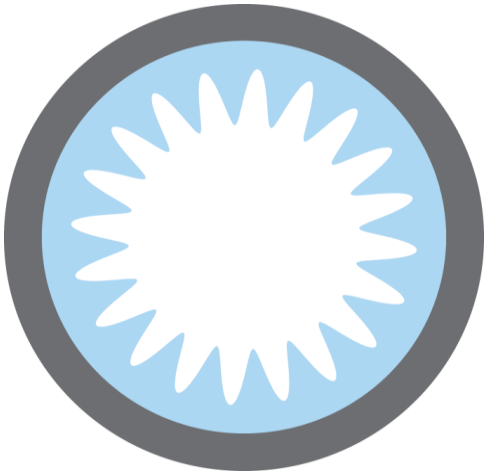

Beta Layering

Local Defects

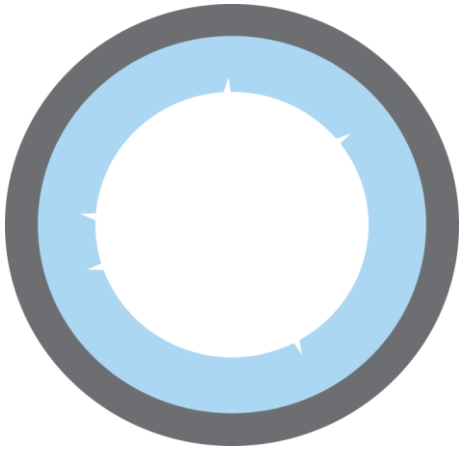

Target Fab Issue

NIF Power Reqmt (1D)

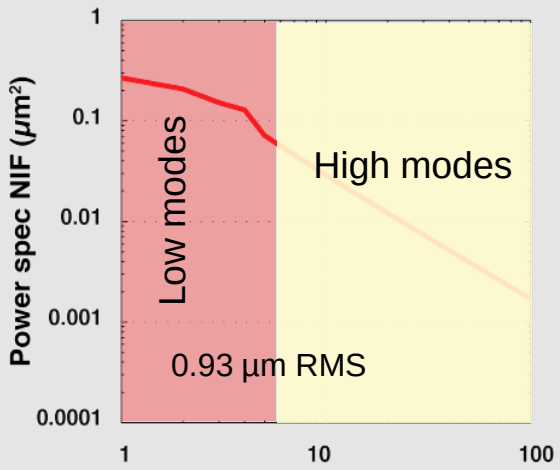

NIF Power Reqmt (1D)

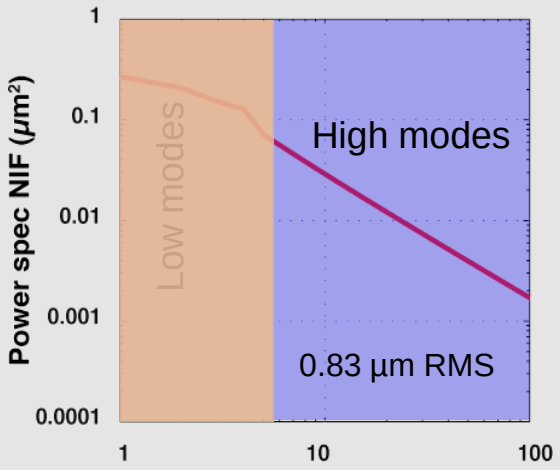

Groove Area and Length

K < 0.7 μm
where

$$K = \sqrt{\frac{1}{V_{fuel}} \sum_{j=1}^{n} A_j^2 \, L_j}$$

And
Max groove area < 200 μm²

The main source of roughness in high quality layers is grooves between low angle grain boundaries

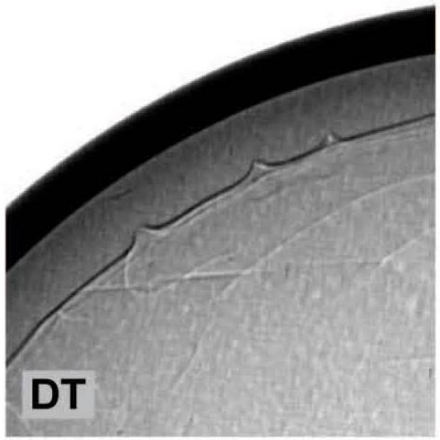

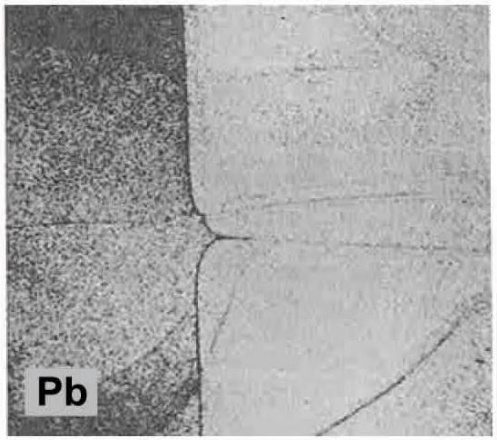

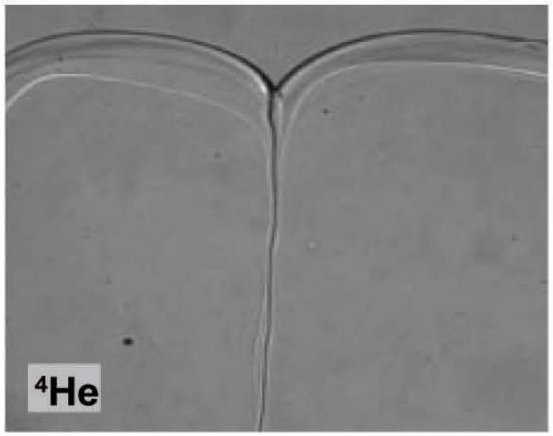

Thermal grooving at grain boundaries is a common phenomenon in materials science

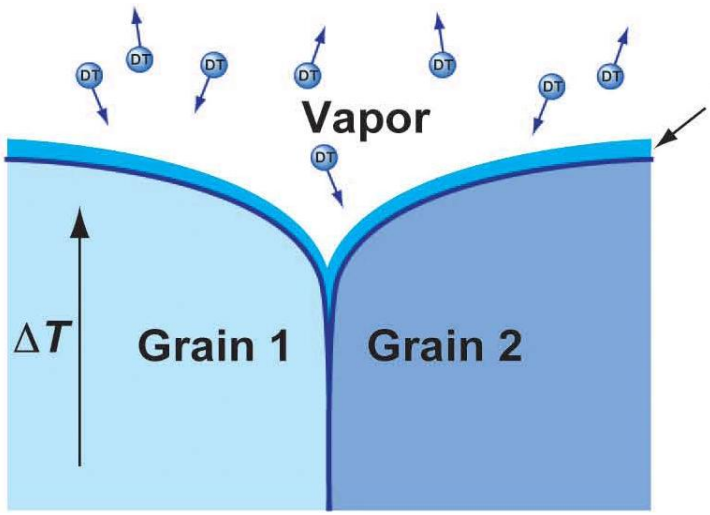

Transport mechanisms:

- **Evaporation/condensation**
- **Surface diffusion**
- **Grain boundary diffusion**
- **Bulk diffusion**

Thermal gradient provided by the tritium makes the grooves stationary.

The main source of high mode roughness in high quality layers is grooves between low angle grain boundaries

Orthogonal optical and x-ray images

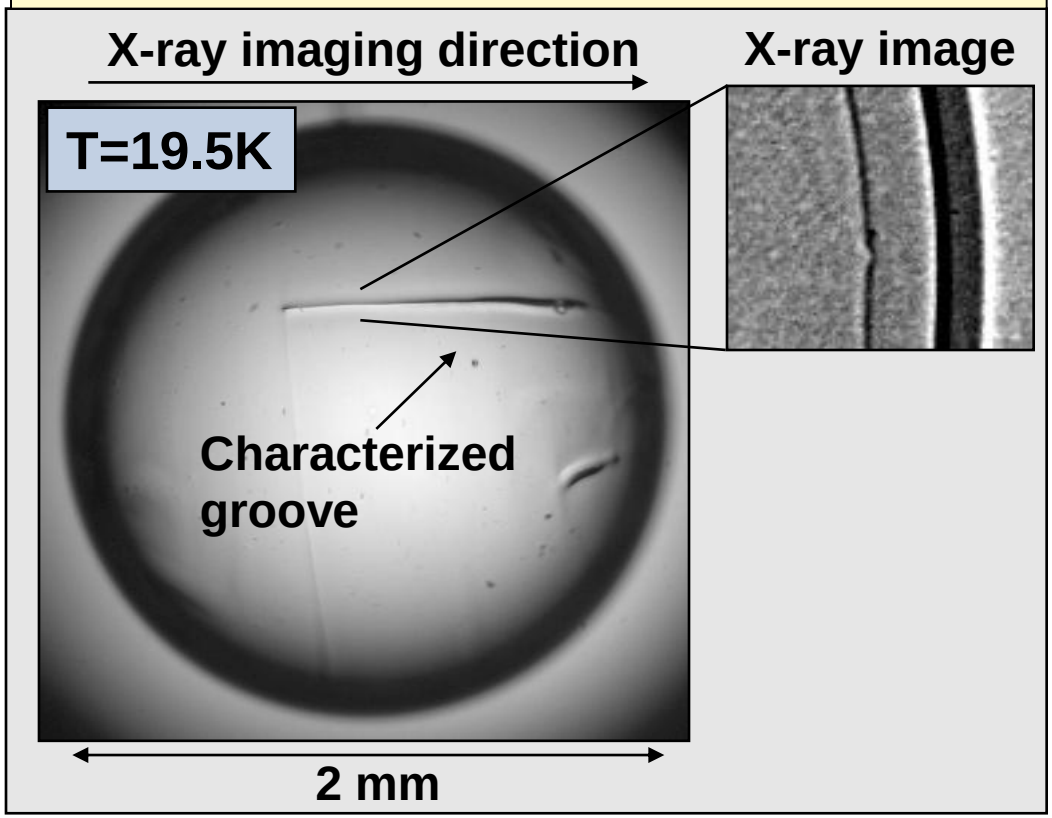

Measured Profiles

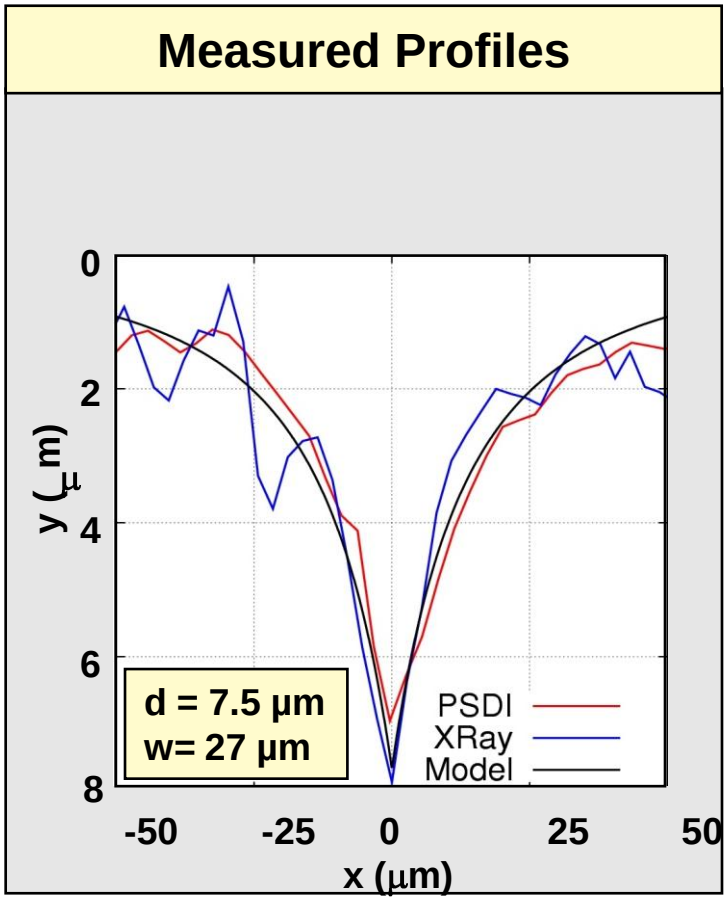

Local defects are vapor-etched grooves formed at small-angle grain-boundaries

Formation of grain boundary grooves is a common phenomenon in crystalline materials

High quality DT layers are formed by single crystal growth

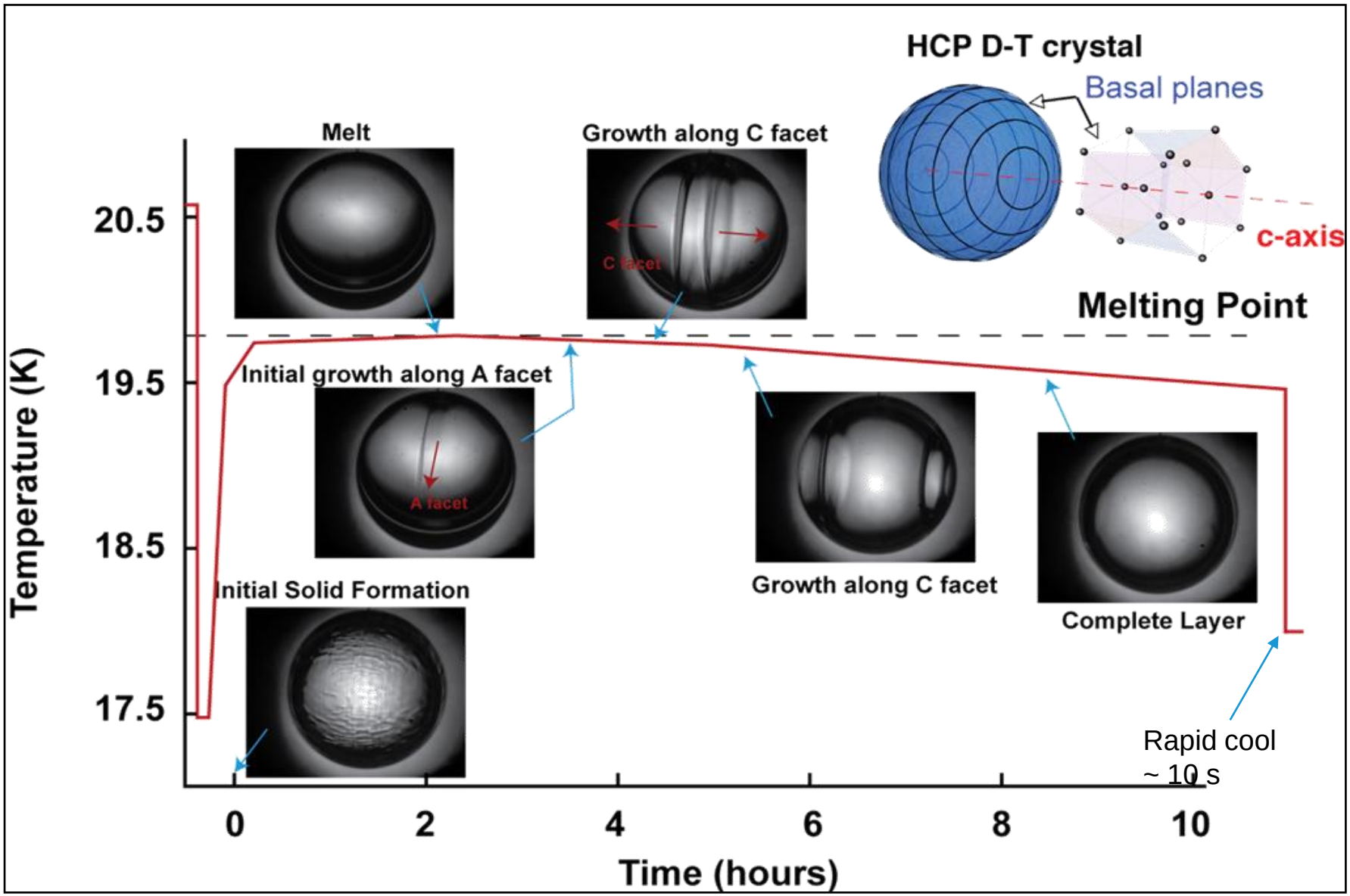

Layer produced in spherical hohlraum, vertical fill-tube. C-axis in the plane of the image

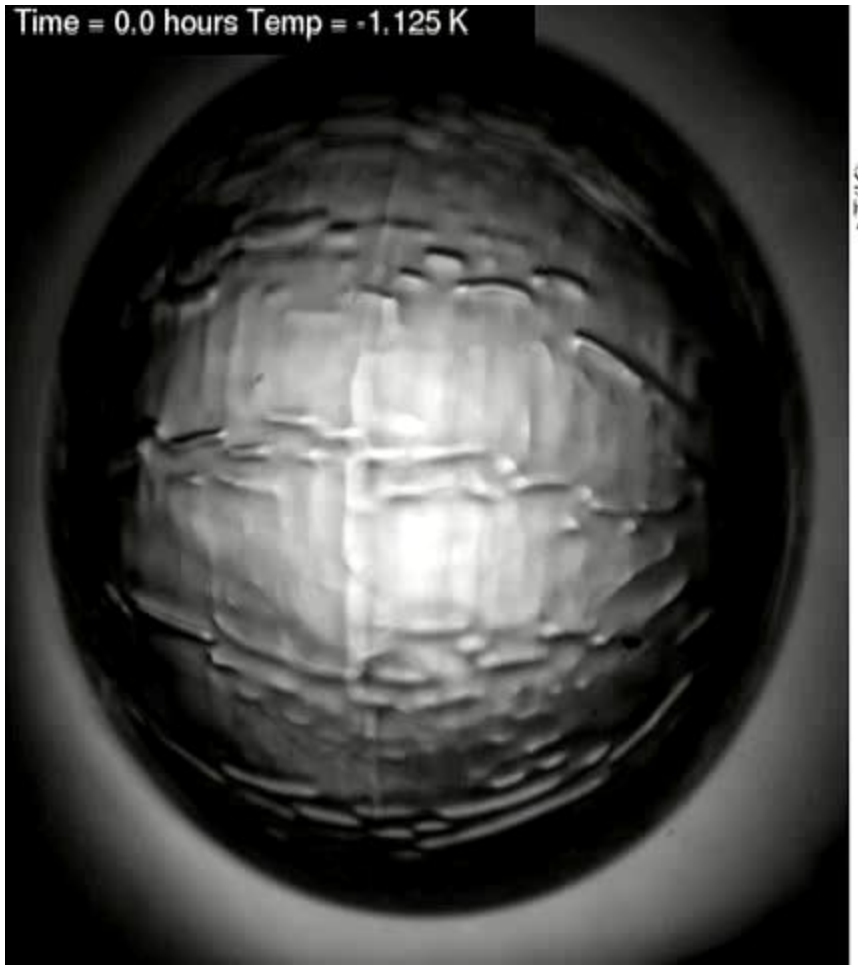

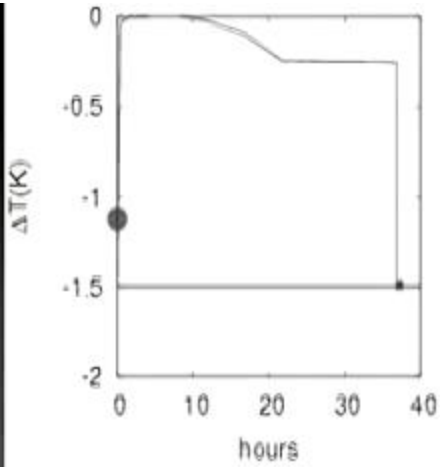

Layering-FastCool-092907-S

First ice layer in a THD target meeting all measureable ice specifications

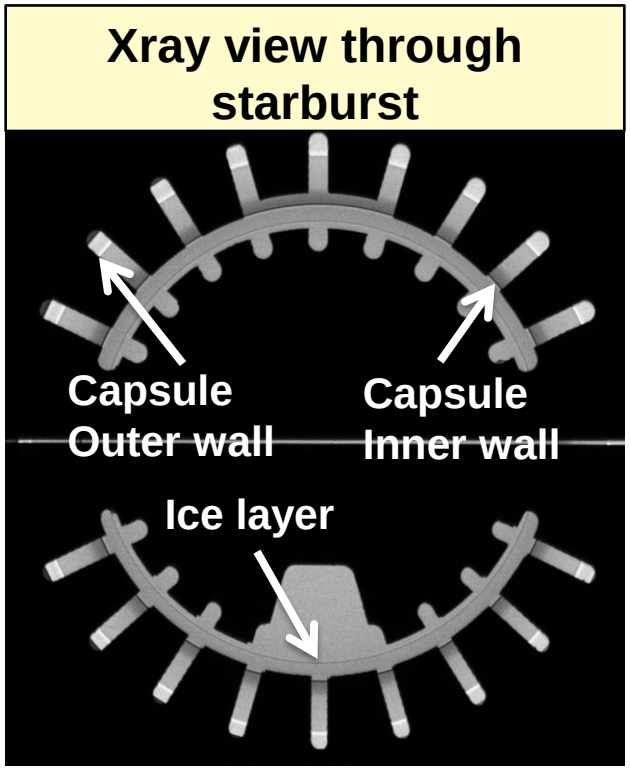

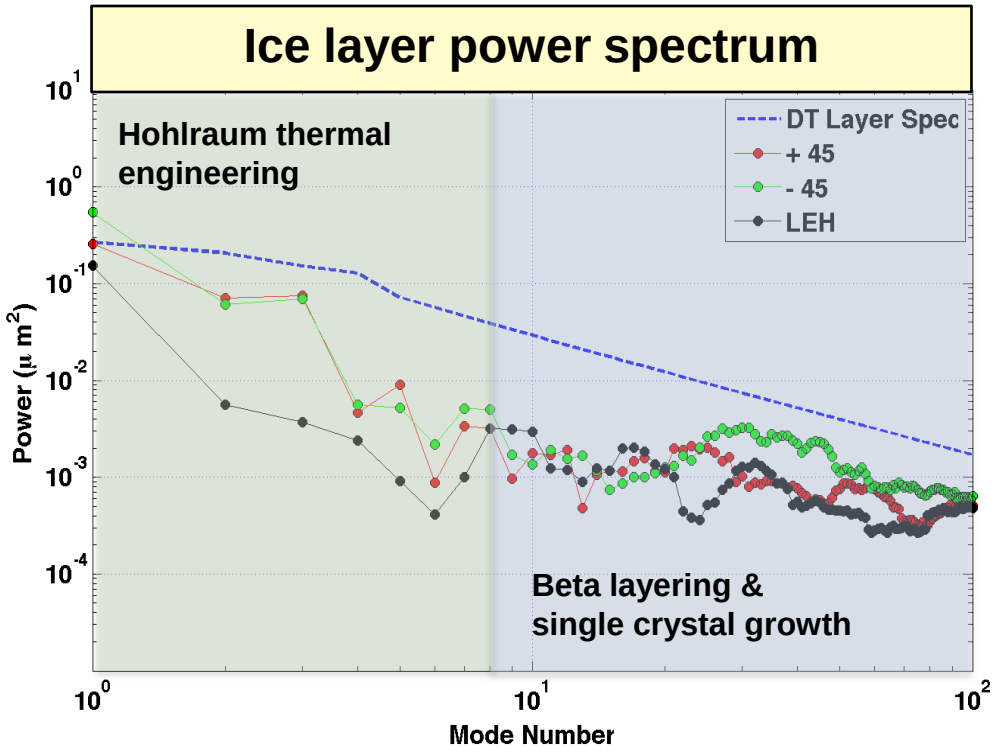

Low Mode Sum – Spec = 0.93 μm		High Mode Sum – Spec = 0.83 μm
+ 45	0.65	0.31
- 45	0.83	0.39
LEH	0.41	0.28

Acceptable layer yield 30%

New Scientific Capabilities Are Required to Meet the Challenges of Fast Ignition Capsules

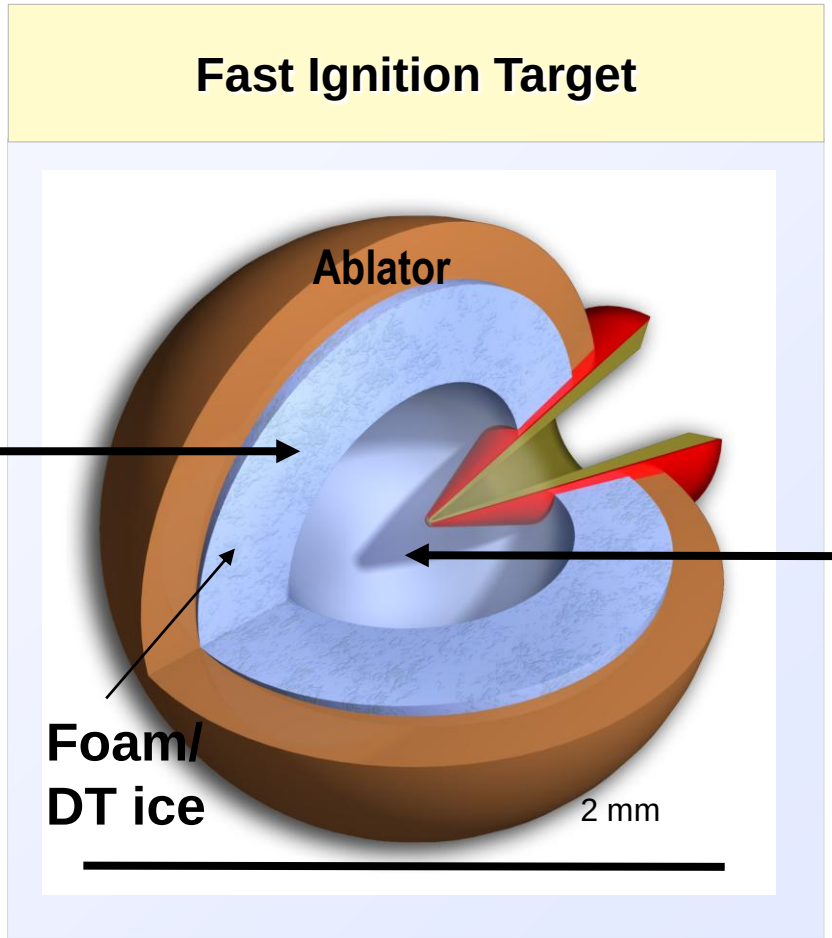

New Challenge

- **Low density, open cell, hydrocarbon foam shell, robust enough to handle wetting by hydrogen**

Our Natural Starting Point is Sol-Gel Chemistry

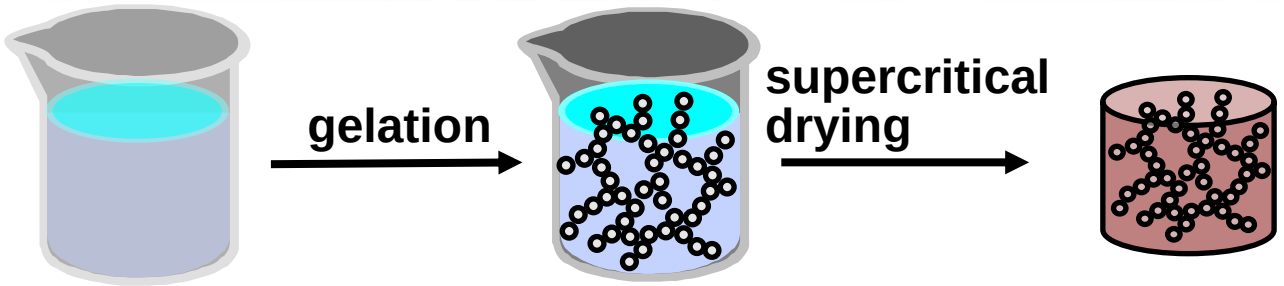

Solution Wet Gel Aerogel

1 H Hydrogen 1.00794																	2 He Helium 4.003
3 Li Lithium 6.941	4 Be Beryllium 9.012182											5 B Boron 10.811	6 C Carbon 12.0107	7 N Nitrogen 14.00674	8 O Oxygen 15.9994	9 F Fluorine 18.9984032	10 Ne Neon 20.1797
11 Na Sodium 22.989770	12 Mg Magnesium 24.3050											13 Al Aluminum 26.981538	14 Si Silicon 28.0855	15 P Phosphorus 30.973761	16 S Sulfur 32.066	17 Cl Chlorine 35.4527	18 Ar Argon 39.948
19 K Potassium 39.0983	20 Ca Calcium 40.078	21 Sc Scandium 44.955910	22 Ti Titanium 47.867	23 V Vanadium 50.9415	24 Cr Chromium 51.9961	25 Mn Manganese 54.938049	26 Fe Iron 55.845	27 Co Cobalt 58.933200	28 Ni Nickel 58.6934	29 Cu Copper 63.546	30 Zn Zinc 65.39	31 Ga Gallium 69.723	32 Ge Germanium 72.61	33 As Arsenic 74.92160	34 Se Selenium 78.96	35 Br Bromine 79.904	36 Kr Krypton 83.80
37 Rb Rubidium 85.4678	38 Sr Strontium 87.62	39 Y Yttrium 88.90585	40 Zr Zirconium 91.224	41 Nb Niobium 92.90638	42 Mo Molybdenum 95.94	43 Tc Technetium (98)	44 Ru Ruthenium 101.07	45 Rh Rhodium 102.90550	46 Pd Palladium 106.42	47 Ag Silver 107.8682	48 Cd Cadmium 112.411	49 In Indium 114.818	50 Sn Tin 118.710	51 Sb Antimony 121.760	52 Te Tellurium 127.60	53 I Iodine 126.90447	54 Xe Xenon 131.29
55 Cs Cesium 132.90545	56 Ba Barium 137.327	57 La Lanthanum 138.9055	72 Hf Hafnium 178.49	73 Ta Tantalum 180.9479	74 W Tungsten 183.84	75 Re Rhenium 186.207	76 Os Osmium 190.23	77 Ir Iridium 192.217	78 Pt Platinum 195.078	79 Au Gold 196.96655	80 Hg Mercury 200.59	81 Tl Thallium 204.3833	82 Pb Lead 207.2	83 Bi Bismuth 208.98038	84 Po Polonium (209)	85 At Astatine (210)	86 Rn Radon (222)
87 Fr Francium (223)	88 Ra Radium (226)	89 Ac Actinium (227)	104 Rf Rutherfordium (261)	105 Db Dubnium (262)	106 Sg Seaborgium (263)	107 Bh Bohrium (262)	108 Hs Hassium (265)	109 Mt Meitnerium (266)	110 (269)	111 (272)	112 (277)	113	114				

58 Ce Cerium 140.116	59 Pr Praseodymium 140.90765	60 Nd Neodymium 144.24	61 Pm Promethium (145)	62 Sm Samarium 150.36	63 Eu Europium 151.964	64 Gd Gadolinium 157.25	65 Tb Terbium 158.92534	66 Dy Dysprosium 162.50	67 Ho Holmium 164.93032	68 Er Erbium 167.26	69 Tm Thulium 168.93421	70 Yb Ytterbium 173.04	71 Lu Lutetium 174.967
90 Th Thorium 232.0381	91 Pa Protactinium 231.03588	92 U Uranium 238.0289	93 Np Neptunium (237)	94 Pu Plutonium (244)	95 Am Americium (243)	96 Cm Curium (247)	97 Bk Berkelium (247)	98 Cf Californium (251)	99 Es Einsteinium (252)	100 Fm Fermium (257)	101 Md Mendelevium (258)	102 No Nobelium (259)	103 Lr Lawrencium (262)

= Multi-component compositions

= Monolithic compositions prepared

= Organic compositions

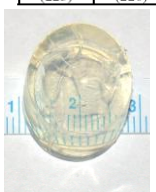

ZrO_2

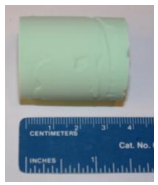

NiO

Lanthanide

SnO_2

Nb_2O_5

WO_3

Aerogels are open cell, low density materials

Chemistry-in-a-capsule

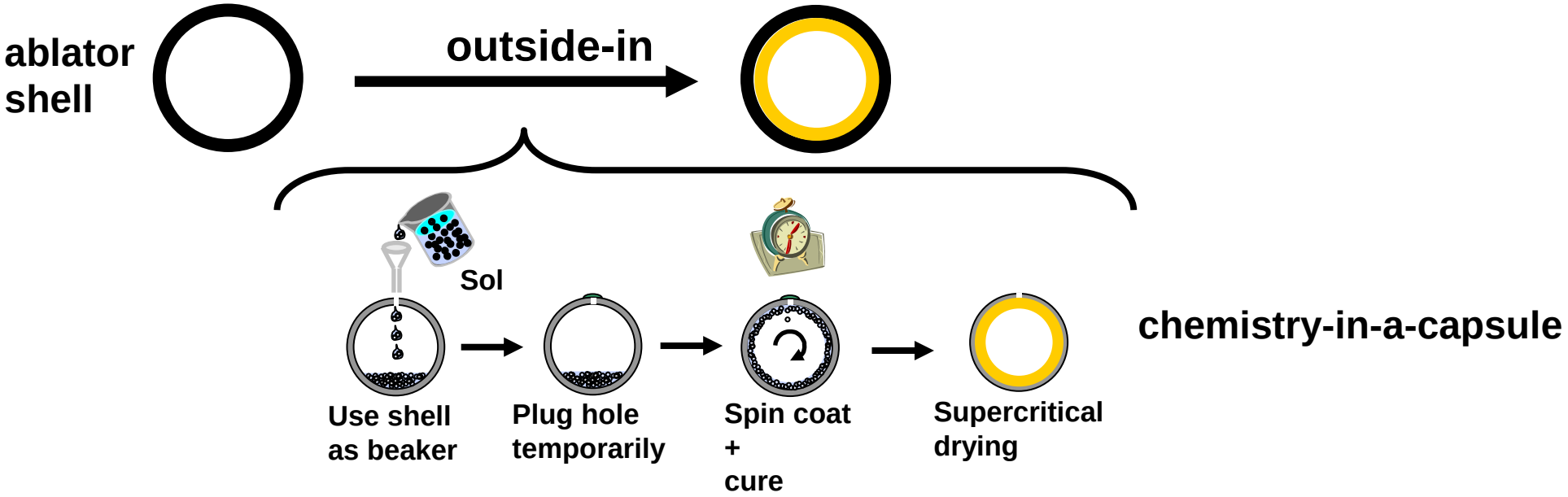

challenges	Effect/problem	solution
Picoliter volumes	*Gibbs–Thomson* effect	Ionic solvents, microfluidics
Mechanical robust and defect free aerogel liner	Shrinkage can induce cracking Aerogel must survive hydrogen wetting	Develop new aerogels
Uniform layer/wetting	Viscoelastic properties at sol-gel transition	Tune aerogel chemistry
Controlled gel time	Catalyst deactivation by surface groups	Surface engineering

Picoliter delivery of aerogel precursor solution

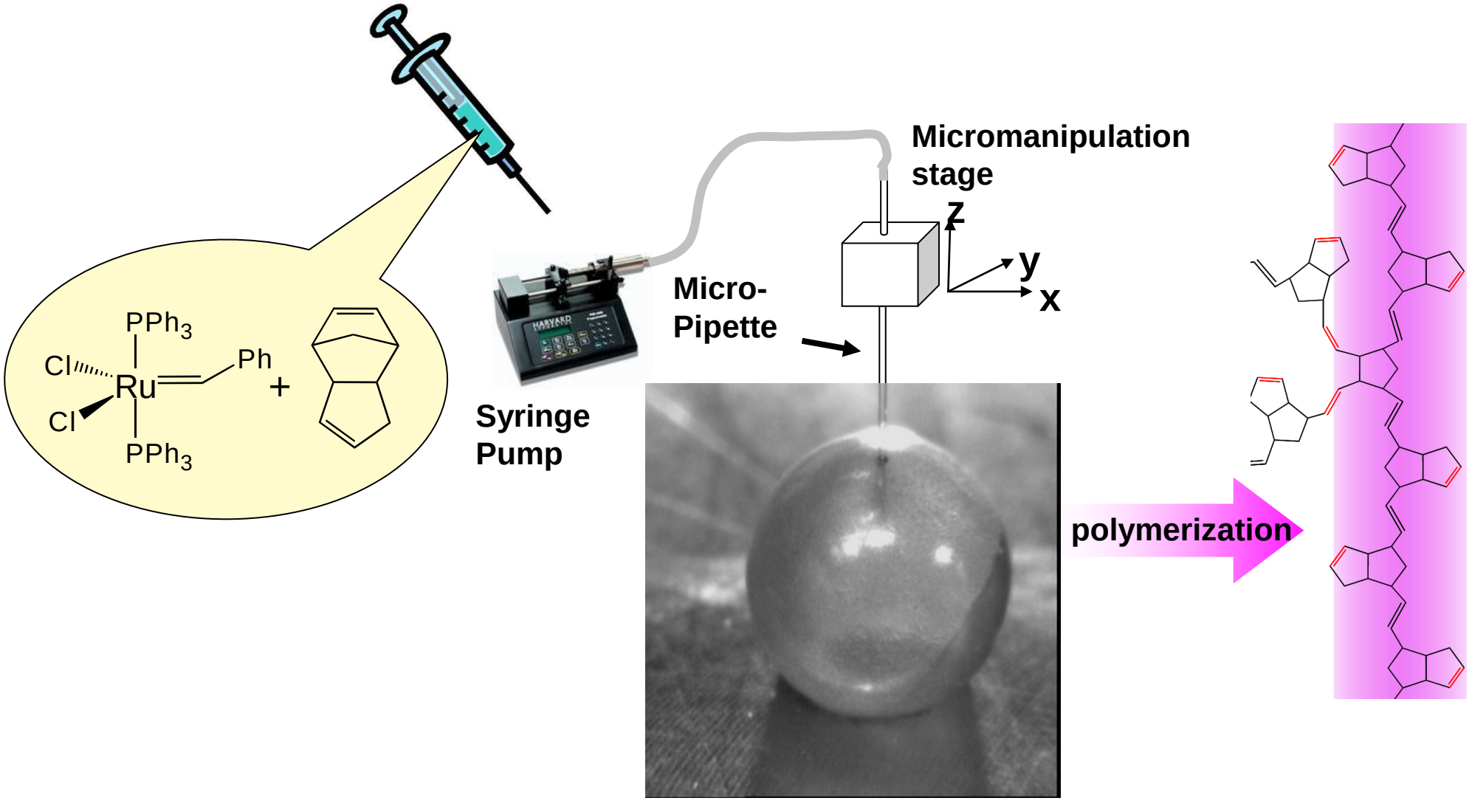

Developed new non-shrinkage low-Z aerogel

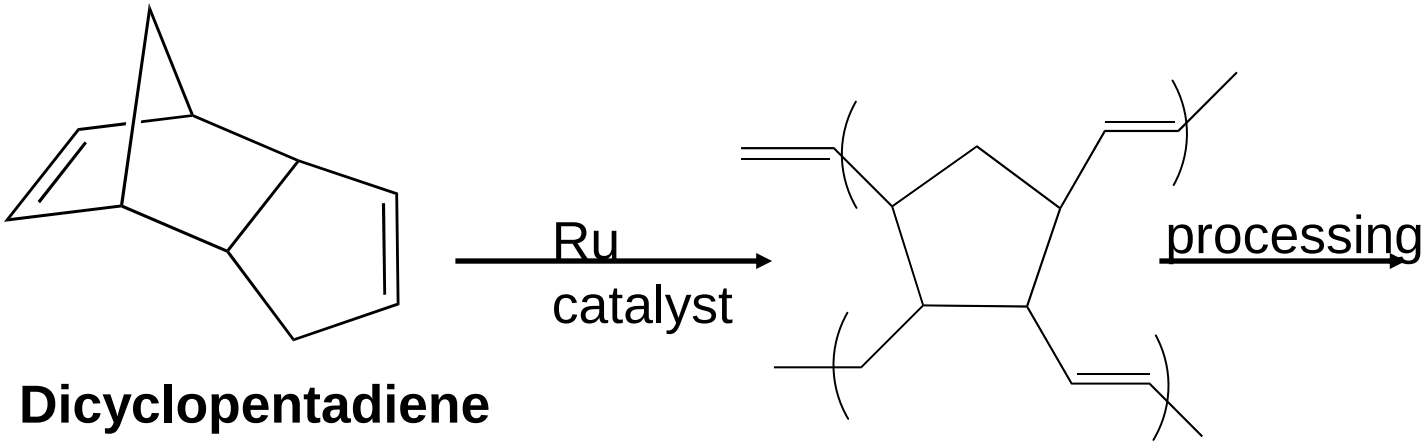

Dicyclopentadiene (DCPD) monomer

DCPD crosslinked polymer network

Image of 200 mg/cc DCPD aerogel

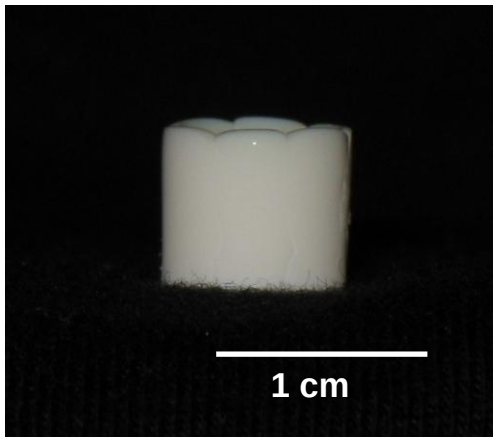

- **density range: 30-300 mg/cc**
- **surface area: 200- 400 m^2/g**
- **pore size: 20-30 nm**

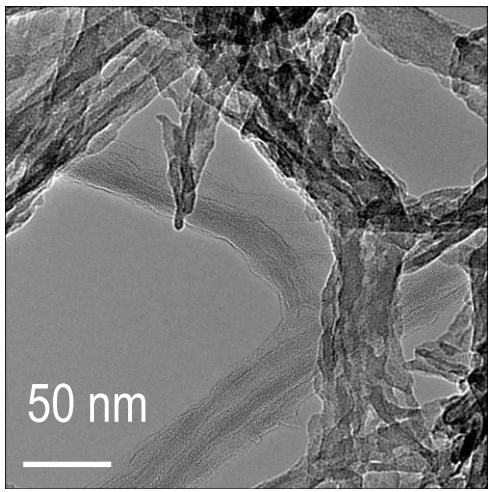

TEM Image of 30 mg/cc DCPD aerogel

Aerogels in Liquid & Solid Hydrogen

Slowly freezing: transparent ice with irregular bubble (~12K). (~8K: cracking throughout ice)

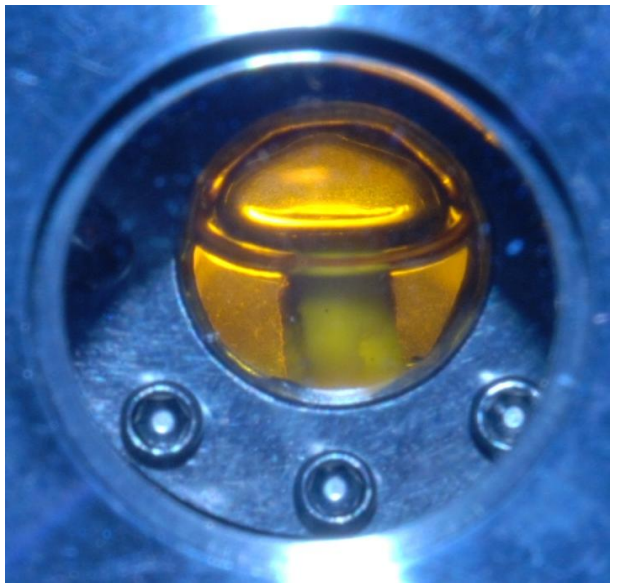

No visual evidence of cracking observed

Synthesis of ultra-low density low-Z aerogels inside a capsule

Radiograph of a capsule completely filled with an iodine-doped DCPD aerogel

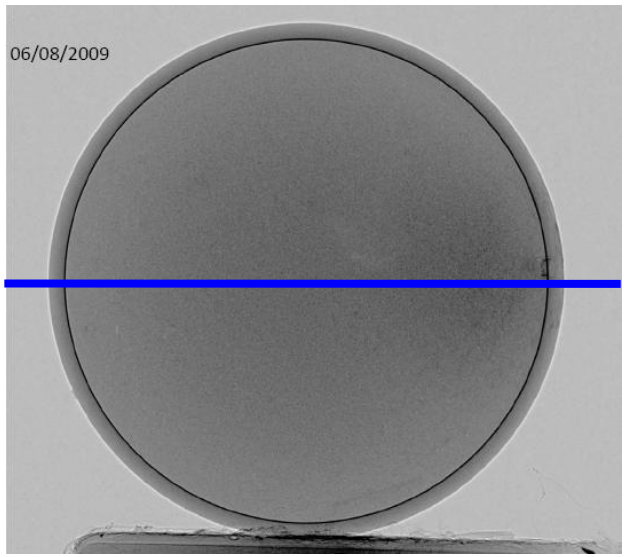

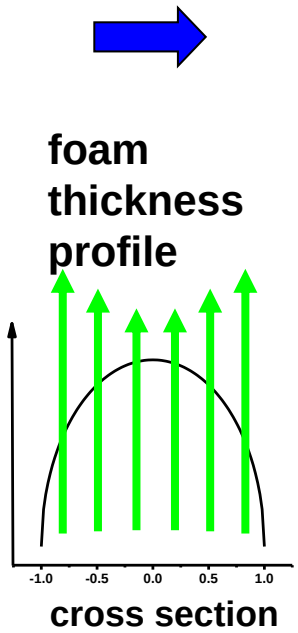

Doping required for aerogel imaging

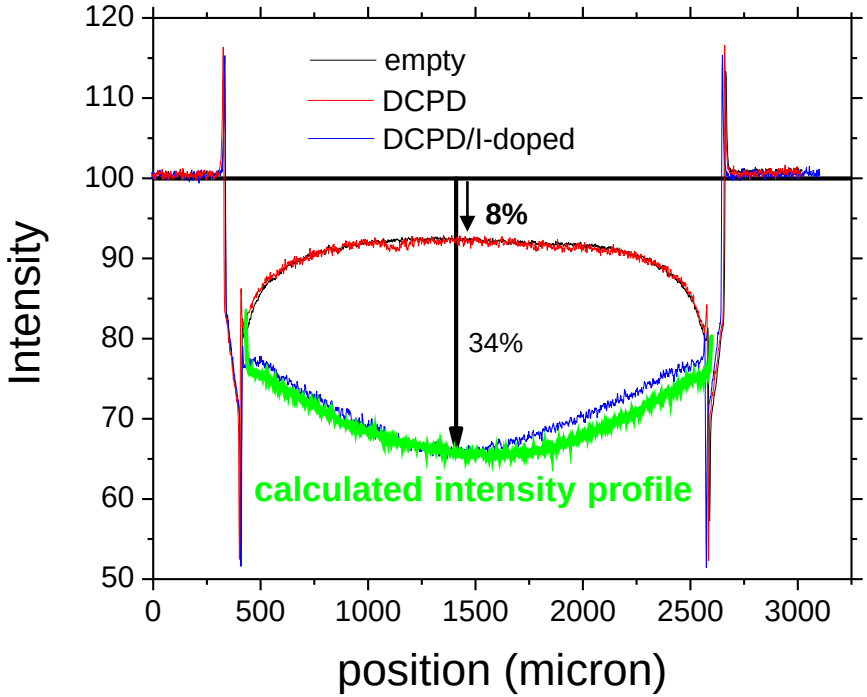

Synthesis of uniform, low density (<30 mg/cc), iodine-doped (10^{19} I/cc = $3x10^{15}$ I in a 20 μm thick foam liner) DCPD aerogels inside a capsule.

Ultrathin nanoporous foam liner

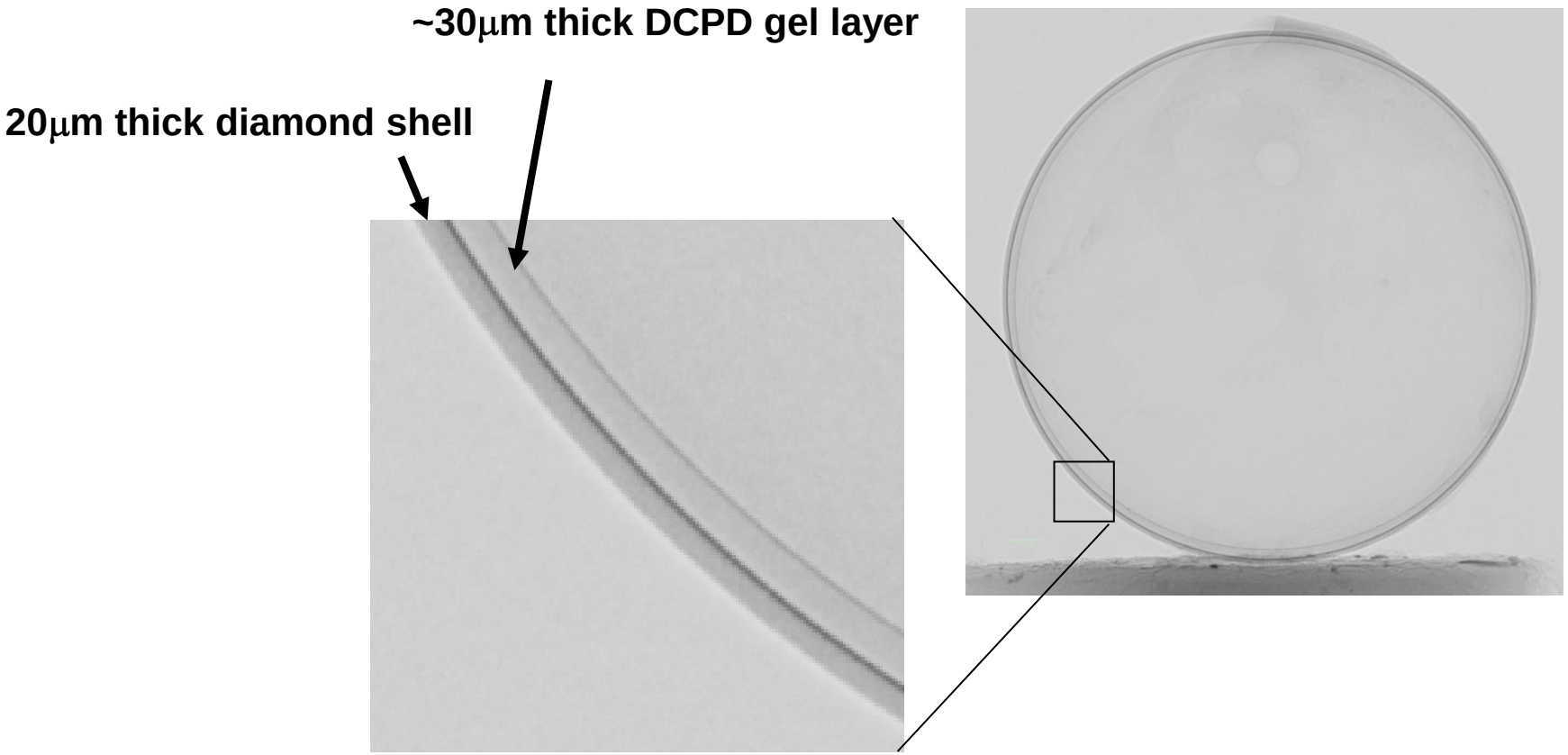

Problem: Uniformity

Alternative capsule liner materials

Carbon nanotube reinforced carbon aerogels

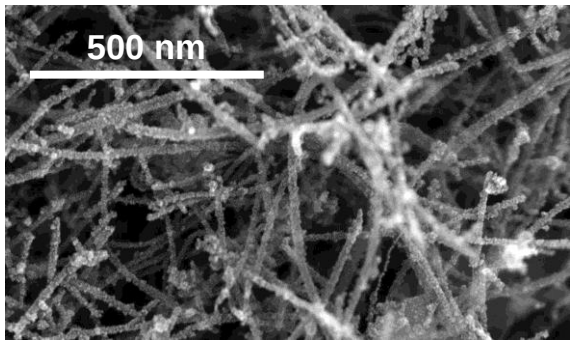

Requires high temperature pyrolysis, but elastic behavior up to very large (~90%) strains

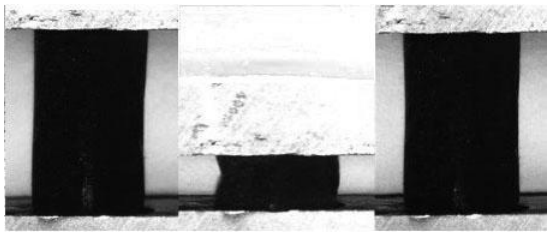

Worsley M.A. *et al.* 2009 *Appl. Phys. Lett.* 94, 073115
Worsley M.A. *et al.* 2009 *J. Mater. Chem.* 19, 3370
Worsley M.A. *et al.* 2008 *Langmuir* 24, 9763

Cross-linked polymer brushes

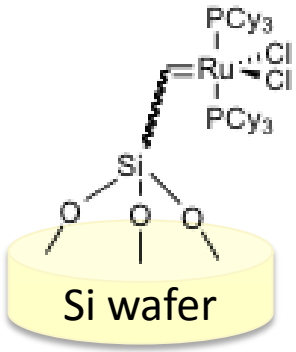

DCPD **Ru catalyst**

Crosslinked DCPD

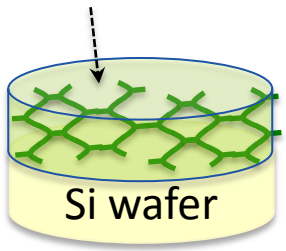

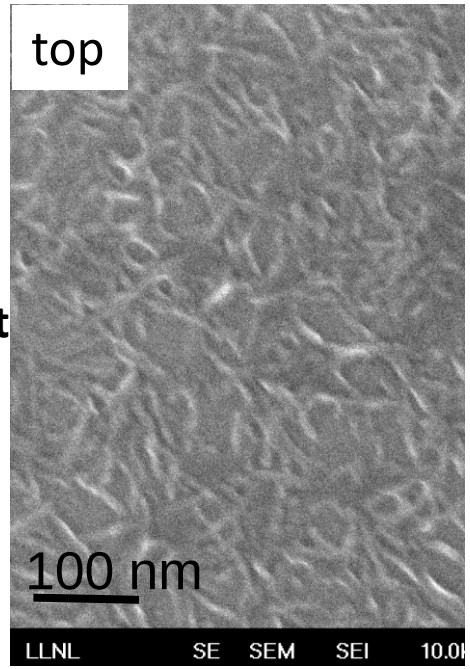

Fabrication of the ignition double-shell target is a Grand challenge

Nanoporous materials

- Ultra-low-density (<100 mg/cm^3) foam, sub 500-nm pore size (never done) [highest risk]

- High-strength inner shell capsule to contain 790-atm DT (never done at this small scale) [high risk]
- Density graded metallic shells (never done) [high risk]

Advanced high-strength materials

Ignition Double Shell

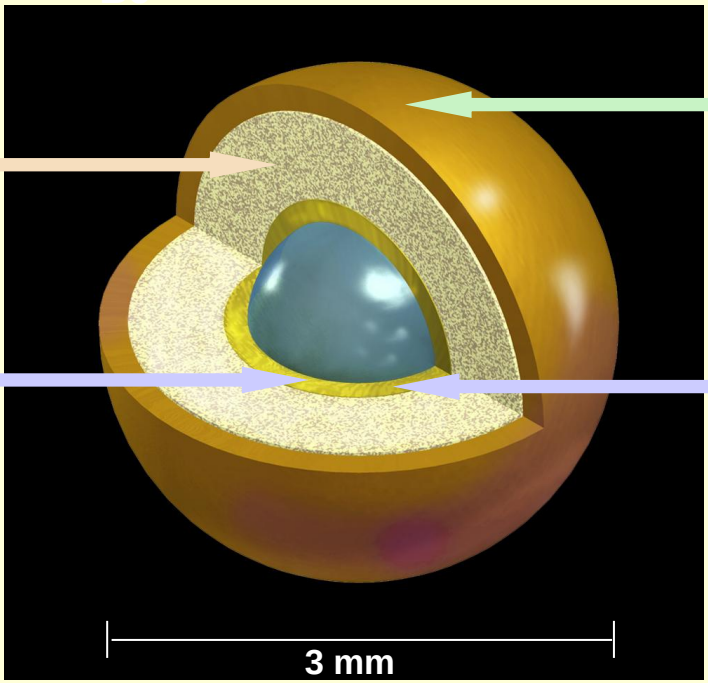

Novel 3D Fab

- Microassembly with precision to less than 2 μm (concentric shells done to 1.4 μm) [low risk]
- Assemble with 790 atms DT gas intact until shot time (never done) [medium risk]

- Filling metallic inner shell to 790-atm DT gas without introducing shell defect (never done at this scale) [higher risk]

Advanced high-strength materials

Hydrodynamic instability mitigation is a key issue

Challenge: Control of hydrodynamic growth

Unstable design

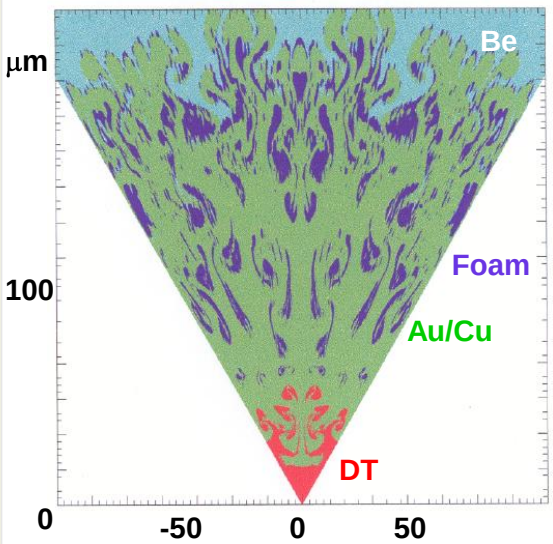

Potential Solution:

Graded electro-deposition of Au/Cu + mid-Z foam

Stable design

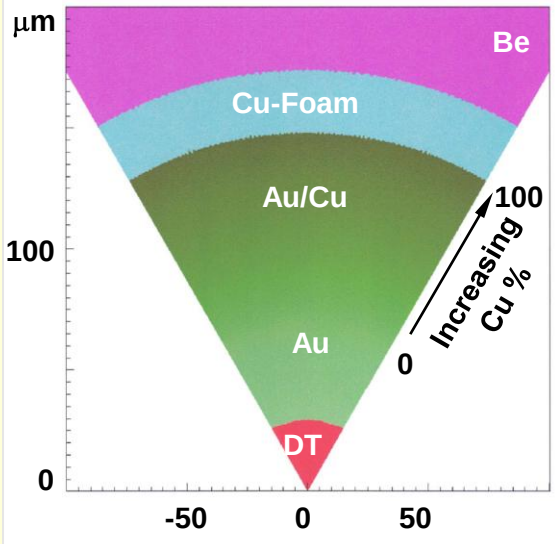

Capsule dimension at peak neutron yield

A significant effort has gone into developing Double Shells with unprecedented concentricity

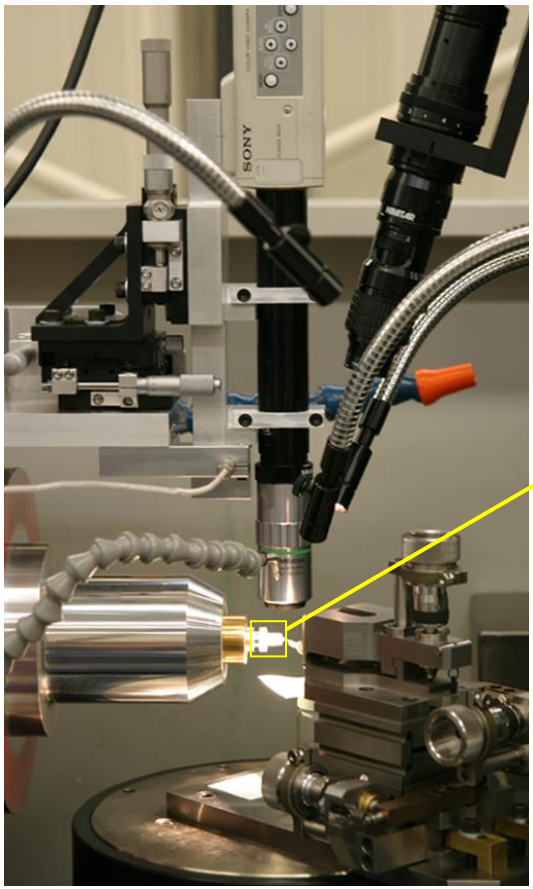

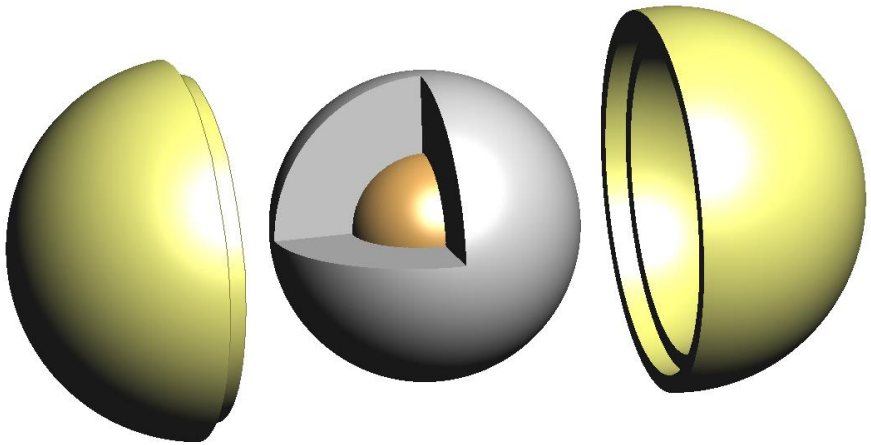

There is no longer a seam in the aerogel

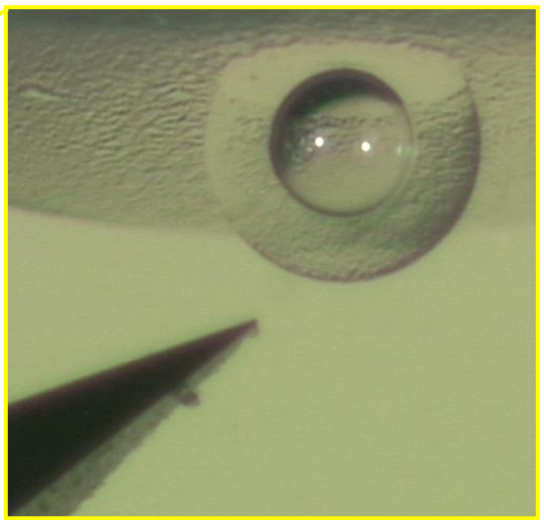

Improved optics allow in-situ metrology with 1-2 µm accuracy to machine aerogel concentric to an embedded capsule

Assembly of the double shell target is a major accomplishment

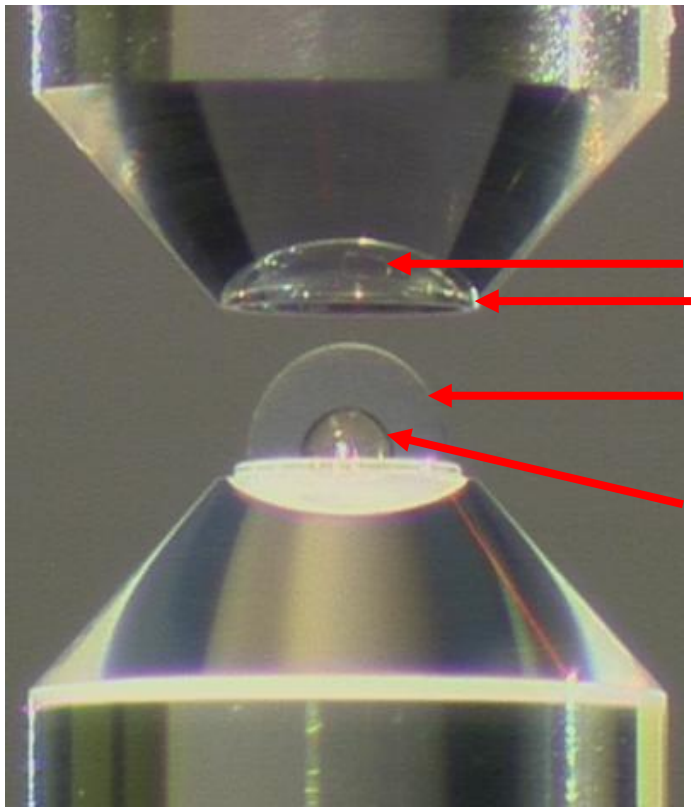

2% Brominated plastic outer shell

SiO_2 foam

SiO_2 inner capsule

100 nm channel

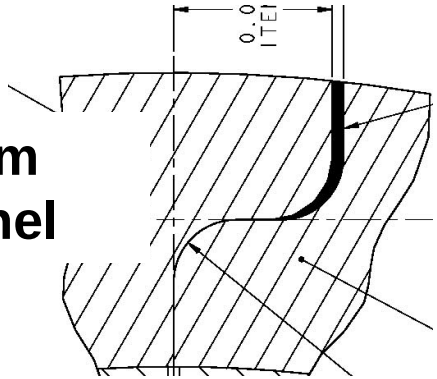

- Simulations showed the joint between the hemishells must be filled and density matched to avoid instability
- We picked 1% brominated cyanoacrylate to match the 2% bromine doped CH ablator

Newly developed capabilities have led to Double Shell targets that meet all of the specifications

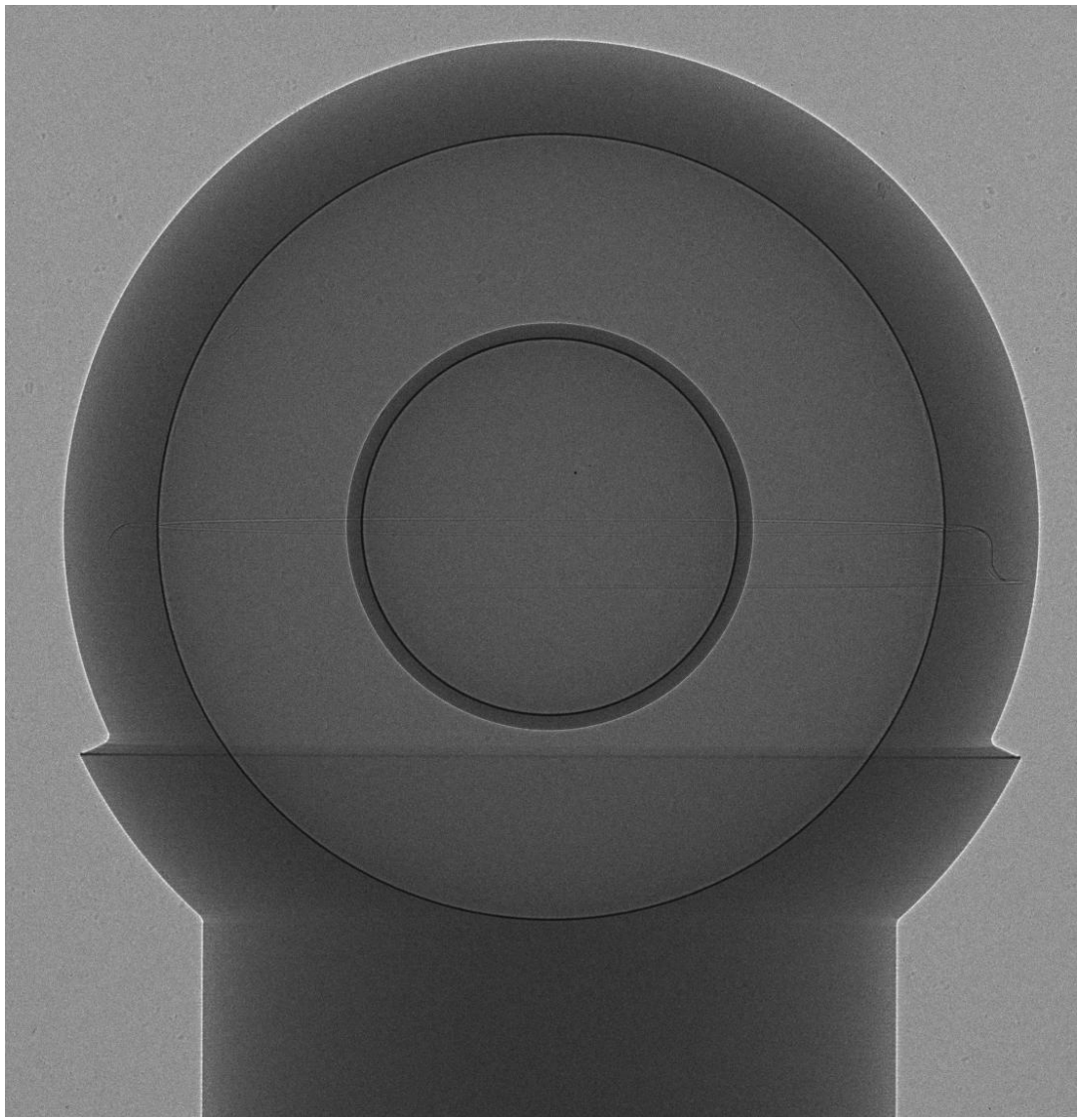

Transmission radiograph of Double Shell target

First article results

Feature	Spec	Measured value
Concen-tricity	3 μm	**1.40 μm**
Δr at joint in the ablator	0.5 μm	**< 0.5 μm**
Voids or gaps	< 10 μm	**No visible voids**
Ablator t uniformity	1 μm	**1 μm**

Finished Double Shell

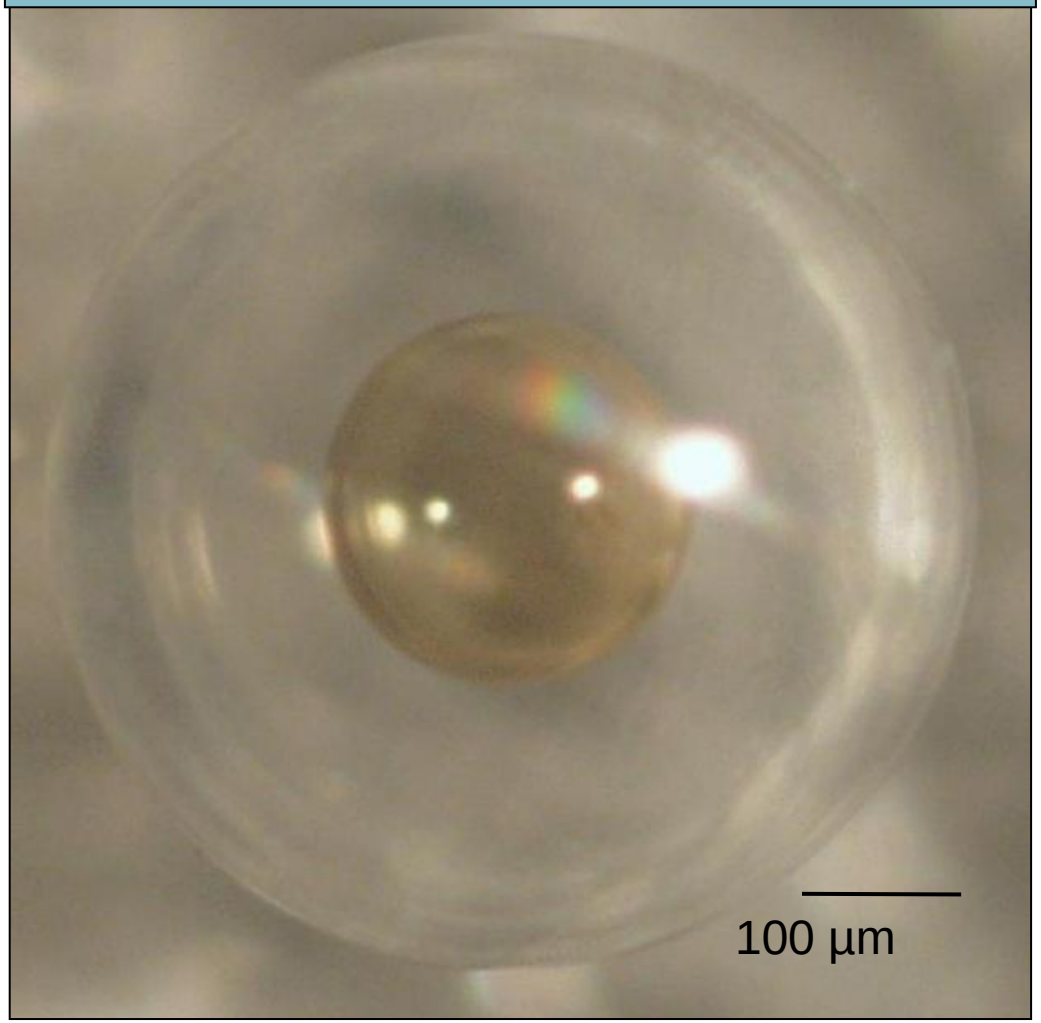

We are engineering materials with high strength by controlling grain size

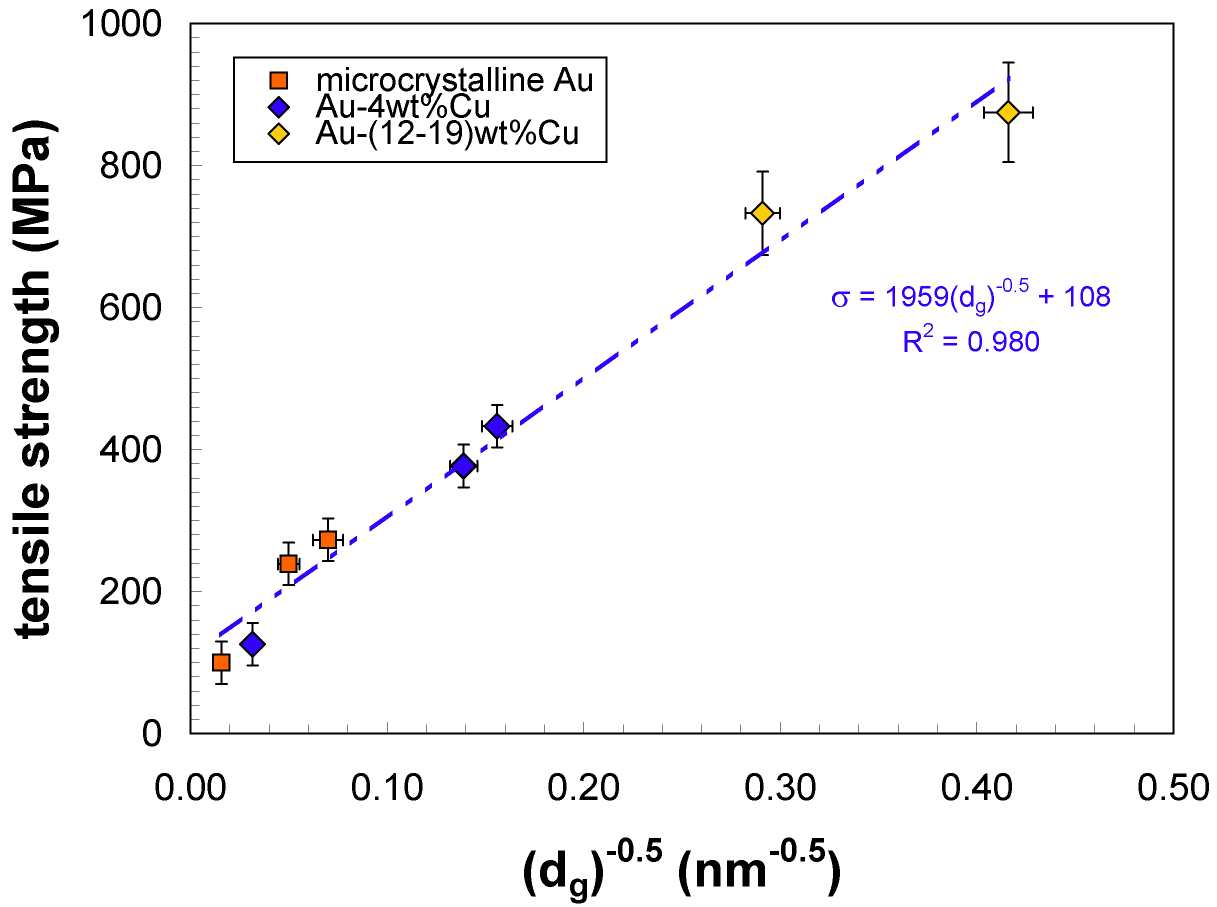

A Hall-Petch plot of grain size $d^{-0.5}$ ($nm^{-0.5}$) with strength σ (MPa) for Au [1] as well as upper-bound strength values for nanocrystalline Au-4 wt.%Cu, and Au-(12-19)wt.%Cu.

[1] R.D. Emery and G.L. Povrik, Acta Mater., 51 (2003) 2079

Tin doping maintains Au/Cu alloy strength after annealing at 430 C

Sn doped graded composition Au/Cu maintains nanograin size (10-20nm) at 430 C

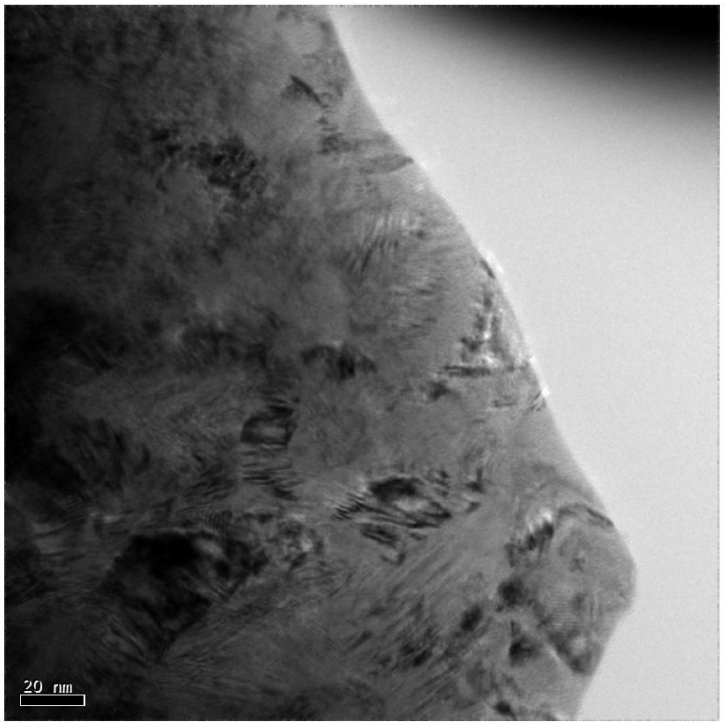

Sn doped graded composition Au/Cu maintains strength at temperature 430 C

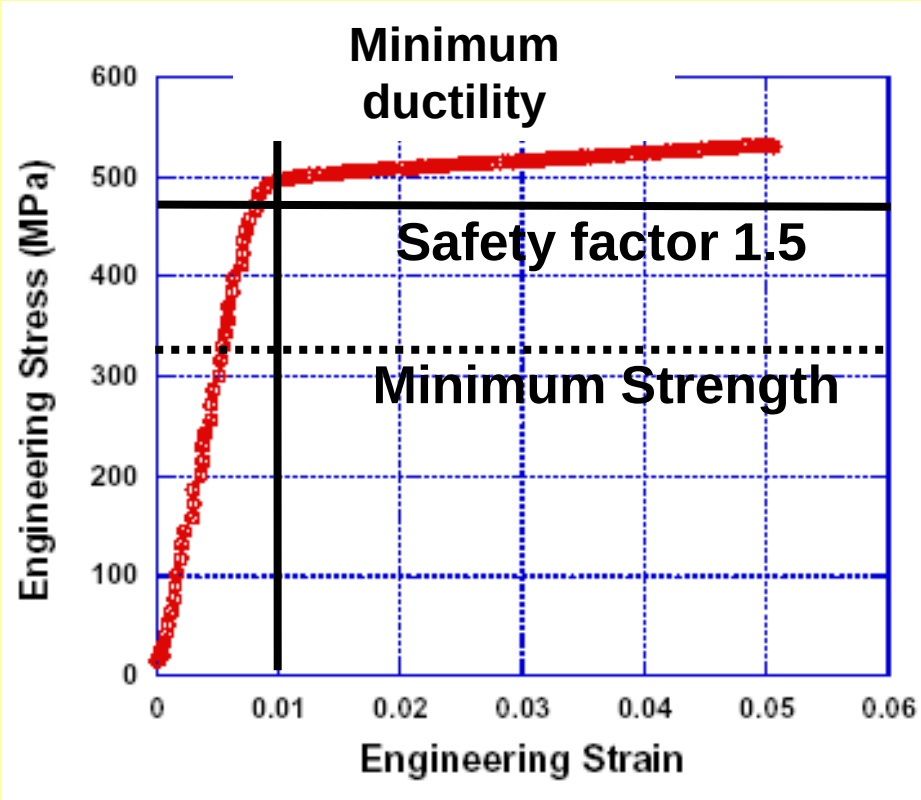

Composition graded Au/Cu from 90wt% to 40wt% Au
Sn doping 5 wt%

We are making progress producing Au/Cu shells

10 micron thick Au/Cu shell electro-deposited on glass mandrel

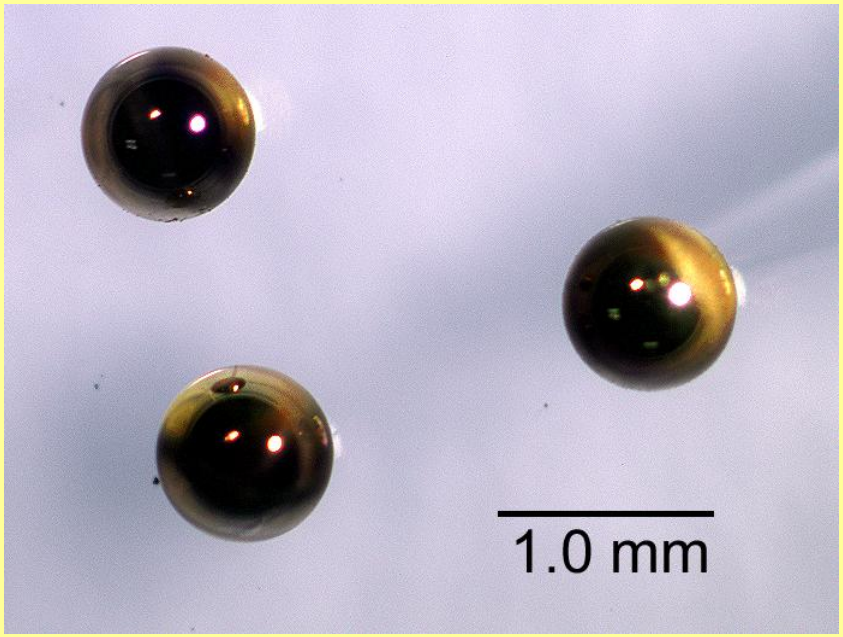

Thicker shells are required; smoothness specification is needed

We have made ~35 μm thick Au/Cu/Sn capsules

Polished capsule courtesy of GA

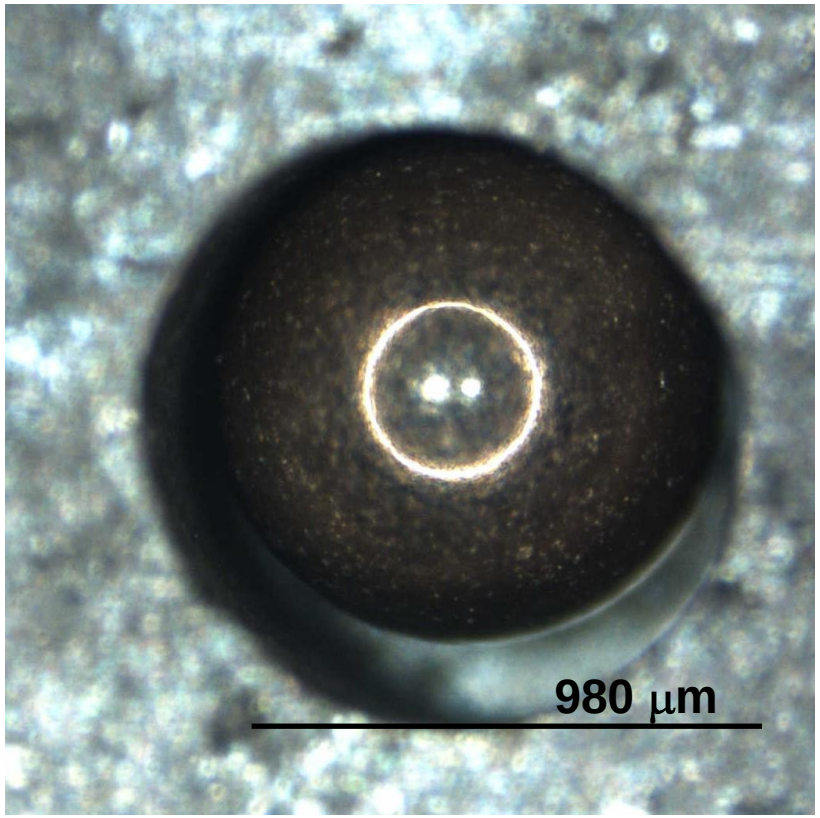

SEM of FIB cross-section of Au/Cu/Sn capsule

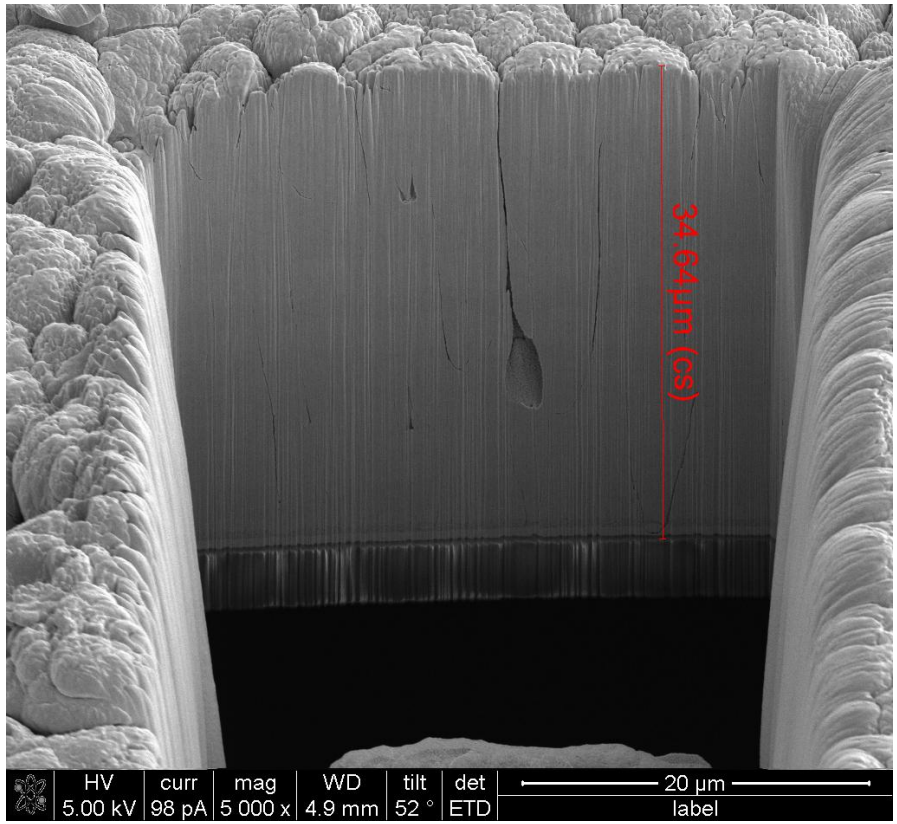

76%Au/20%Cu/4%Sn

Have not yet been successful at filling

Glass mandrels courtesy of GA

We have developed the ability to make low density pure metal foams

Nanoporous materials: Gold

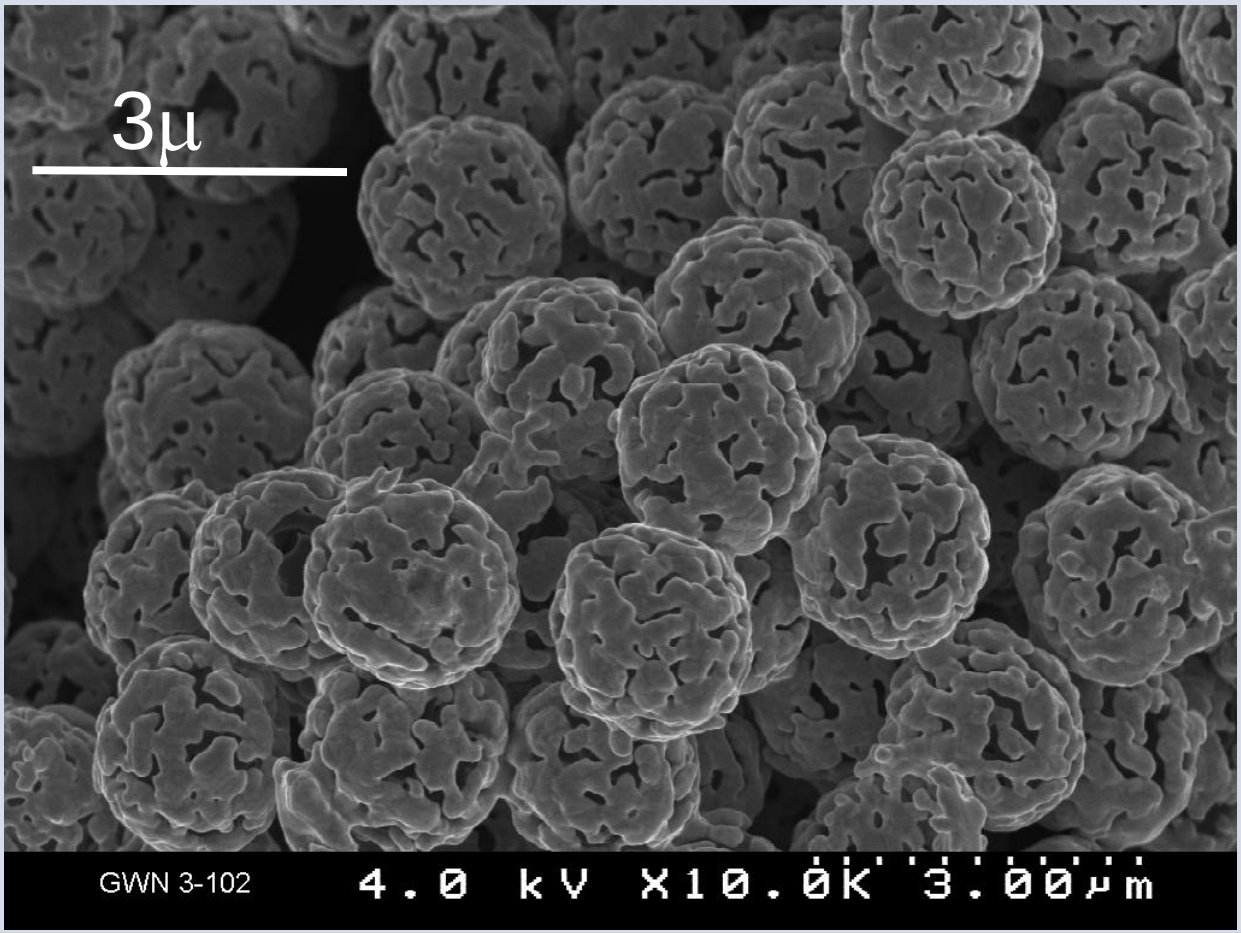

Ultralow density 2% relative density

Nyce, G. W, et al., "Synthesis and characterization of hierarchical porous gold materials," CHEMISTRY OF MATERIALS 19 (3): 344-346 FEB 6 2007

We can produce 10% relative density copper foam

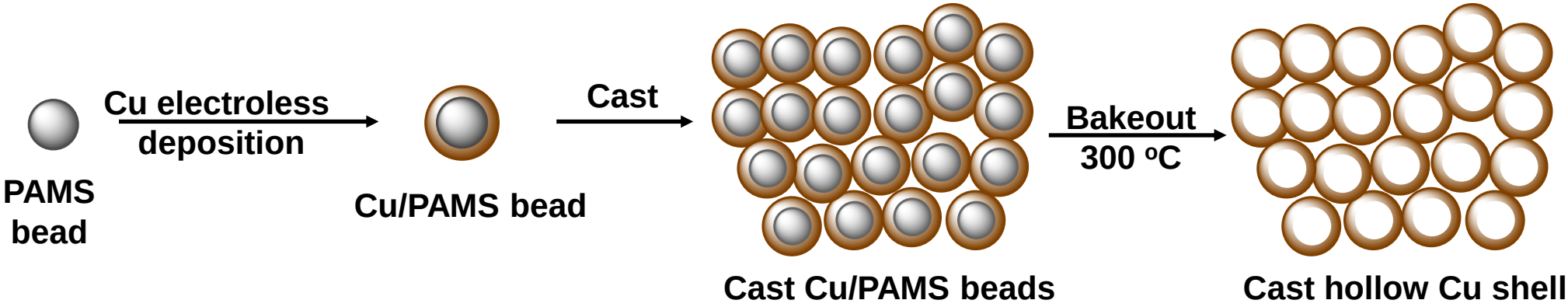

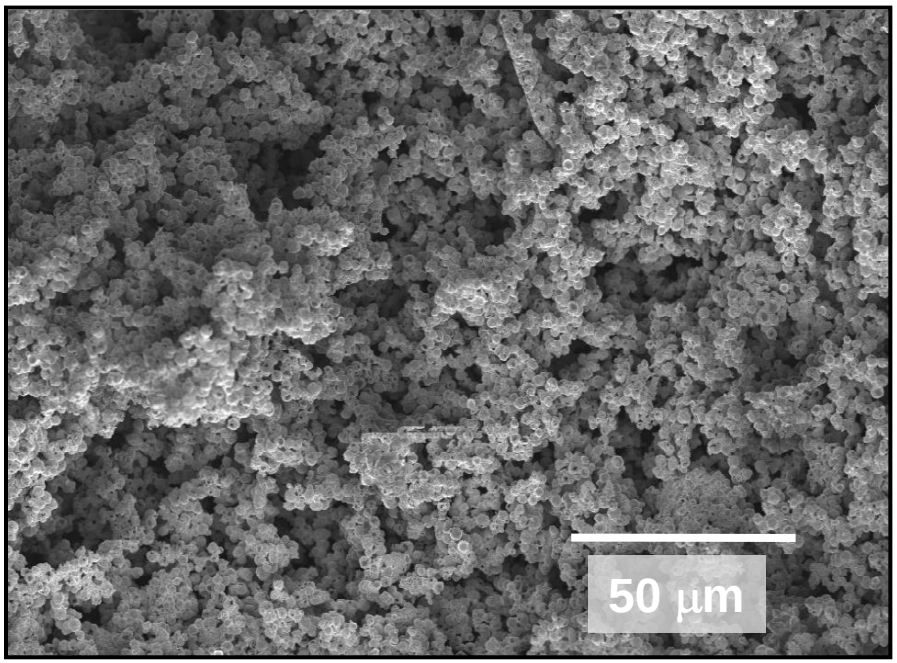

SEM image of Cu foam (10% rd)

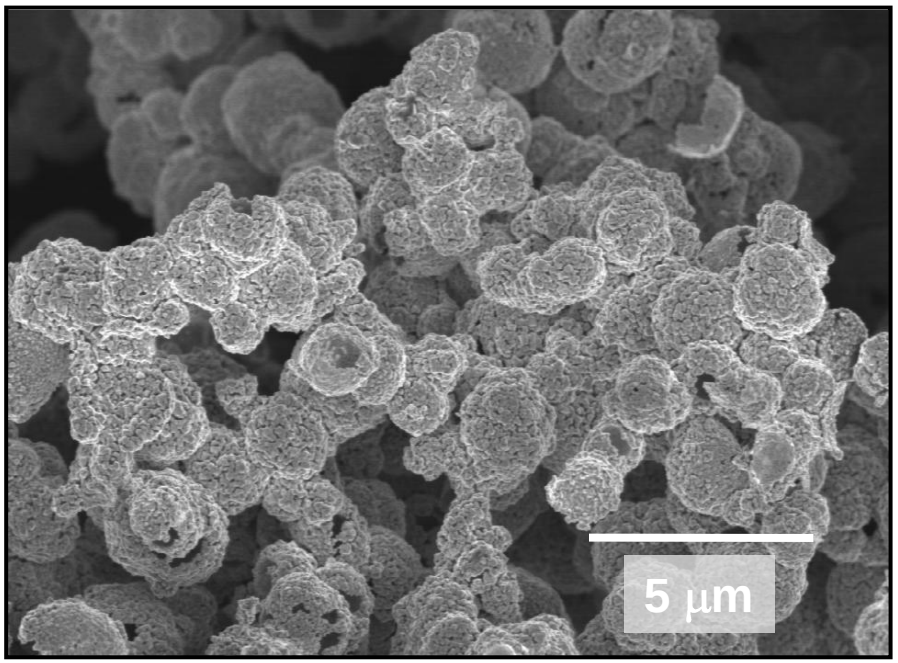

SEM image of Cu foam (10% rd)

Copper foam is surprisingly robust

Machined Steps in 10% relative density Copper foam

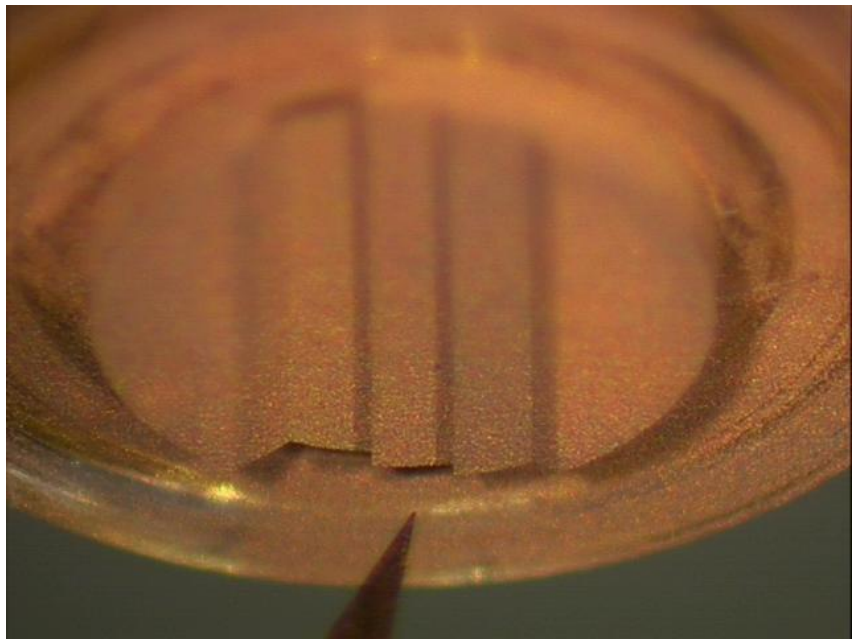

Top View

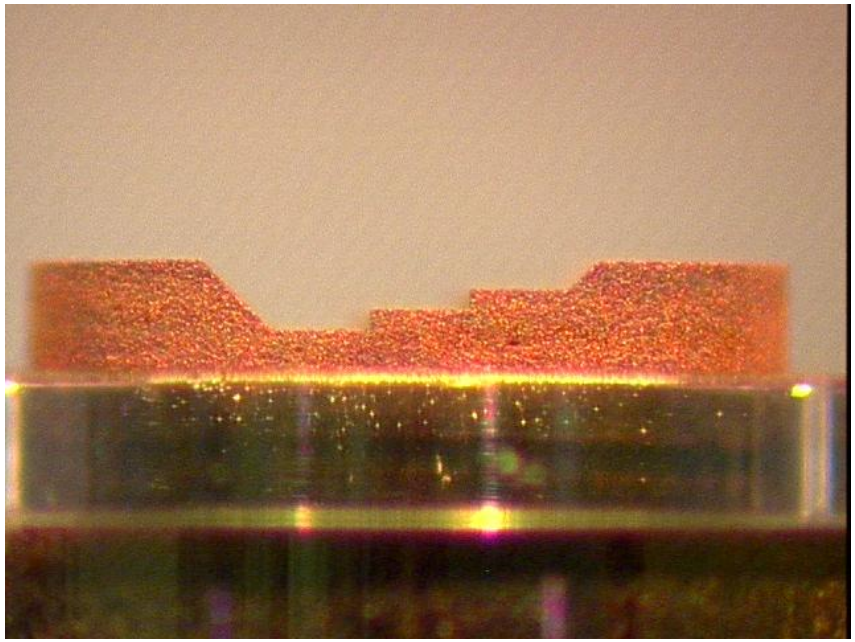

Side View

Ligament size determines strength

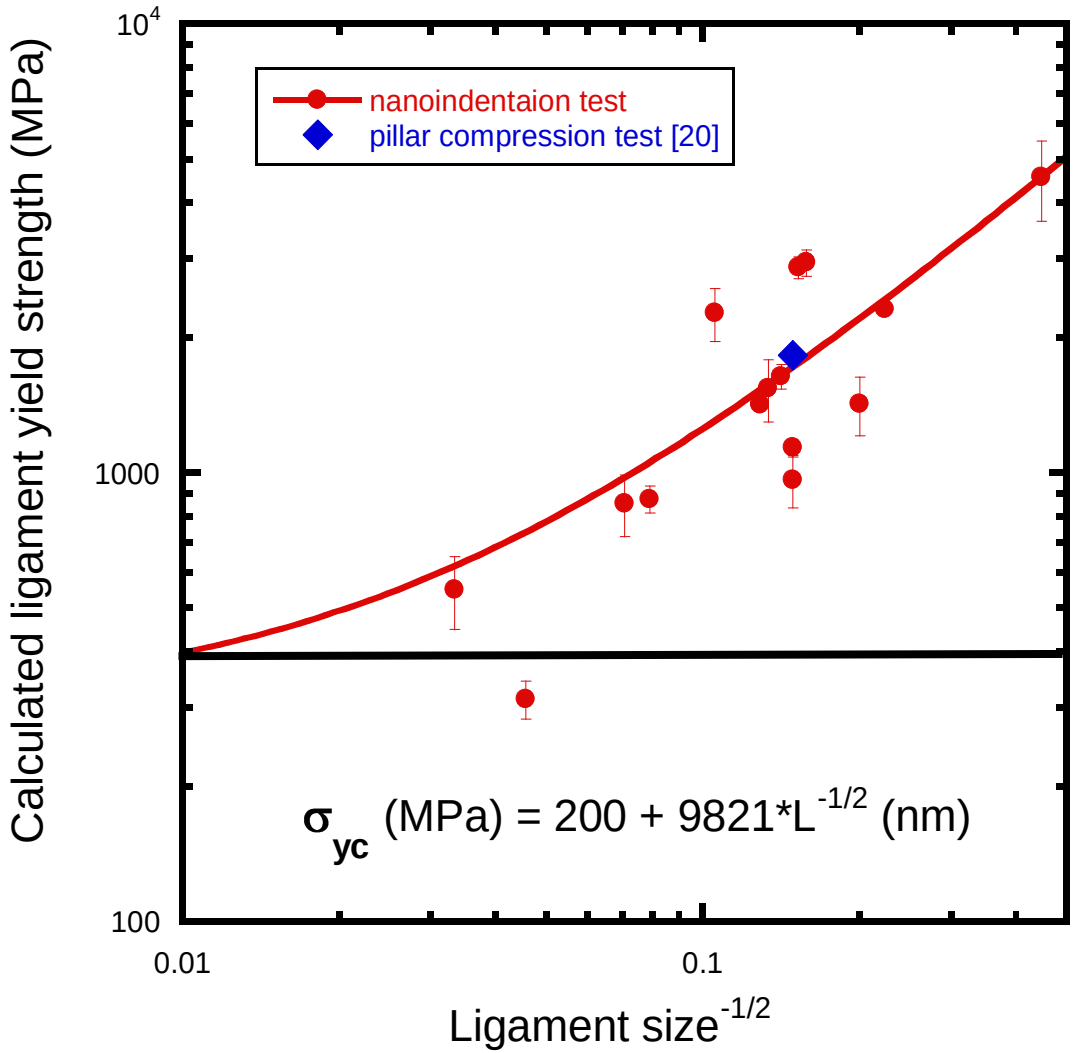

Nanoporous gold is surprisingly strong

Robust CuO aerogel at 50 mg/cc has been synthesized

CuO aerogel billet on lathe

Diamond turned CuO aerogel

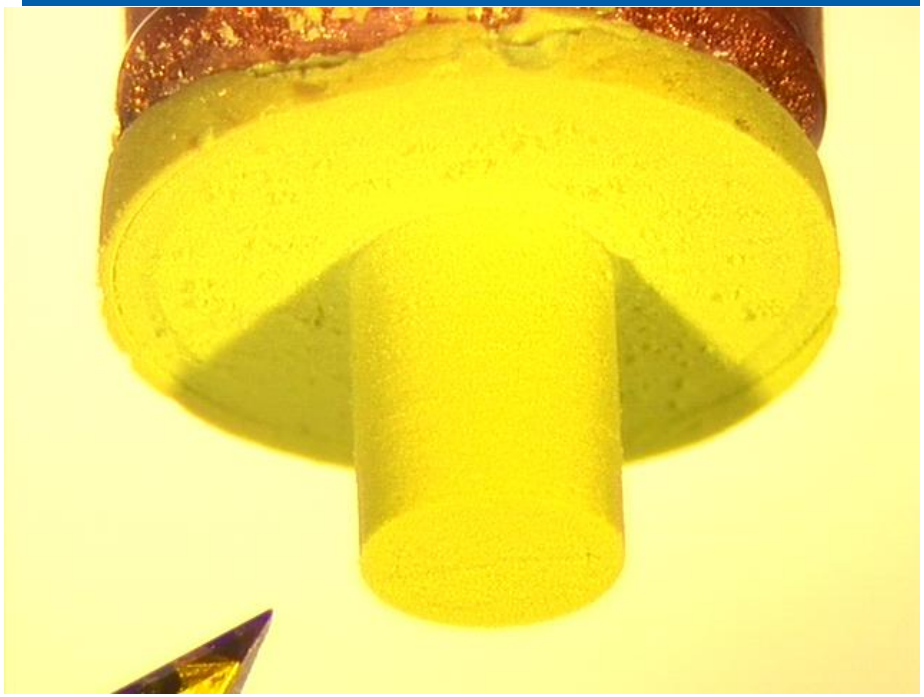

Could we build a miniature sun on earth?

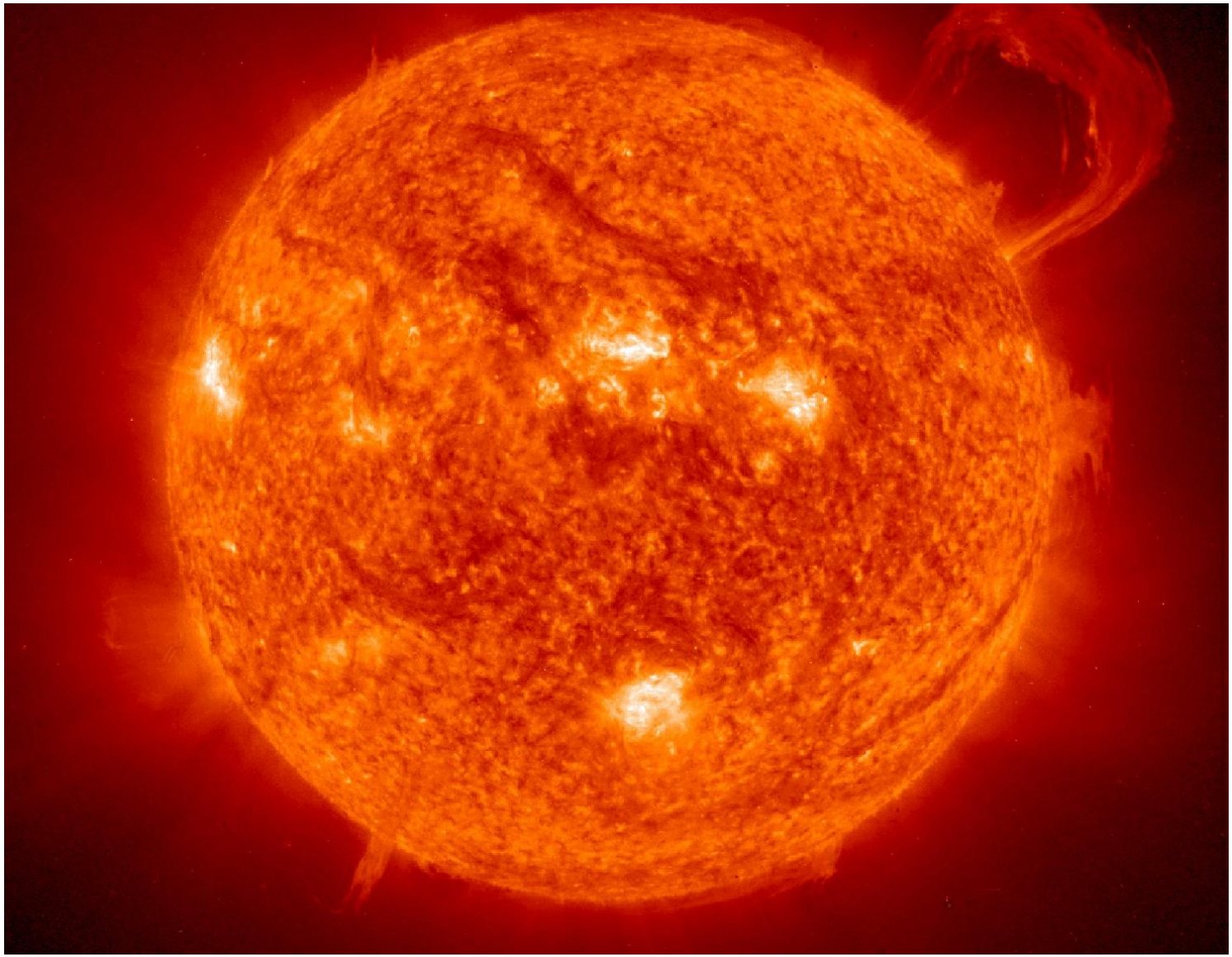

NIC

A new CFTA Mapper will combine confocal microscopy with a 4π manipulator to quantify capsule cleanliness prior to final assembly

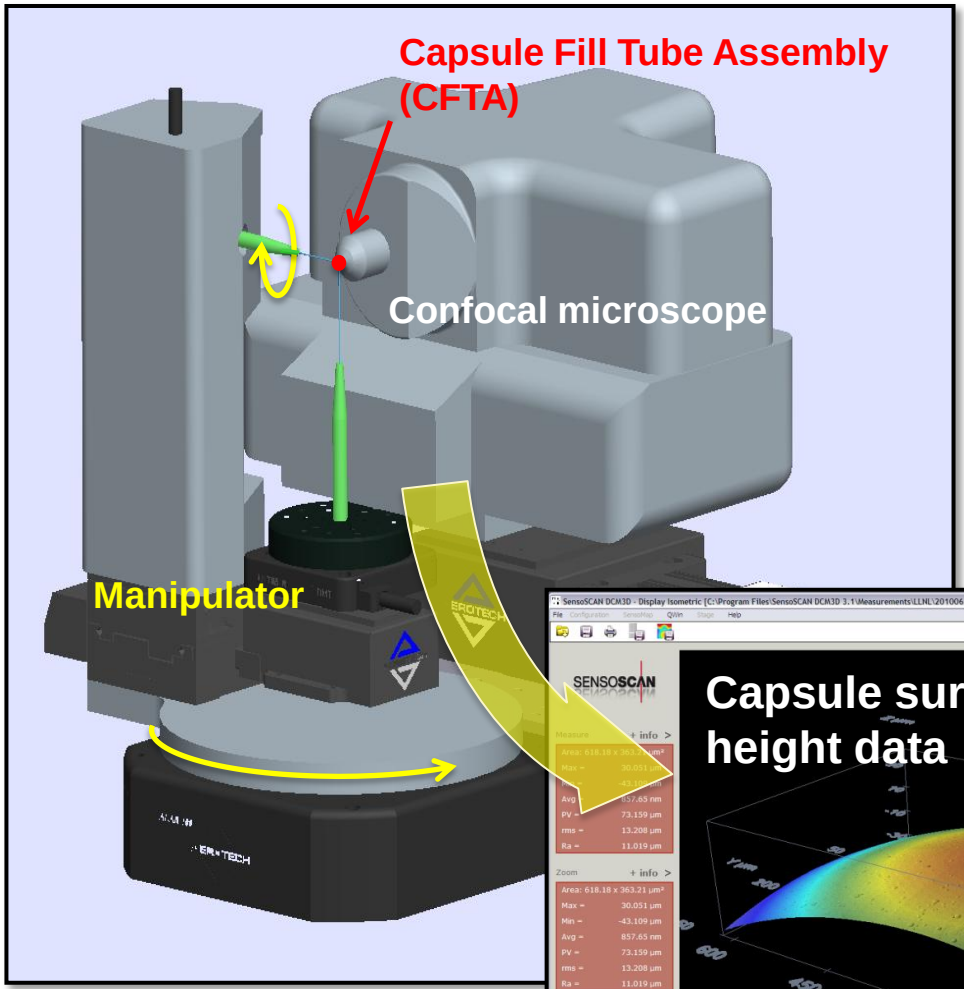

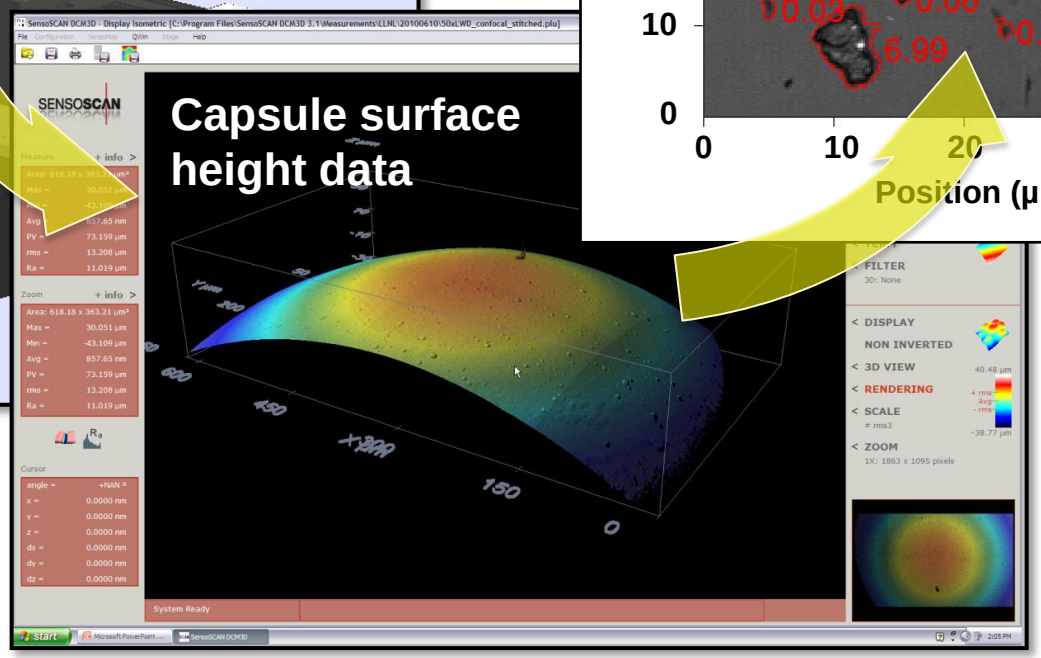

Data post-processed to locate particles and determine their volumes

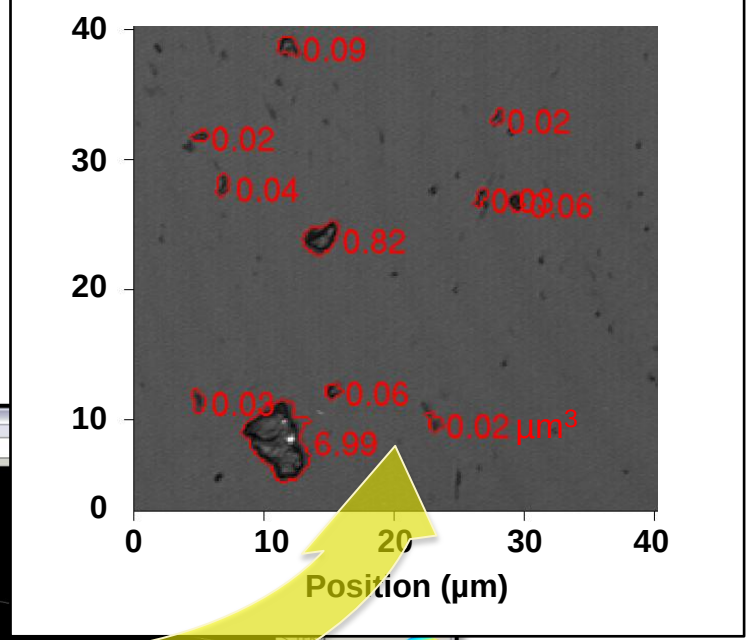

Precision radiography measures optical depth variations around the capsule in ignition shells

Precision Radiograph

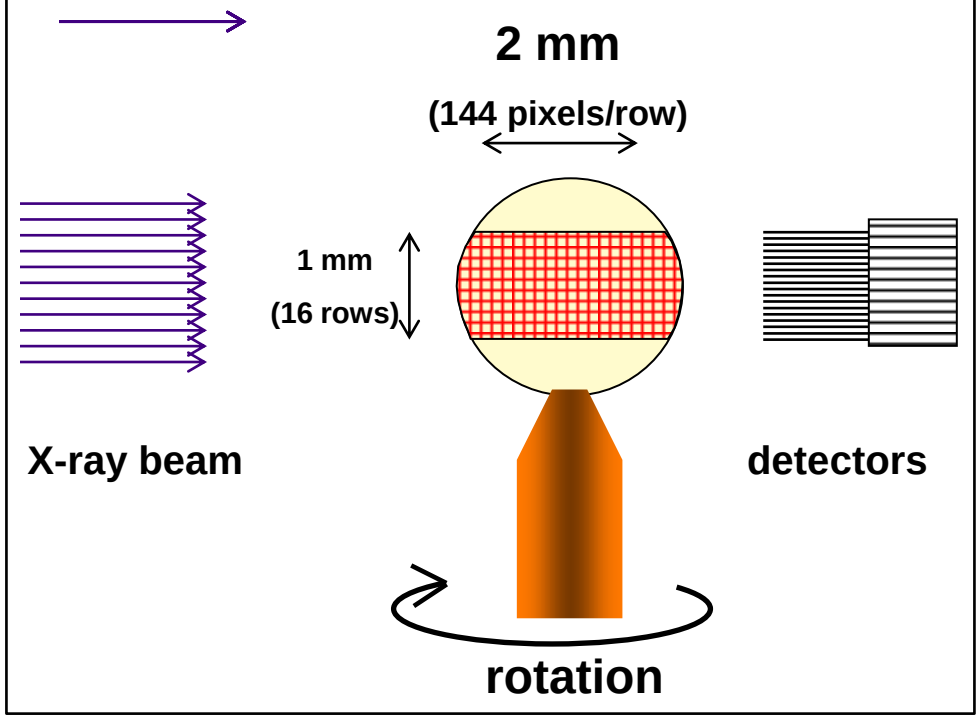

Optical depth variations

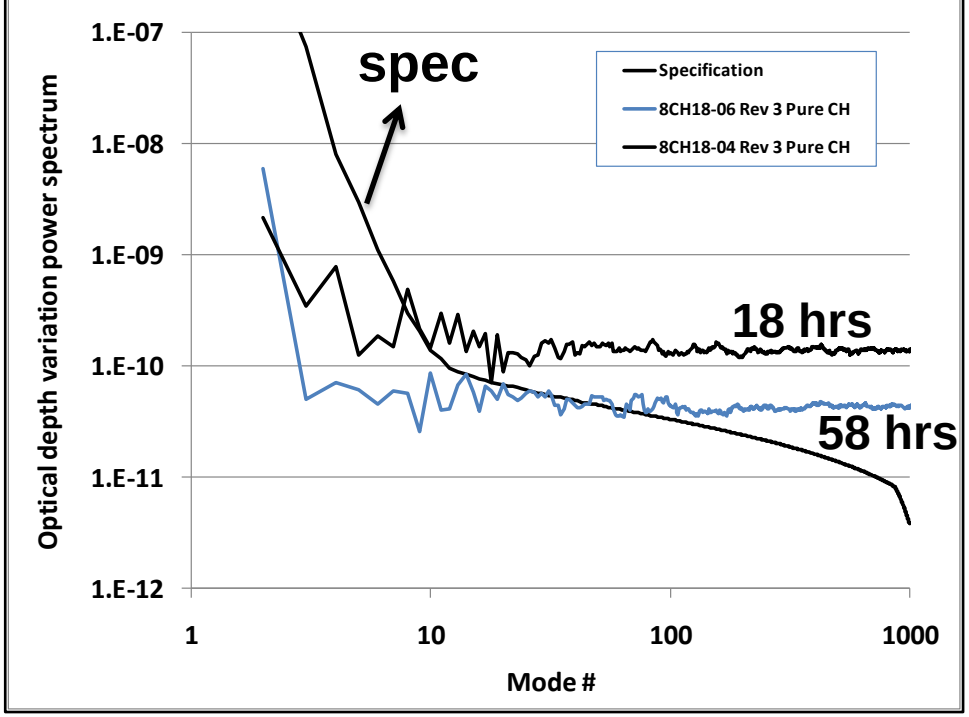

- 120 um resolution (~ < mode 25)
- Source size and brightness
- Detector size
- S/N : Poisson statistics driven by counting time
- Optical depth : thickness OR density (including dopant) non-uniformity

- Shells produced meet the optical depth variations to within noise floor and instrument resolution
- Longer counting time drops noise floor
- Synchrotron imaging currently to reach modes of interest (~ 60)

Atomic Force Microscopy is used to characterizes shell surfaces

1) AFM measures rotating shell on equator

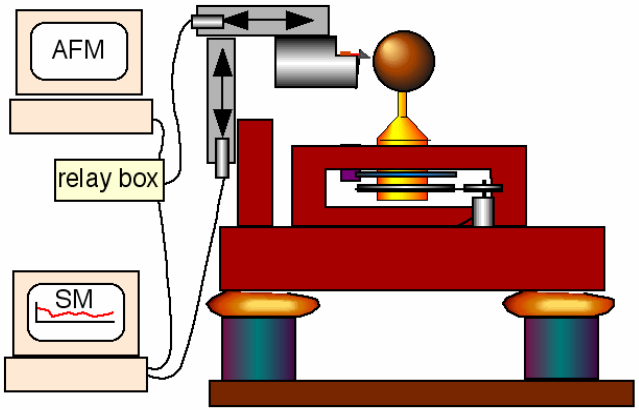

2) 1 equatorial & 18 polar traces cover the surface.

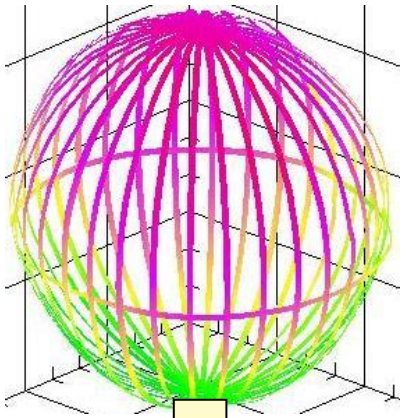

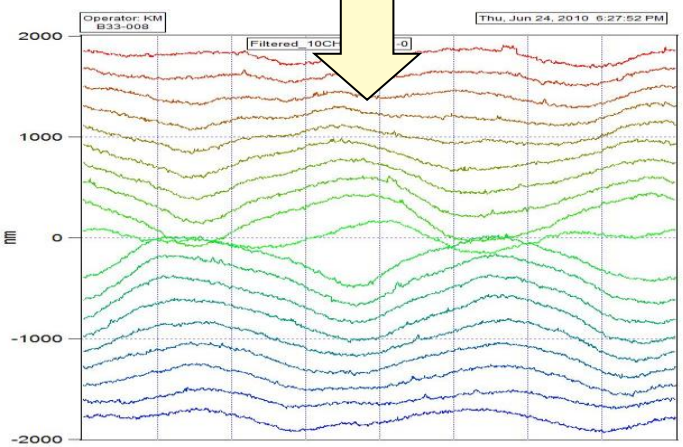

3) Traces capture surface figure and roughness

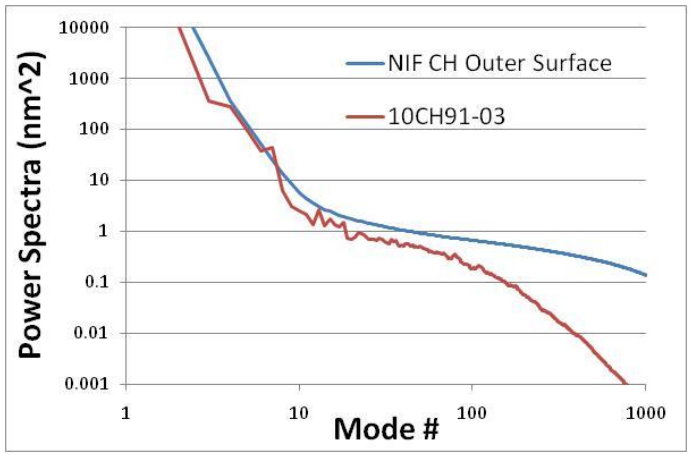

4) Power spectra compares to NIF spec

AFM is good for a Fourier analysis of the surface, but not for isolated defects

Phase sensitive diffractive interferometry (PSDI) is used to characterize localized defects

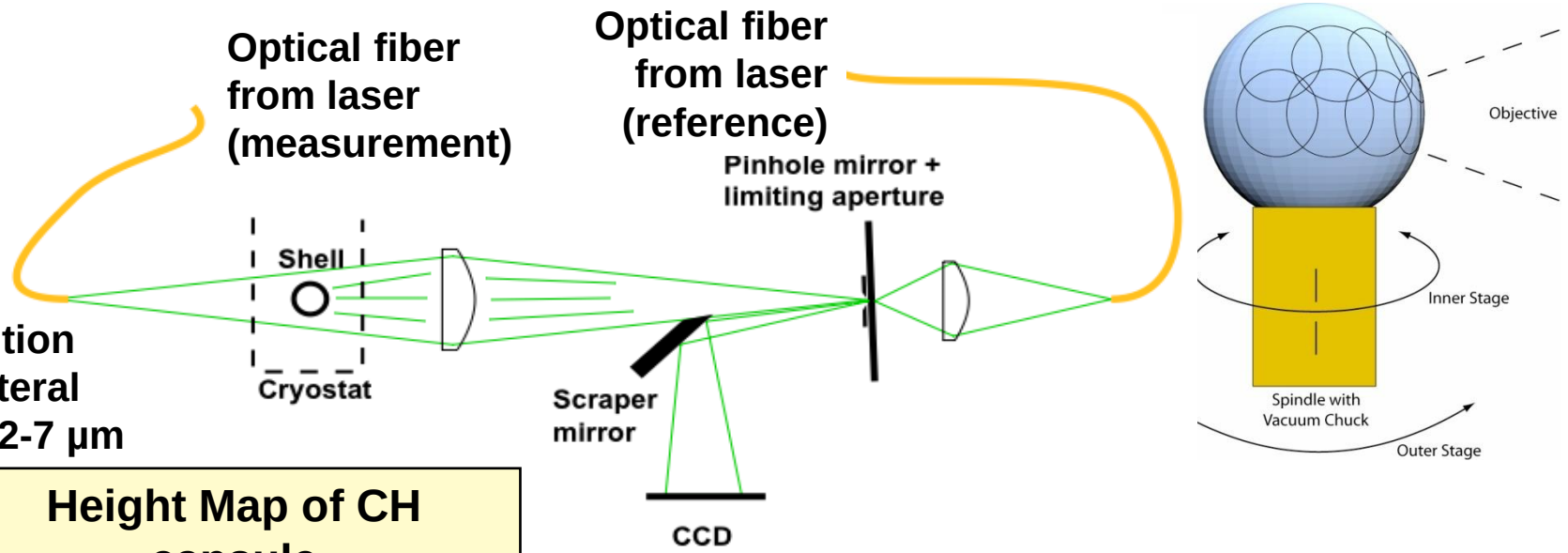

Depth resolution ~ 0.01 μm, lateral resolution ~ 2-7 μm

Height Map of CH capsule

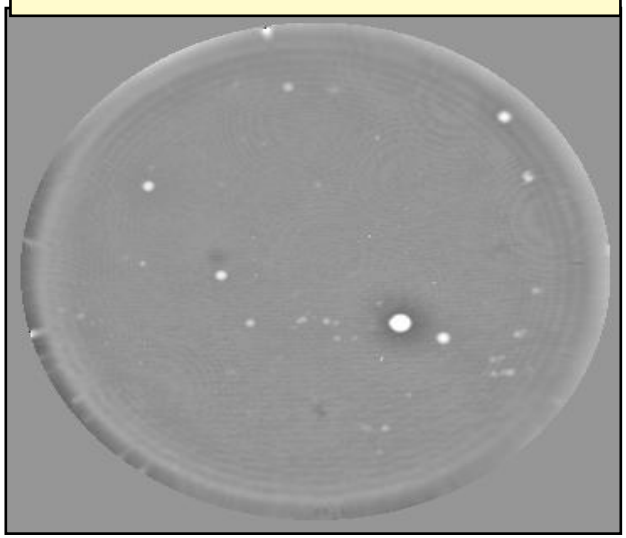

500 μm

PSDI covers 100% of the surface area

- ~140 medallions with ~2x oversampling

New finishing process can significantly reduce/eliminate mixed mass by reducing bump heights

Pre-Polish (Optical micrograph & PSDI measured defects)

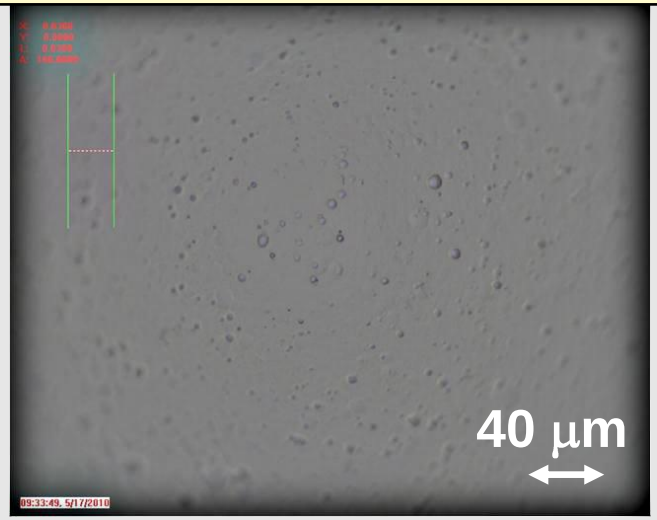

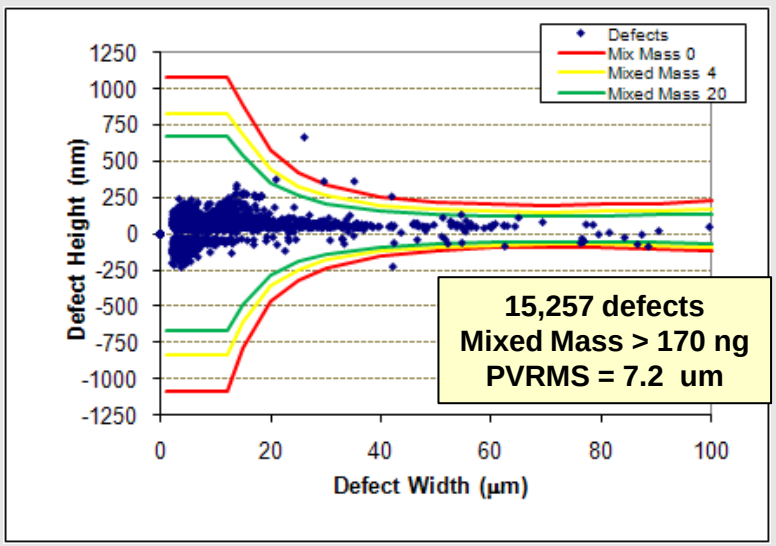

Polished (Optical micrograph & PSDI measured defects)

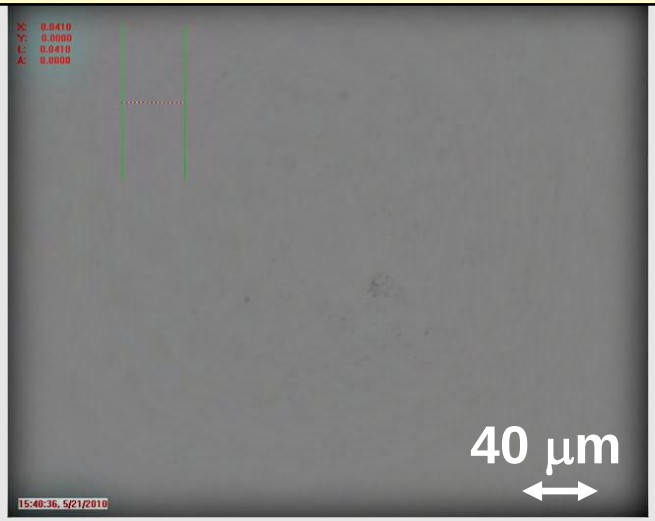

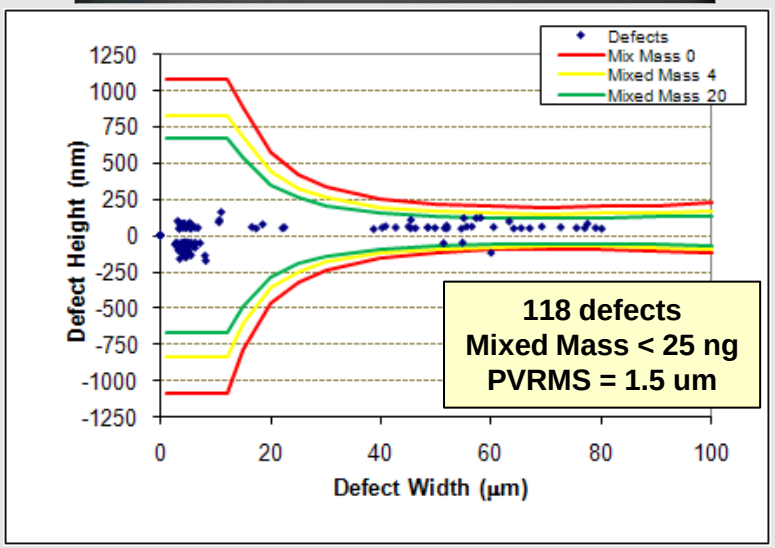

*First Pre-pilot capsule at GA after Facilitization (10CH70-07) 5-20-2010

Fuel layers that meet measurable specifications are being formed

Radiograph of Shimmed HT

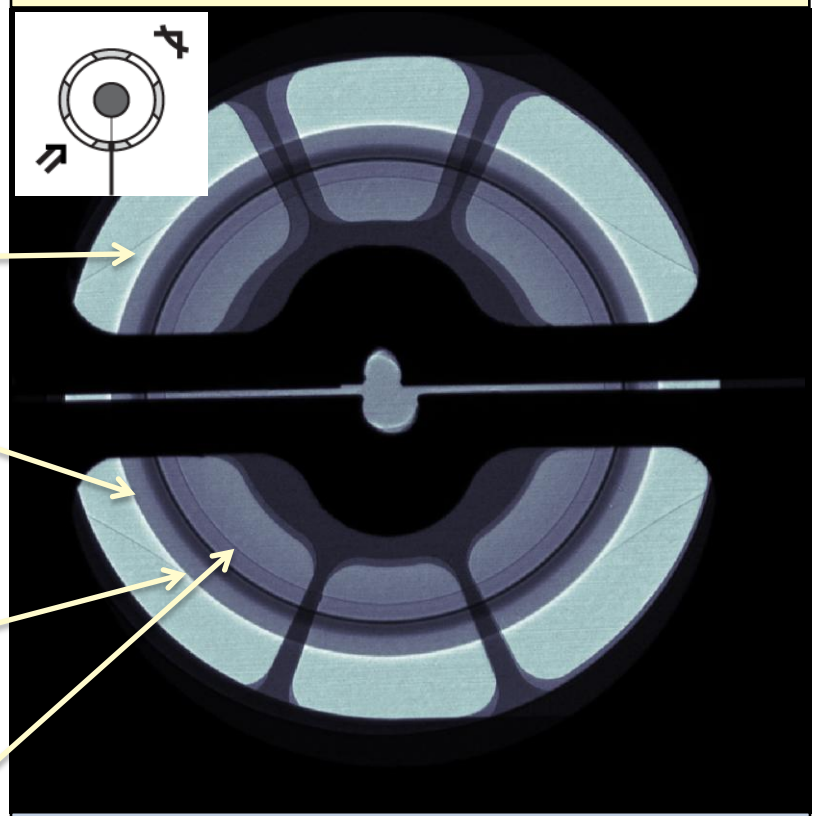

66 micron thick HT layer in 0.93 scale Be shell

Power Spectra of 3 views

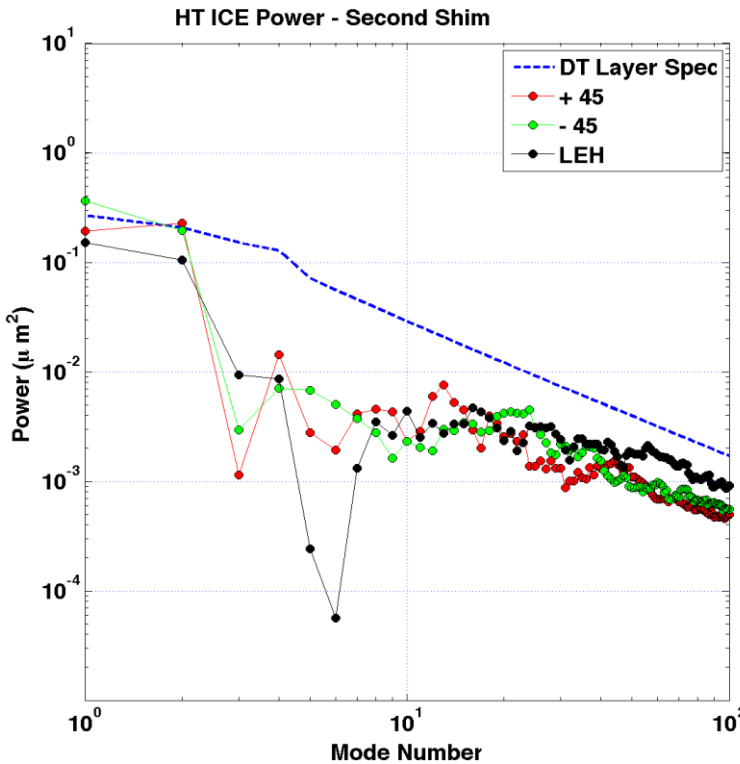

Meets both high and low mode PSD specs

- Yield of layers that meet specifications is ~30%
- Similar yield for HT and DT layers

Modes 1 to 6 are controlled by the thermal field of the hohlraum

- **Modes are conventionally described as a fourier series.**

$$R = R_0 + \sum a_n \cos(n\theta) + b_n \sin(n\theta)$$

- **Modal amplitudes b_1 and a_2 are actively controlled by "shimming" heaters**
- **All other low modes are controlled by the geometry of the hohlraum and quality of the assembly.**

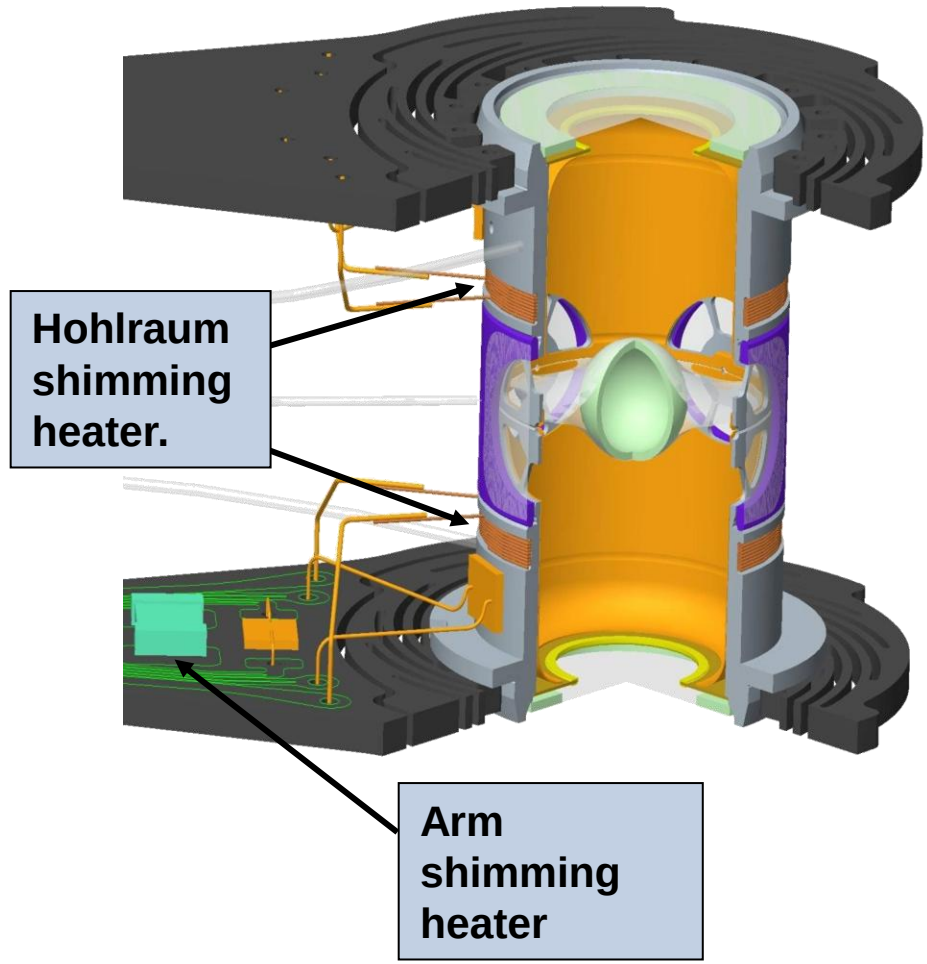

Layering timeline at NIF

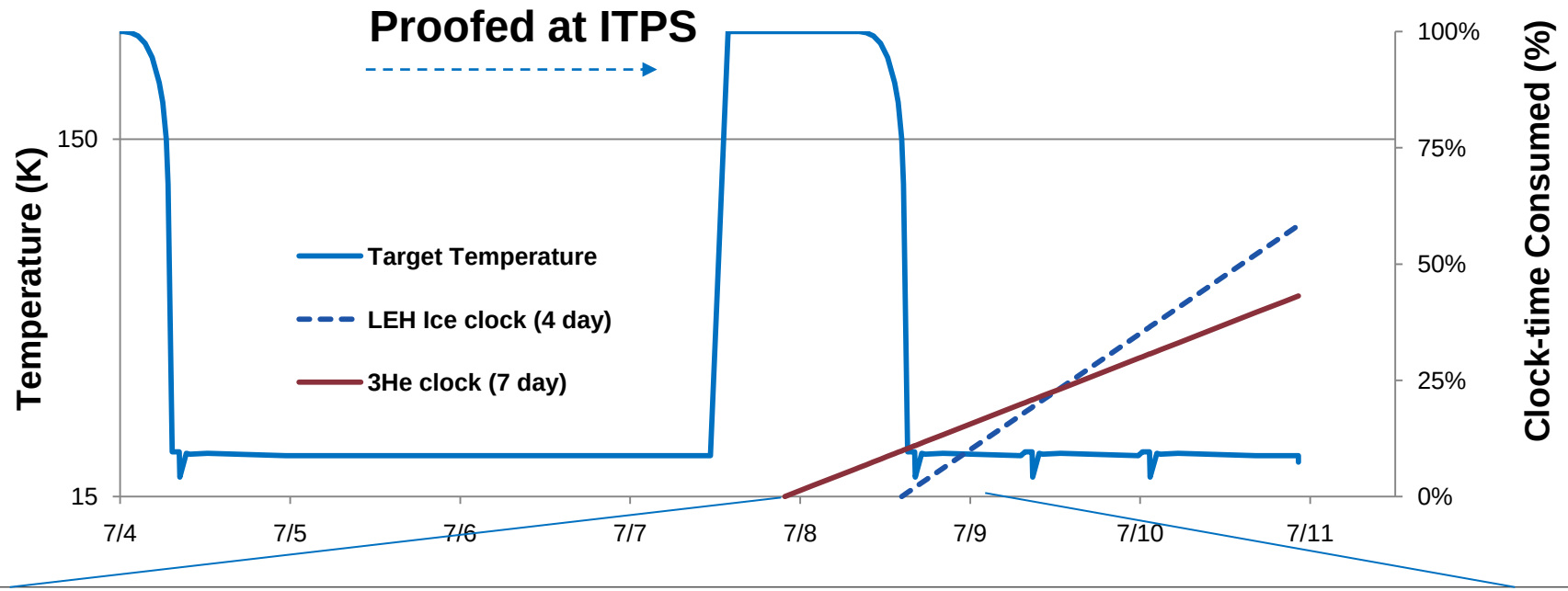

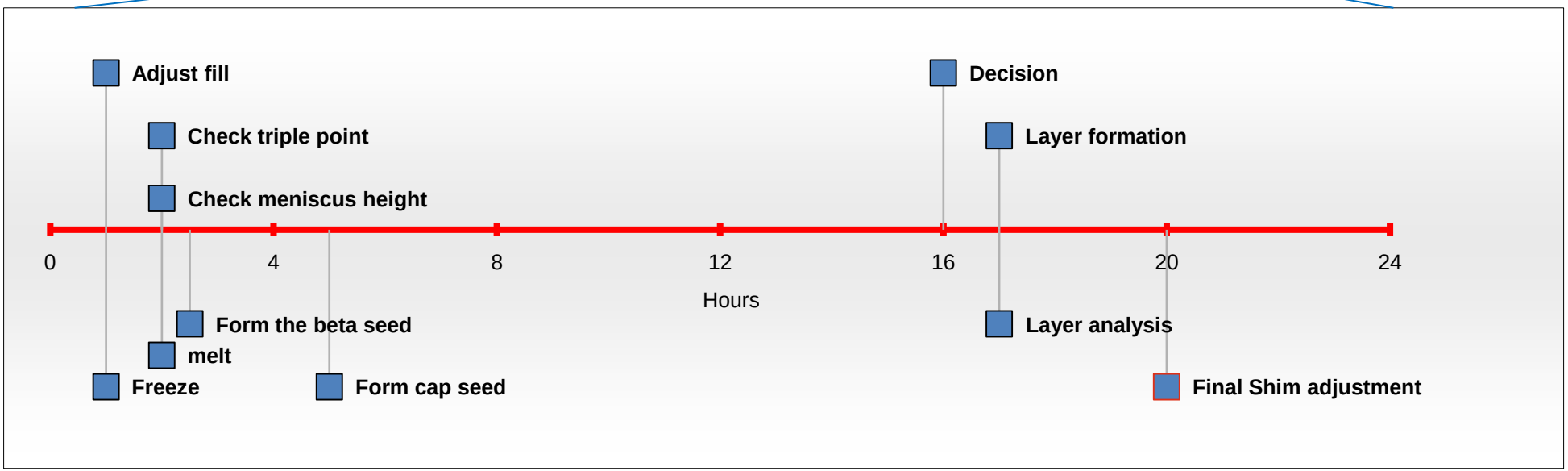

Three X-ray views limits the isolated defects that we can detect

At NIF presently we have a limited view of defects

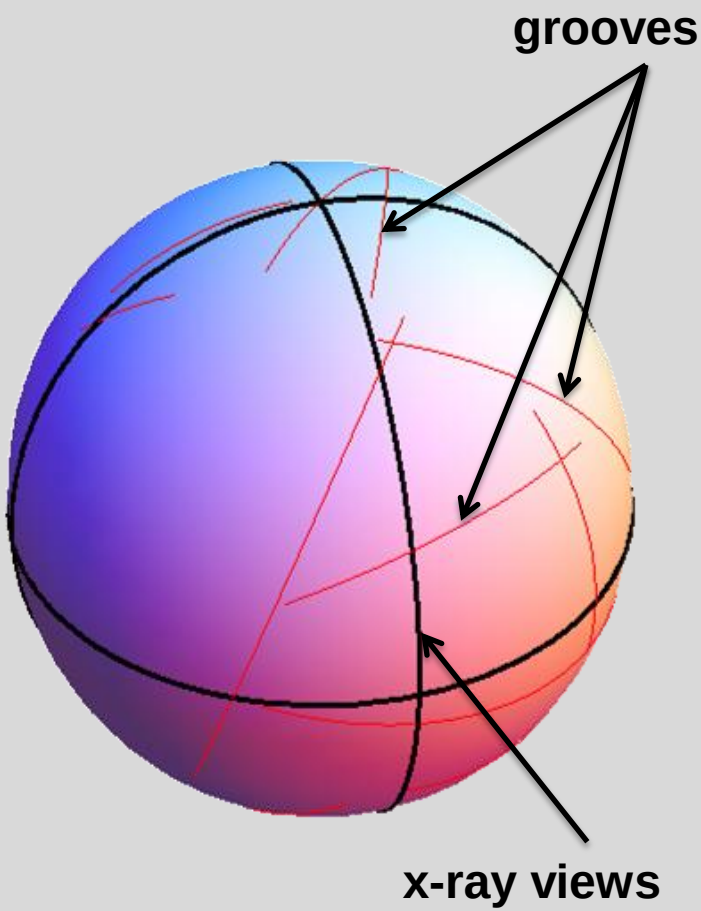

There is more information in the LEH view if we can enhance contrast

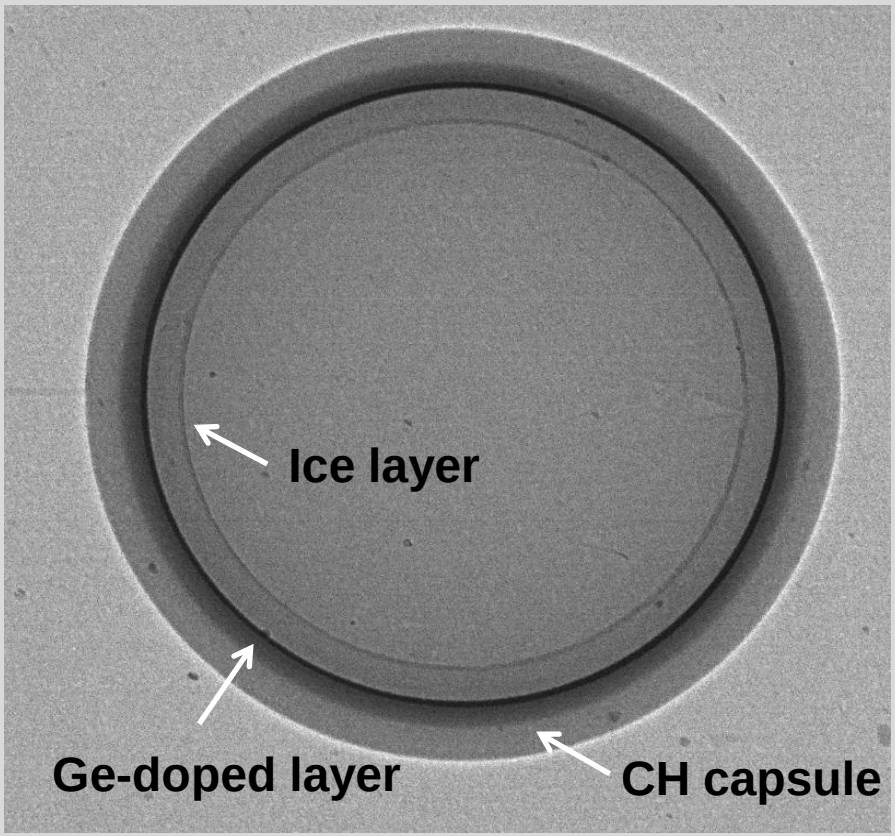

We are exploring using phase contrast, the "Talbot effect," to find defects not on a limb

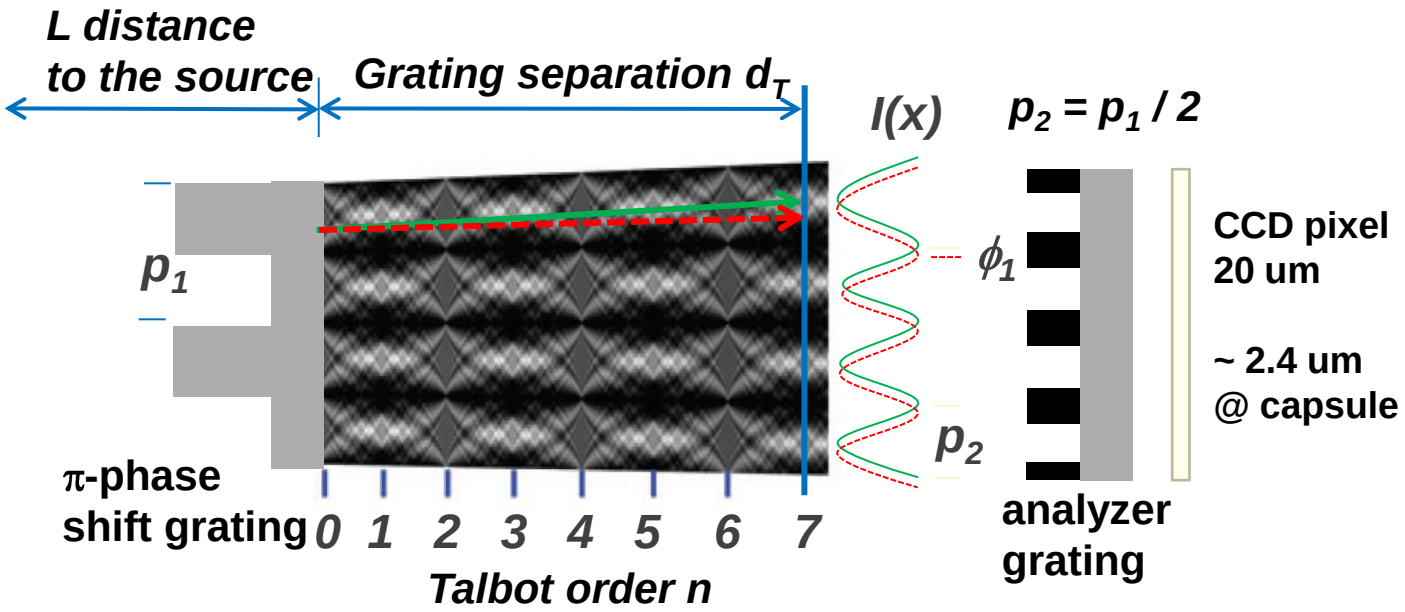

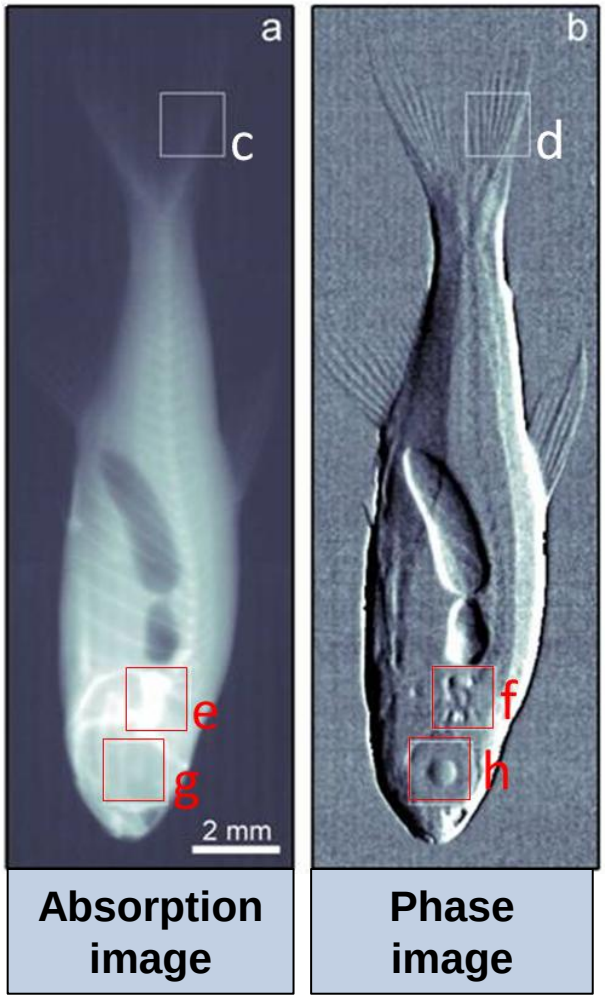

The interference pattern I(x), as seen by the CCD, is

$I(x) = a_0(x) + \Sigma a_m^{\infty}(x) \cos(2\pi m x/p_2 + \phi_m(x))$; m is the diffraction mode $m = 1$

$a_0(x)$ provides absorption "brightfield contrast" information
$a_1(x)/a_0(x)$ provides coherence "darkfield contrast" information
$\phi_1(x)$ provides beam deflection angle "differential phase contrast" information

M. BECH , "X-ray imaging with a grating interferometer," *Ph.D Thesis, Niels Bohr Institute, University of Copenhagen, May 2009*

CryoTARPOS in the Integrated Test Facility just prior to packaging for the move

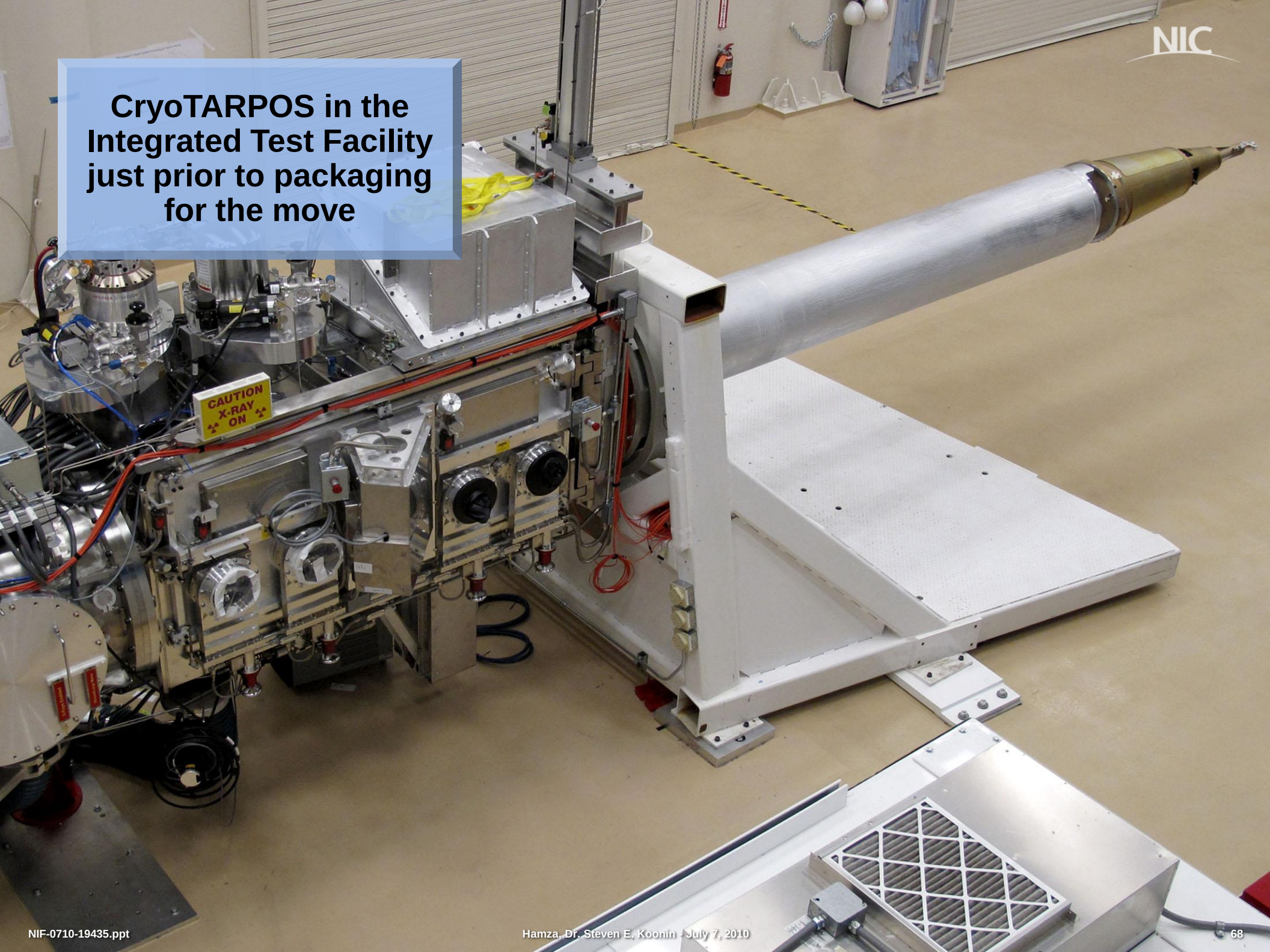

ITPS for layering development and proofing of THD/DT targets
CAUTION
X-RAY
ON

K spec impact on ITF

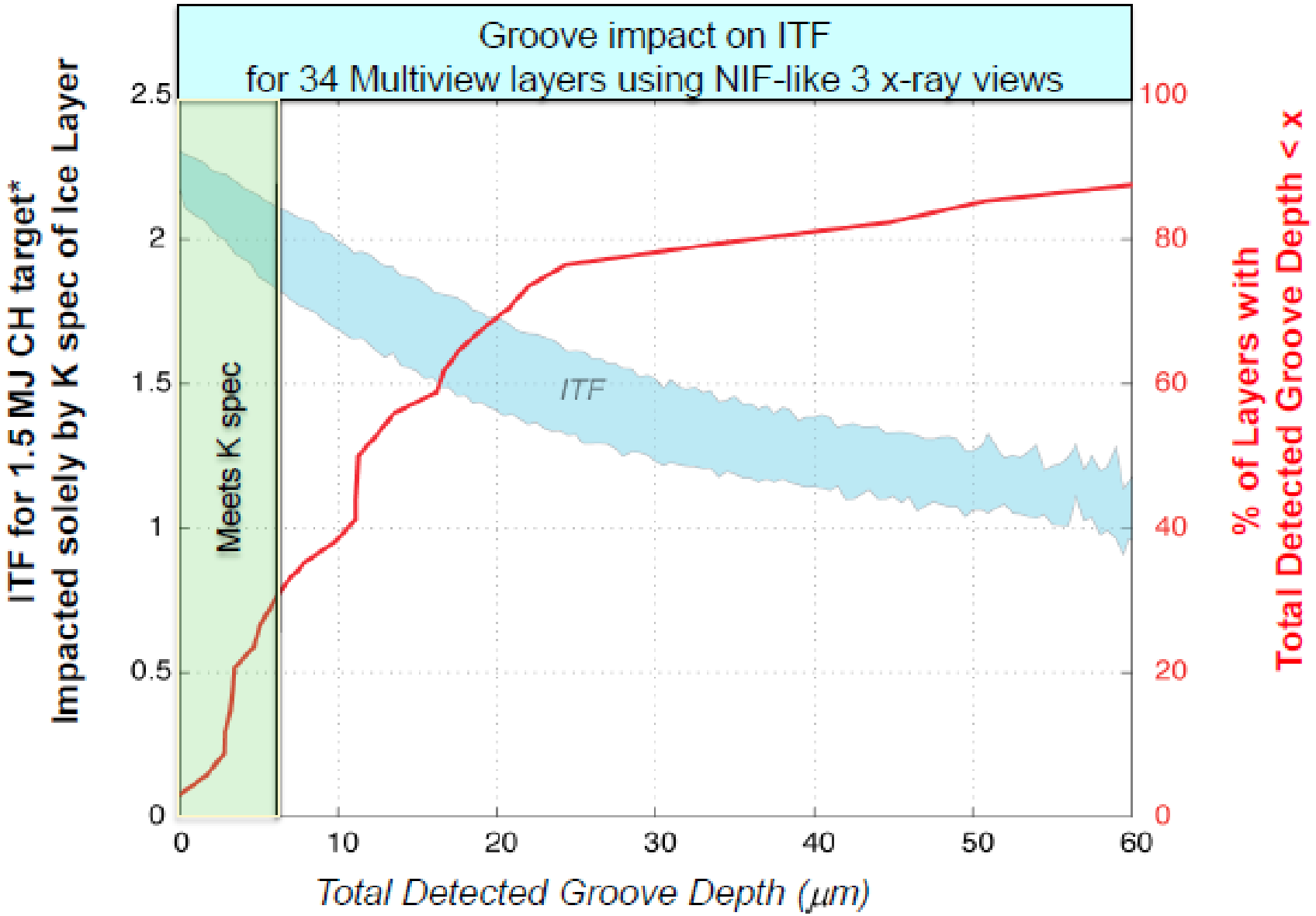

*At 1.3 MJ (2010 scale), ITF is smaller by 15%

Parham

Layering behavior for DT and HT is similar

Isotopic composition influences:

- **Effective potential ⇒ Bond strength:**
  - **Lattice constants**
  - **Melting point**
  - **Vapor pressure**
  - **Molecular mobility**
  - **Surface energy**
  - **Mechanical properties**
  - **Etc.**
- **Beta-decay rate (∝ T content):**
  - **Thermal gradient**
  - **Electronic excitation**
  - **Alloy fractionation**

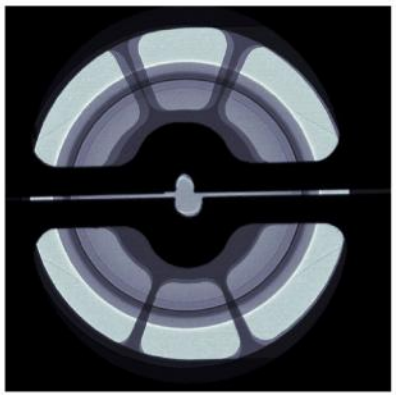

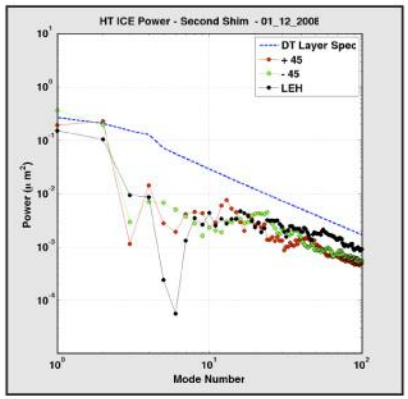

	T_m (K)	P (kPa)	D_0 (10^{-8} m^2/s)	E_d (K)
H_2	14.0	7.2	14	191
D_2	18.7	17.2	4	276
T_2	20.6	21.6	2	340

NIF quality HT layers have been demonstrated

Advances in target fabrication improve margin over uncertainty

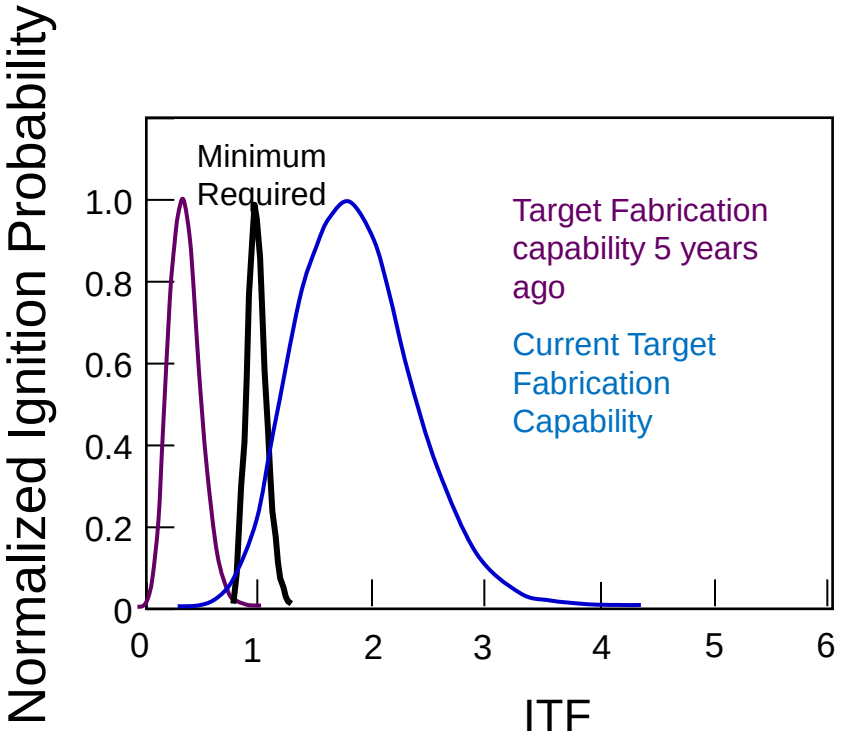

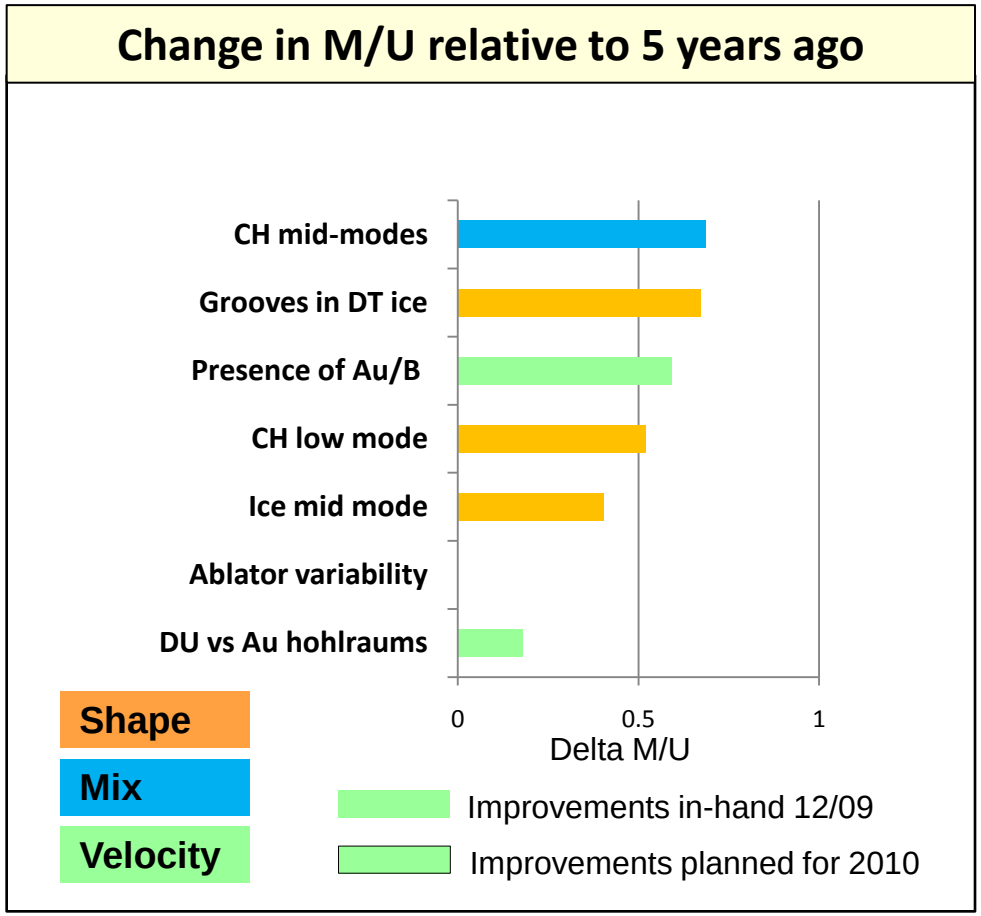

Advances in target fabrication improve margin over uncertainty

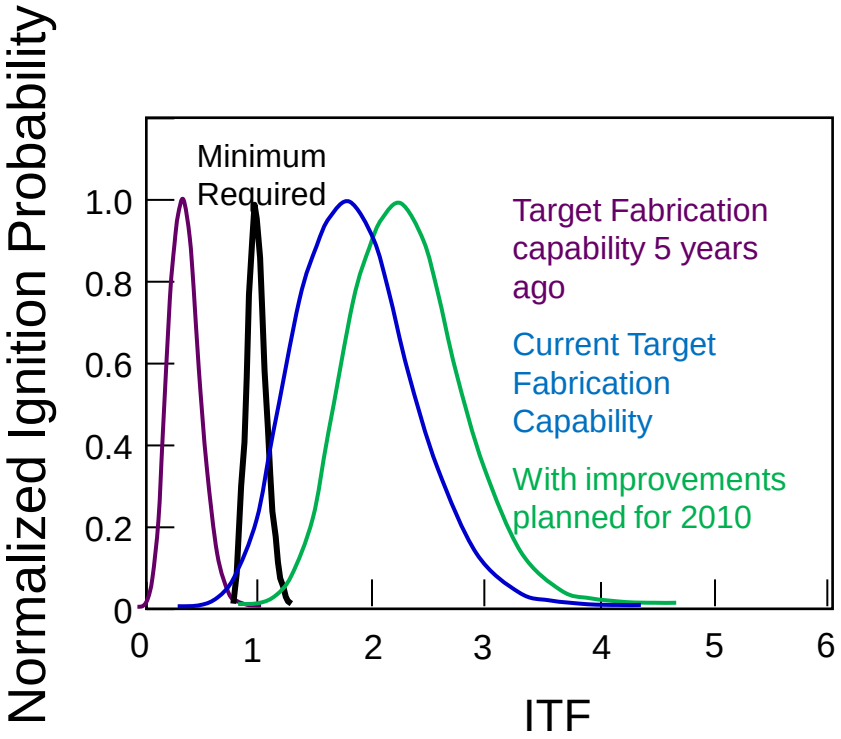

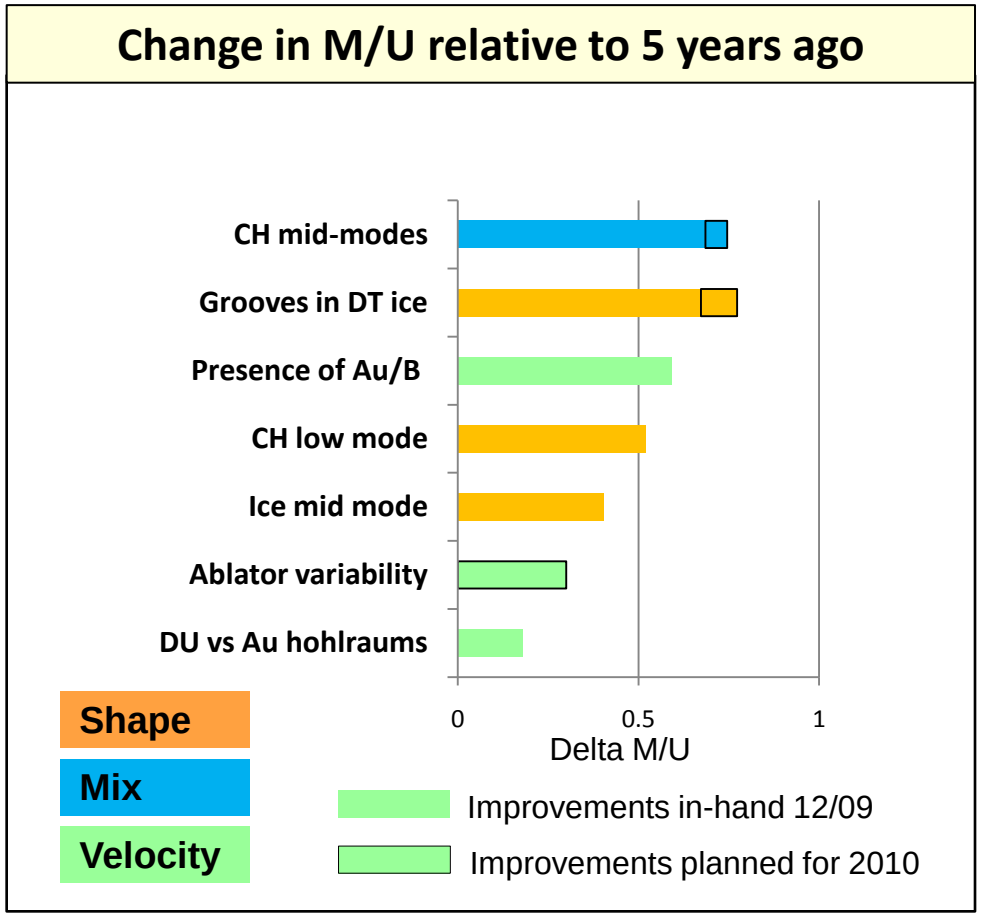

The removal rate for polishing is modeled using a Modified Preston Equation for insights on process

$$\frac{dh}{dt} = k_p \, \mu \, \sigma \, \bar{v}_r \, f_c \, f_t$$

Preston Constant	Friction Coefficient	Pressure at contact	Relative velocity	Fraction of surface area in contact	Fraction of time in contact
• Fundamental material removal of polishing compound	• Function of slurry composition, relative velocity, and viscosity	• Average pressure at capsule-media contact	• Time and spatial average velocity between media and capsule	load and mechanical properties of capsule	• Function of load and mechanical properties of capsule
From polishing literature	Stribeck Curve	Elastic Contact Momentum balance	Estimate from kinematic measurements	Hertzian Contact Mechanics	Hertzian Contact Mechanics
$k_p \cong 8 \cdot 10^4 \frac{nm/hr}{psi \cdot m/\sec}$ for colloidal silica	$\mu \cong 0.7$ in contact mode	$P = 1.54 \left(\frac{}{}\right)^{3/5} \left(\frac{}{}\right)^{2/5} v_N^{6/5} r^2$ $\sigma \approx \frac{P}{\pi \left(\frac{4kPR}{3E^{sh}}\right)^{2/3}}$		$E^{sh} \cong 2.3 E_s \left(\frac{t}{R}\right)^2$ $f_c = \frac{\left(\frac{4kPR}{3E^{sh}}\right)^{2/3}}{d^2}$	$f_t \approx \frac{2\left(\frac{4kPR}{3E^{sh}}\right)^{1/3}}{d}$

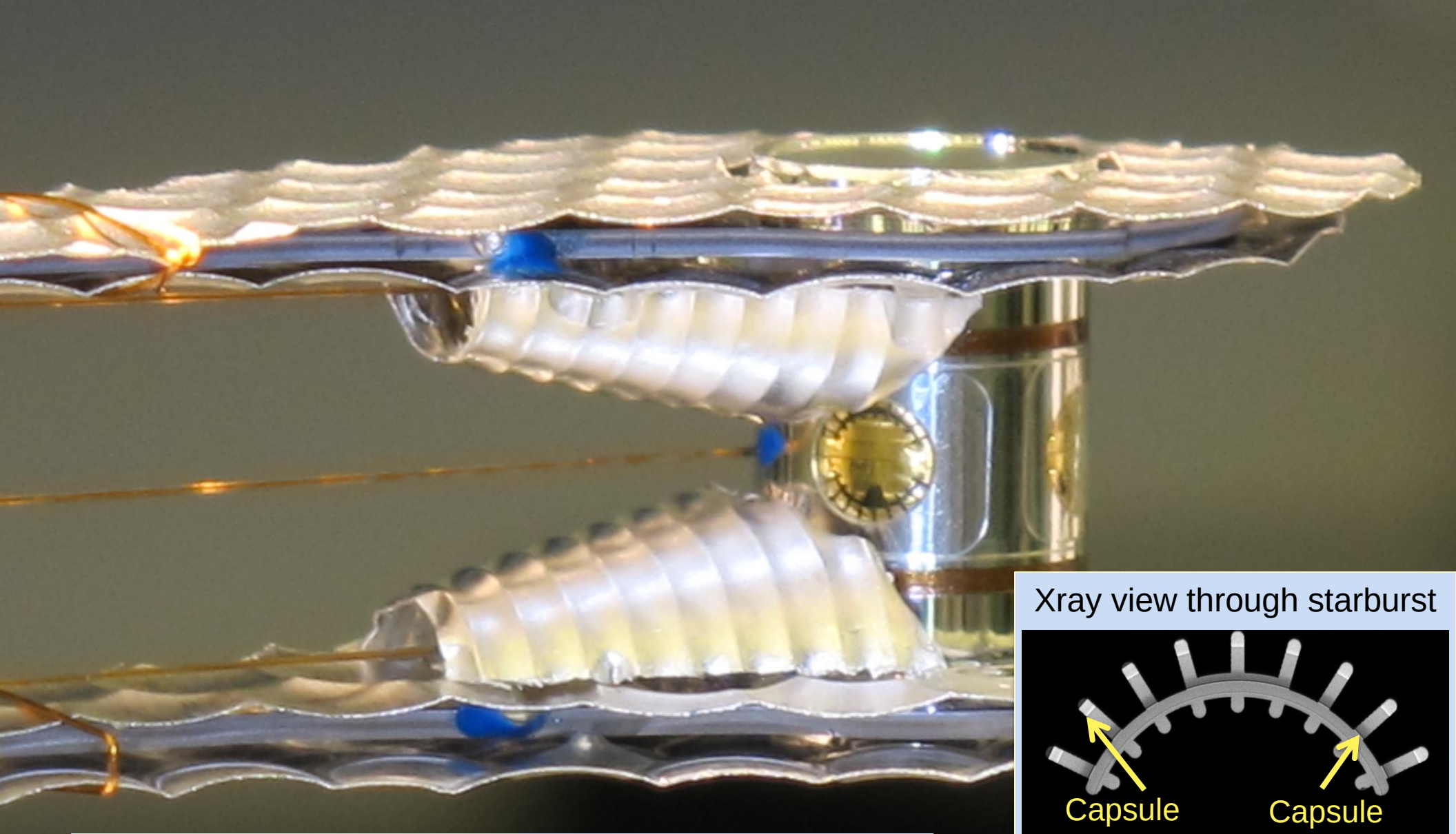

Xray view through starburst

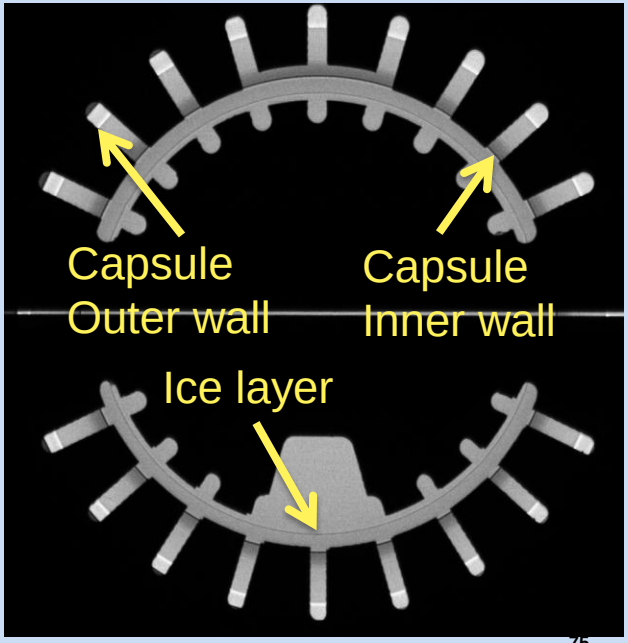

First ice layer in a THD target meeting all measureable ice specifications (CH capsule, ICCS controls, NIF-like cryo system, NIF-like xray metrology)

Layering done in Ignition Target Proofing System (ITPS) in B298

Radiographs from synchrotron run

0 degrees

90 degrees

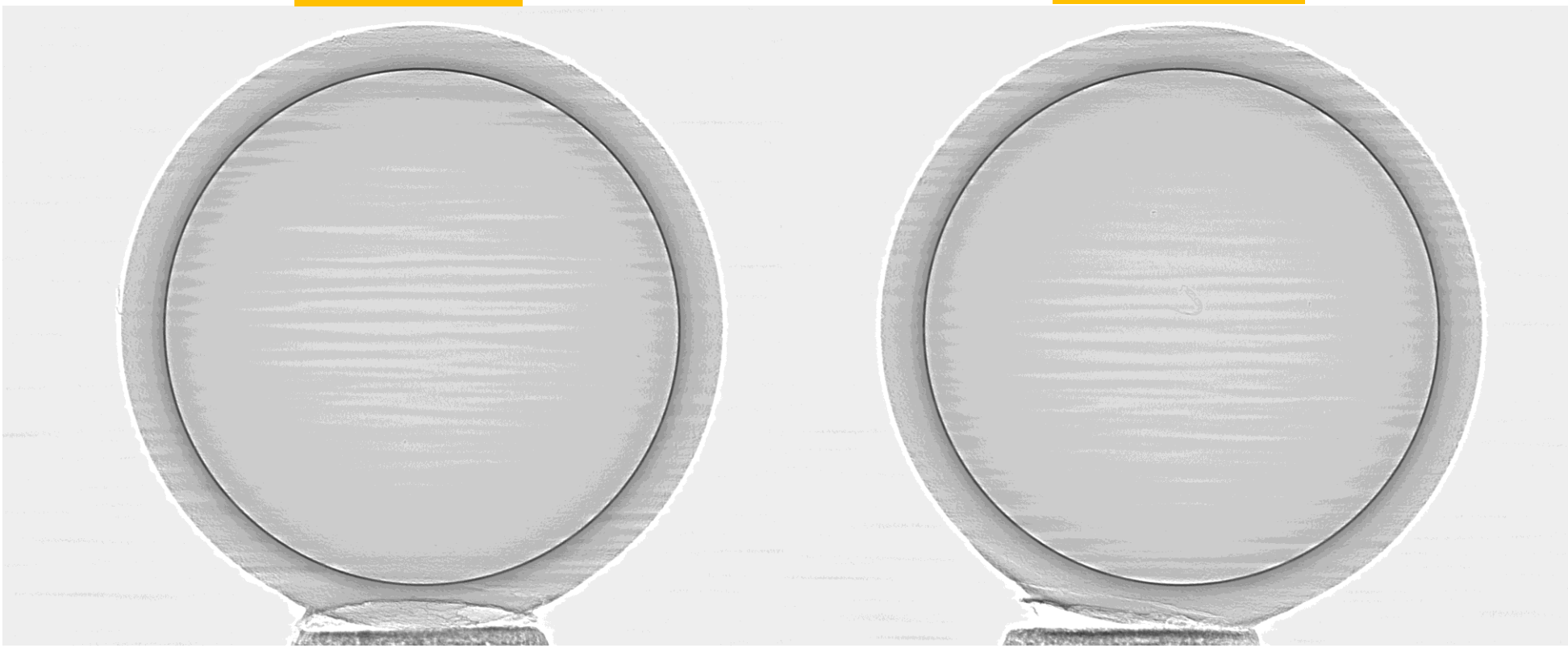

Tomographic slice of capsule being evaluated for homogeneity

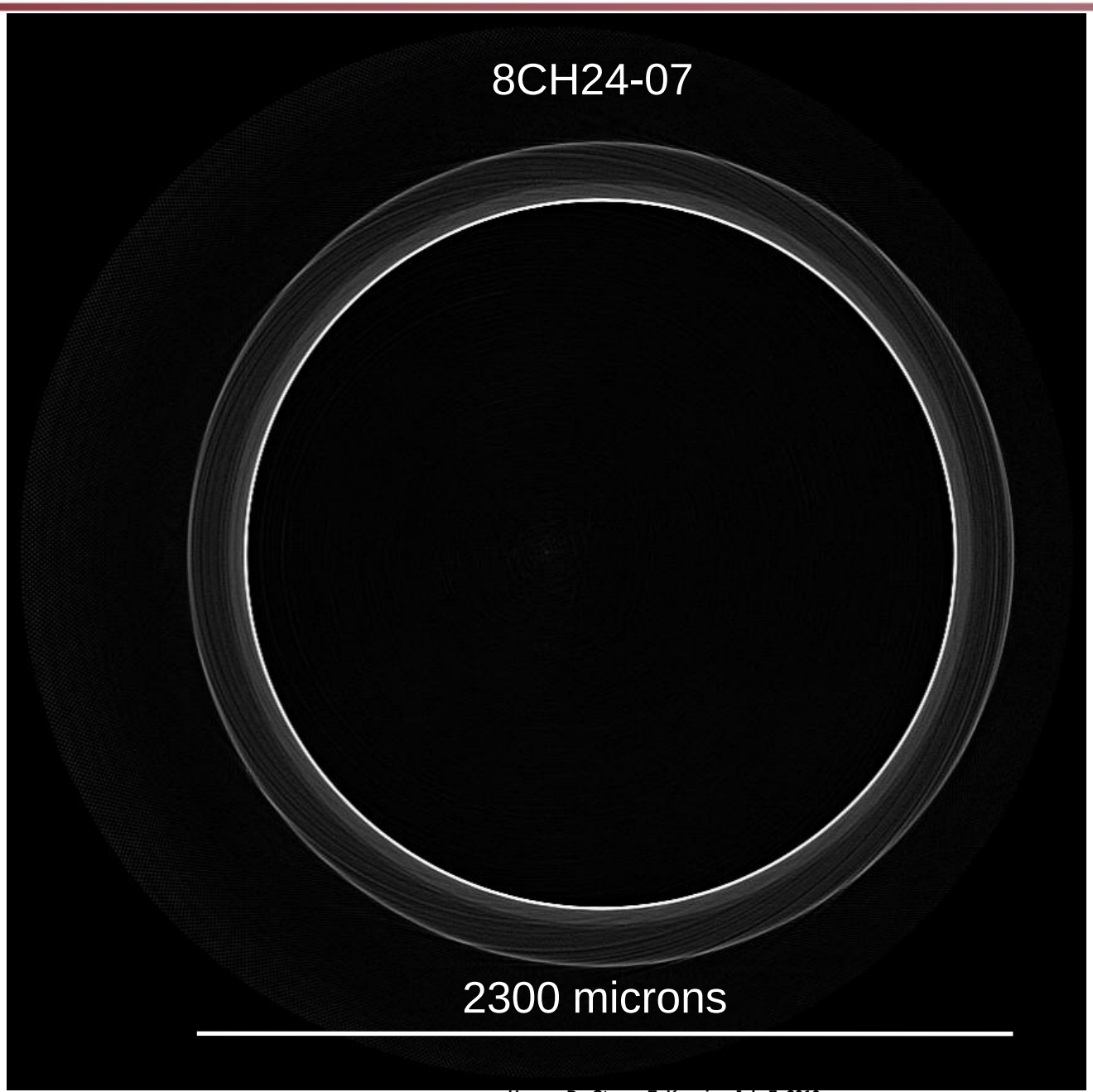

We can estimate the small refraction angle of x-rays at a DT ice groove with an area of 200 um^2

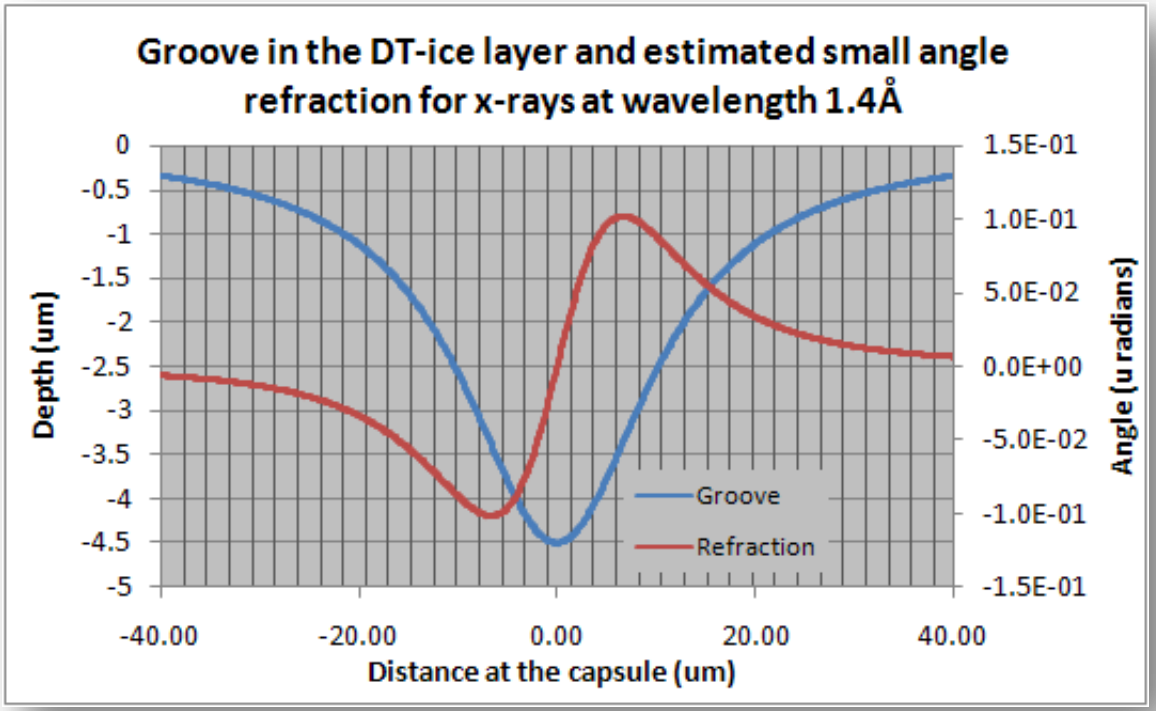

$$g(x) = \frac{D}{1+(x/w)^2}$$

Groove area = π D w

D = -4.5 μm
W = 11.5 μm

Note that each minor division
one pixel at the CCD

From Snell's law

$\alpha_R = -\delta\, \Delta y/\Delta x \quad = -\delta_{DT}\, g'(x)$

where δ_{DT} is the refractive index of DT ice

The resulting phase shift at the interferomete

$\phi_1(x) = 2\pi\, \alpha_R(x)\, d_T / p_2$

$\phi_1(x) \geq 12.5$ mrad for $\alpha_R(x) = 100$nrad

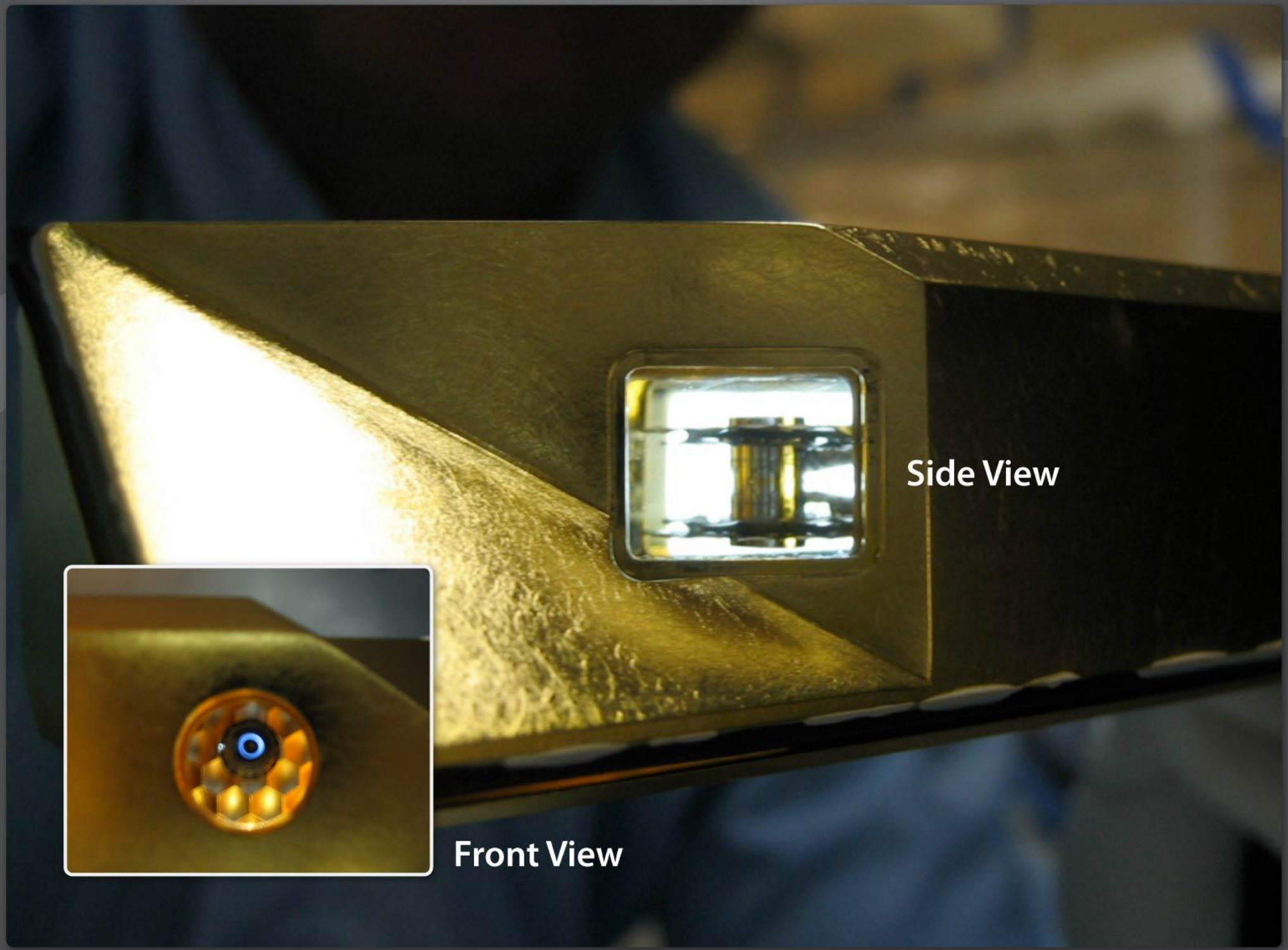
Side View
Front View

NIC